Design and Synthesis of Molecular Models for Photosynthetic Photoprotection

by

Kul Bhushan

A Dissertation Presented in Partial Fulfillment
of the Requirements for the Degree
Doctor of Philosophy

Approved April 2012 by the
Graduate Supervisory Committee:

Devens Gust, Chair
Ana Moore
Mark Hayes

ARIZONA STATE UNIVERSITY

May 2012

ABSTRACT

Most of the sunlight powering natural photosynthesis is absorbed by antenna arrays that transfer, and regulate the delivery of excitation energy to reaction centers in the chloroplast where photosynthesis takes place. Under intense sunlight the plants and certain organisms cannot fully utilize all of the sunlight received by antennas and excess redox species are formed which could potentially harm them. To prevent this, excess energy is dissipated by antennas before it reaches to the reaction centers to initiate electron transfer needed in the next steps of photosynthesis. This phenomenon is called non-photochemical quenching (NPQ). The mechanism of NPQ is not fully understood, but the process is believed to be initiated by a drop in the pH in thylakoid lumen in cells. This causes changes in otherwise nonresponsive energy acceptors which accept the excess energy, preventing oversensitization of the reaction center.

To mimic this phenomenon and get insight into the mechanism of NPQ, a novel pH sensitive dye 3’6’-indolinorhodamine was designed and synthesized which in a neutral solution stays in a closed (colorless) form and does not absorb light while at low pH it opens (colored) and absorbs light. The absorption of the dye overlaps porphyrin emission, thus making energy transfer from the porphyrin to the dye thermodynamically possible. Several self-regulating molecular model systems were designed and synthesized consisting of this dye and zinc porphyrins organized on a hexaphenylbenzene framework to functionally mimic the role of the antenna in NPQ.

When a dye-zinc porphyrin dyad is dissolved in an organic solvent, the zinc porphyrin antenna absorbs and emits light by normal photophysical processes. Time resolved fluorescence experiments using the single-photon-timing method with excitation at 425 nm and emission at 600 nm yielded a lifetime of 2.09 ns for the porphyrin first excited singlet state. When acetic acid is added to the solution of the dyad, the pH sensitive dye opens and quenches the zinc porphyrin emission decreasing the lifetime of the porphyrin first excited singlet state to 23 ps, and converting the excitation energy to heat.

Under similar experimental conditions in a neutral solution, a model hexad containing the dye and five zinc porphyrins organized on a hexaphenylbenzene core decays exponentially with a time constant of 2.1 ns, which is essentially the same lifetime as observed for related monomeric zinc porphyrins. When a solution of the hexad is acidified, the dye opens and quenches all porphyrin first excited singlet states to <40 ps. This converts the excitation energy to heat and renders the porphyrins kinetically incompetent to readily donate electrons by photoinduced electron transfer, thereby mimicking the role of the antenna in photosynthetic photoprotection.

This work is dedicated to my loving parents for their continuous support and motivation during the graduate program.

ACKNOWLEDGEMENTS

I would like to thank my research advisor Professor Devens Gust for his erudite guidance and support throughout my graduate program at Arizona State University. He has been a continuous source of encouragement and inspiration. I would also like to thank Professor Ana Moore and Professor Mark Hayes to serve on my dissertation committee and providing important feedback. My sincere thanks also go to Professor Thomas Moore along with all of the members of Gust/Moore/Moore groups for their help and stimulating discussions about the research which helped me accomplish my goals.

Special thanks to Dr. Yuichi Terazono and Dr. Paul Liddell for sharing their expertise of organic synthesis and providing some of the synthetic compounds. Thanks to Dr. Michael Hambourger for conducting electrochemistry experiments, and James Bridgewater and Bradley Brennan for doing solar cell experiments on several compounds. Special thanks to Dr. Gerdenis Kodis for his work on steady state and time resolved spectroscopic studies of the model compounds and final target molecules.

I wish to acknowledge all of my friends, especially, Vikas Garg, Pallav Kumar, and Devendra Chauhan for their scholarly discussions, help and encouragement. Special thanks to my loving family for their necessary support and encouragement throughout this great endeavor.

TABLE OF CONTENTS

CHAPTER Page

LIST OF FIGURES

Figure Page

Figure Page

Figure Page

Figure Page

LIST OF SCHEMES

Scheme Page

Chapter 1

INTRODUCTION

The sunlight is the main source of the energy and life on earth. It is abundant and readily available in sufficient amount to fulfill the energy needs of the world if harvested properly. Most of the energy being used today is solar energy harvested by plants and organisms in its current form like petroleum products, coal, and natural gas etc. However, these dwindling sources of energy based on fossil fuels are limited and likely to be consumed by the end of this century. The energy problem is one of the most significant challenges faced by humans today. The consumption of these fossil fuels produces carbon dioxide and other greenhouse gases, which harm the environment. Therefore, new sources of clean alternative energy are required to cope with the enormous energy demands of the ever growing human population. Many different sources of alternative energy such as geothermal, wind, solar, hydroelectric, and biomass have been explored.[1]

For almost one century, the harnessing of solar energy has been considered an important alternative to the energy derived from fossil fuels.[2] Although the solar energy reaching earth every hour can be sufficient for one full year, only about 0.01% of this energy is being harnessed. The sunlight is diffuse, and depends on the time, season, and weather conditions. Therefore, it needs to be harvested and stored in a suitable form such as batteries. Current practical methods of solar energy conversion and storage, including photovoltaic cells based on inorganic semiconductors, organic semiconductors, and dye-sensitized

solar cells, do not compete with that of the fossil fuels. Therefore, efficient, inexpensive, and environmentally benign methods of solar energy conversion and storage technologies are required to decrease our dependence on nonrenewable fossil fuels.

To harness the sunlight energy in a useful form such as chemical or electrical energy, it is important to understand the underlying principles and mechanisms of natural photosynthesis which have been successfully developed and employed for billions of years by plants and organisms for their energy requirements. To solve this problem one of the approaches is to utilize artificial photosynthesis which mimics the techniques employed by natural photosynthesis. Artificial photosynthesis also holds promise in organic photovoltaic solar cells, nanoscale molecular machines, and optoelectronic devices.

Plants and organisms efficiently harvest the sunlight for their energy requirements using the antennas and reaction centers, but the sunlight received by many of them, in various geographical locations, is much more than what they can utilize. This has led to them develop alternative methods to avoid this excess energy. Plants and organisms use various mechanisms to dissipate this excess energy, one of the most prominent methods of dissipating this excess energy as heat is non-photochemical quenching (NPQ). It is very difficult to understand the actual mechanisms involved in NPQ due to extremely complex structures of the cells, but it is believed to be initiated by a signal by a drop in the pH of thylakoid lumen, and by a series of structural changes in cell components, the excess energy is dissipated as heat by antennas. This phenomenon is called photosynthetic

photoprotection. There have been numerous studies to understand its mechanism. On the basis of artificial photosynthesis, recently, self-regulating molecular models have been synthesized and studied to develop a mechanistic model of photosynthetic photoprotection employed by antenna moieties.[3] This dissertation describes the design, synthesis, and photophysical studies of molecular models for photosynthetic photoprotection.

Natural Photosynthesis

Photosynthesis is a process of converting light energy into chemical energy by green plants, algae and certain bacteria. Carbon dioxide is consumed and oxygen is evolved in this process which helps maintain the balance of greenhouse gases in the environment. Cyclic tetrapyrroles (e.g. chlorophylls and porphyrins) act as efficient antennas and photoprotectors due to their ability to absorb light in the visible region of the solar spectrum. Photosynthesis occurs within cell membranes where the components are embedded within a protein matrix (Figure 1).[4] Photosynthesis begins with the absorption of light by photosynthetic chromophores that function as antennas for light harvesting. Absorption of light generates singlet excited states of the chromophores which by a series of physical and chemical processes, lead to the conversion of excitation energy to chemical energy through transmembrane charge separation.[4]

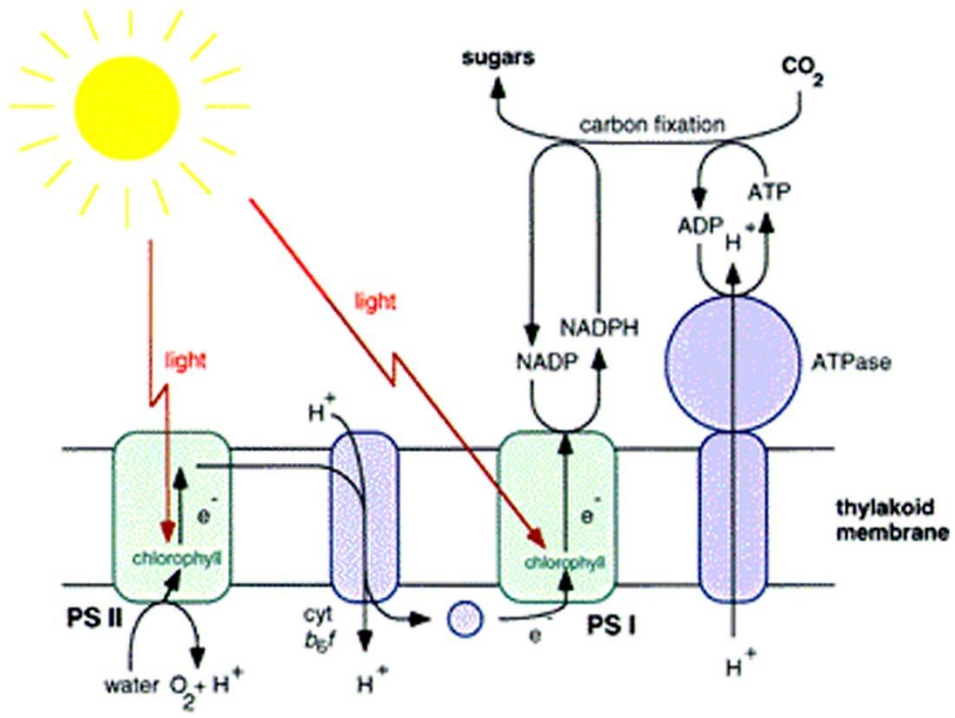

Figure 1. An overview of the photosynthetic processes in plants, algae, and cyanobacteria.[4]

The purple bacterium *Rhodopseudomonas virdis* utilizes less complex photosynthesis machinery than that of higher plants. A well-arranged symmetrical reaction center complex of this bacterium consists of four molecules of bacteriochlorophyll (Bchl), two molecules of bacteriopheophytin (BPh), and two quinones. Photosynthesis in this bacterium utilizes photoinduced electron transfer and energy transfer processes in an ensemble of well organized antenna arrays around the reaction center. A number of chlorophylls and carotenoid antennas are packed near the surface of the cell membranes. These antennas absorb most of the sunlight, and transfer this energy ultimately to the reaction center by singlet-singlet energy transfer processes through a cascade of chromophores.

Photoinduced electron transfer from a Bchl special pair (SP) to a quinone acceptor generates a long-lived charge-separated state due to the reaction energetics and topological factors which discourage the charge recombination. This provides sufficient time for the potential energy stored in charge-separated state to be used in further chemical reactions. The most important biological resource for sustaining life is the production of proton motive force which is driven by the potential energy derived from this process. By a series of reactions, energy-rich adenosine triphosphate (ATP) is formed from adenosine diphosphate (ADP), thereby storing the solar energy in the chemical bonds of ATP. This cyclic process powers the energy requirements of the bacterium. Photosynthesis in higher plants involves two photosynthetic reaction centers, photosystem I and II. Each photosystem plays a vital role in photosynthesis. In photosystem II, oxidation of water takes place to generate molecular oxygen, and in photosystem I, carbon dioxide is converted into sugars and carbohydrates.[5, 6]

Artificial Photosynthesis

Artificial photosynthesis is the design and study of artificial constructs synthesized and assembled in a laboratory setting to mimic the natural structures, and understand the underlying principles of natural photosynthesis technologies employed by plants and organisms. Artificial photosynthesis is an important aspect of the science to understand the natural photosynthesis better, and use the information gained to design light harvesting materials and media to effectively harness the solar energy. A number of artificial photosynthetic reaction centers

based on donor-acceptor molecules have been developed to understand basic mechanistic electron transfer and energy transfer processes.[5, 7-17] Two of the main desired qualities of artificial reaction centers are to get a 100% quantum yield of the final charge-separated state and to produce a long-lived charge-separated state between the donor-acceptor moieties so that they could be practically used to harness solar energy. Artificial reaction centers utilize photoinduced electron transfer and energy transfer processes to harvest the solar energy. Some artificial reaction centers utilize non-biological components such as semiconductors and metal complexes, but most of them employ organic chromophores because they are similar to the chromophores found in natural photosynthetic systems.

It is exceptionally difficult in a lab setting to mimic the exact reaction centers found in nature due to their extremely complex structures. This has led to the rational design and synthesis of less complex architectures of artificial donor-acceptor systems. The components in artificial reaction centers need to be at optimum distances for electronic coupling for effective and efficient energy and electron transfer. These systems use covalent linkage between donor-acceptor and antenna moieties to control spatial orientation. There are some examples of self-assembled reaction centers,[18-20] but most of the reaction centers employ covalent linkages for optimum performance. Advances in synthetic organic methodologies have enabled the scientists to build macromolecules and macroarrays for better mimicking of the complex natural photosynthetic systems.

Energy Transfer in Reaction Centers

In photosynthetic reaction centers when a donor D absorbs the light its electronically excited singlet state D^* is generated. Energy transfer then occurs from this excited state moiety to an acceptor A to generate excited singlet state A^*, and the donor returns to its ground state A. The energy transfer from the donor to acceptor may occur by two pathways. First pathway is called the Förster mechanism where the energy transfer occurs through space, and an orbital overlap of donor-acceptor molecules is not required. This mechanism allows the chromophores to be far apart (10-100 Å). The rate of energy transfer (k_{EnT}) is given by the Förster equation (1)[22, 23]

$$k_{EnT} = 0.529\ \kappa^2\ \Phi_D\ J\ /\ n^4\ N\ \tau_D\ R^6 \qquad (1)$$

where κ is the orientation factor (related to the relative spatial orientation of donor and acceptor transition dipole moments and taken as 2/3 for a random distribution of interacting dipoles), Φ_D is the quantum yield of fluorescence of the donor in the absence of acceptor, *J* is the spectral overlap integral of the acceptor's absorption and donor's emission, *n* is the dielectric constant of the medium, *N* is Avogadro's number, τ_D is the excited state lifetime of the donor in the absence of acceptor, and *R* is the interchromophoric distance in cm.

The second pathway for energy transfer is called the Dexter mechanism where the donor and acceptor molecules are covalently attached to each other, and an effective overlap of donor and acceptor orbitals is necessary for effective

energy transfer. Therefore, it operates on shorter distances (10 Å) between donor and acceptor. It has stronger dependence on interchromophoric distances than the Förster mechanism. When the Dexter mechanism is operating, the rate of energy transfer (k_{EnT}) is given by Dexter equation (2)[24]

$$k_{EnT} = KJ \exp(-2R/L) \qquad (2)$$

where *K* is related to specific orbital interactions, *J* is the spectral overlap integral normalized for the extinction coefficient of the acceptor, and R is the separation of the donor and acceptor relative to their van der Waals radii, L.

Electron Transfer in Reaction Centers

If an electron acceptor of appropriate redox potential is in close proximity of the donor then instead of transferring its energy to an acceptor, an excited donor D^* can also come to ground state D by spending its energy to transfer an electron to the electron acceptor by photoinduced electron transfer. This process leads to a charge-separated state, and it is competitive with other deactivation pathways such as fluorescence emission, intersystem crossing (ISC) to the triplet state, and internal conversion (IC) to the ground state. Photoinduced electron transfer leads to the decreased lifetime of the donor excited singlet state (τ_f), and the florescence quantum yield (Φ_f).

Photoinduced electron transfer occurring in covalently linked donor-acceptor molecules is described by Marcus, Levich, Hush, and Jortner theory.[25-29] The rate of electron transfer k_{ET} is given by equation (3)

$$k_{ET} = (\pi/\hbar^2 \lambda \kappa_B T)^{1/2} |V|^2 \exp [- (\Delta G^0 + \lambda)^2/4\lambda \kappa_B T] \quad (3)$$

where $\hbar$ is Planck's constant, λ is the total reorganization energy required to transform the product state and its surroundings from the equilibrium configuration of the reactant state. λ is the sum of two energy terms, solvent dependant (λ_s) and solvent independent (λ_i), where λ_s is solvent reorganization energy and λ_i accounts for the energy of structural differences between the reactant and the product. The term κ_B is the Boltzmann's constant, T is the absolute temperature, V is the electronic coupling matrix element between the donor-acceptor molecules, and ΔG^0 is the free energy change for the reaction. k_{ET} is dependent on the electronic interactions between the donor-acceptor, and the free energy of the reaction.

Equation 3 expresses three distinct scenarios of the relationship between ΔG^0 and λ. When the reaction is more spontaneous, ΔG^0 becomes more negative. Just like most reactions, in the Marcus 'normal region' when the thermodynamic driving force is smaller than the overall reorganizational energy ($-\Delta G^0 < \lambda$), the rate of electron transfer between donor-acceptor increases with increasing thermodynamic driving force. When the thermodynamic driving force becomes equal to the overall reorganizational energy ($-\Delta G^0 = \lambda$), the rate of electron

transfer becomes maximum. When the thermodynamic driving force continue to increase ($-\Delta G^0 > \lambda$), the rate of electron transfer begins to decrease (Markus 'inverted region').[29] The rate of charge recombination, in the reaction centers containing fullerenes as electron acceptors, follows this region resulting in long-lived charge separated states. This is one of the reasons that fullerenes have become attractive candidates as electron acceptors in artificial reaction centers.

Artificial Reaction Centers

In an artificial reaction center, chromophores absorb the light and then an electron is transferred from the donor chromophore to electron acceptor by photoinduced electron transfer. This generates a charge-separated state between donor and acceptor moieties. An artificial reaction center stores the excitation energy as chemical potential energy in the charge-separated state. The charge-separated states are usually short-lived due to rapid recombination of the charges and other energy deactivation pathways. It is essential to get a long-lived high energy charge-separated state by controlling the distance and spatial organization of the donor and acceptor molecules, and slow the rate of charge recombination so that the charge separation can be used in a device such as organic photovoltaic solar cell. Many artificial reaction centers consisting of donor-acceptor molecules as well as antennas-donor-acceptor molecules have been synthesized and studied.[30-42] Various antennas and electron donors such as porphyrins, phthalocyanines, and other chromophores, and electron acceptors like quinones and functionalized fullerenes etc. have been explored.

Porphyrins as Antennas and Electron Donors

Porphyrin are the most frequently employed as antennas and electron donors, and sometimes electron acceptors in artificial reaction centers due to their excellent stability, and structural resemblance to the natural chromophores such as chlorophylls (Figure 2).

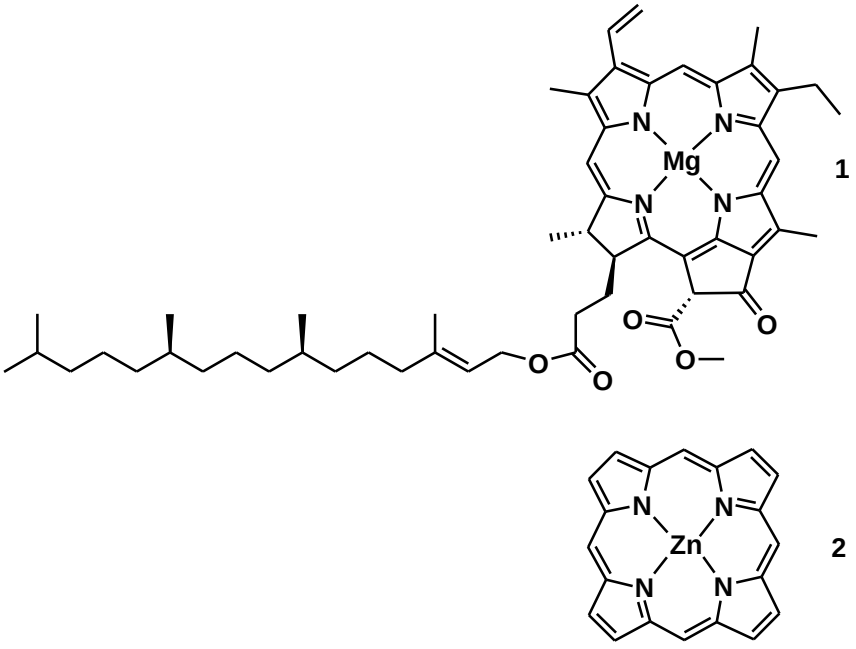

Figure 2. Structures of chlorophyll a **1** and a model zinc porphyrin **2**

This makes the porphyrins and metalloporphyrins attractive candidates for bio-mimicry and artificial photosynthesis. A variety of porphyrins can be synthesized with relative ease in comparison to their naturally occurring counterparts. Porphyrins absorb the light notably in the short as well as less strongly in long wavelengths of the visible region of the solar spectrum. Porphyrins have high

molar extinction coefficients. Photoexcitation of both free-base and zinc porphyrins exhibits high quantum yields, and sufficiently long lifetimes of their first excited singlet states to allow electron transfer process successfully compete other deactivation processes. Additionally, the redox properties of porphyrins can be tuned by altering their substituents and forming different metalloporphyrins. Introduction of redox-active metals in the interior of porphyrins can generate additional redox properties. Moreover, the redox properties of porphyrins and metalloporphyrins can dramatically alter upon photoexcitation which leads to their useful excited states.

Artificial reaction center pentad **3** demonstrates that the porphyrins can act as efficient antennas as well as energy sink (Figure 3).[43]

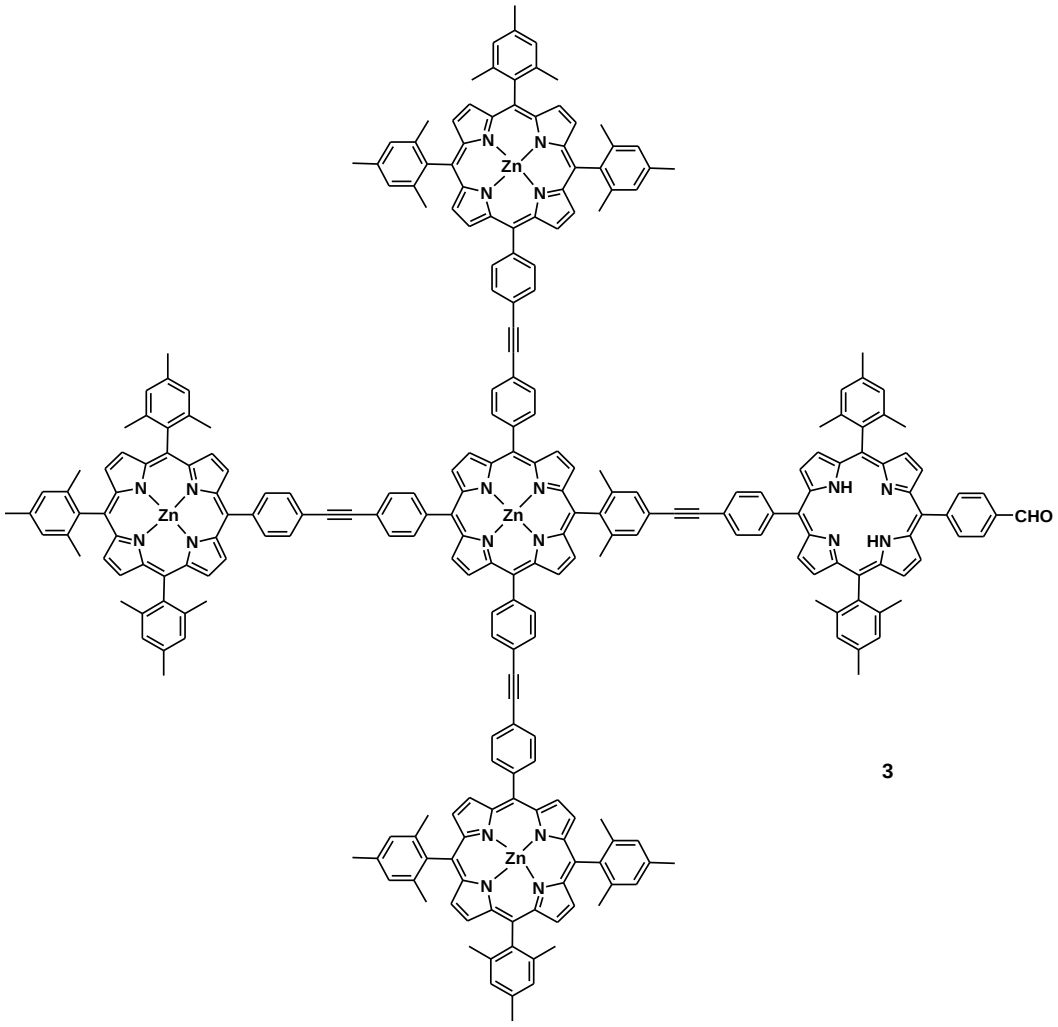

3

Figure 3. A porphyrin-based artificial photosynthetic antenna array pentad **3.**

Pentad **3** features four covalently linked zinc porphyrin chromophores, three at the periphery $(P_{ZnP})_3$ and one at the center (P_{ZnC}). The central zinc porphyrin is covalently attached with three peripheral porphyrins and a free-base porphyrin (P). The energy of first excited singlet state of the free-base porphyrin is 0.15 eV lower than those of the zinc porphyrins, making the energy transfer from zinc porphyrins to free-base porphyrin thermodynamically possible. Time-resolved spectroscopic studies of the pentad revealed that the photoexcitation of the $(P_{ZnP})_3$

results in singlet excitation energy transfer to the P_{ZnC} to produce $(P_{ZnP})_3$-$^1P_{ZnC}$-P with a time constant of 50 ps. First excited singlet state of the central zinc porphyrin then transfers its energy to free-base porphyrin to produce $(P_{ZnP})_3$-P_{ZnC}-^1P with a time constant of 32 ps. First excited singlet state of the free-base porphyrin comes to the ground state in 11 ns by normal photophysical processes. Thus the zinc porphyrins act as efficient antenna array for the free base porphyrin energy sink. The antenna function of the zinc porphyrins was explored in design and synthesis of molecular models for photosynthetic photoprotection described in this dissertation.

Fullerenes as Electron Acceptors

Artificial reaction centers must exhibit a preference of electron transfer over energy transfer at longer distances as the rate of energy transfer rapidly decreases with increasing interchromophoric distances. Fullerenes based electron acceptors are one of the most promising candidates, and commonly used due to their low reduction potentials. The first reduction potential of fullerenes is close to that of the benzoquinone electron acceptors found in natural systems. Fullerenes can efficiently delocalize the acquired negative charge (up to six electrons) due to their symmetrical three dimensional structures and conjugated π bonds. Fullerenes behave like electron deficient alkenes rather than aromatic compounds. They also possess low reorganizational energies and their anions have low sensitivity to solvent stabilization which helps achieve high quantum yield and long-lived charge-separated states. This makes fullerene based artificial reaction centers

superior to two-dimensional acceptors such as quinones. Their versatile and easy functionalization along with the aforementioned properties makes them attractive candidates for bio-mimicry of natural photosynthesis, and their potential use in solar fuel production.[44]

Natural photosynthetic apparatus utilize chlorophyll antenna arrays as the major light harvesting chromophores. Although chlorophylls are efficient in light harvesting but they do not absorb strongly throughout the solar spectrum. To overcome this deficiency natural photosynthetic machinery applies various carotenoid polyenes as auxiliary chromophores to absorb the light where chlorophylls do not absorb. To demonstrate the function of auxiliary chromophores in artificial photosynthetic systems, our research group has recently synthesized and studied energy transfer and photoinduced electron transfer in a wheel-shaped hexaphenylbenzene core based artificial photosynthetic antenna-reaction center complex **4** (Figure 4).[45, 46]

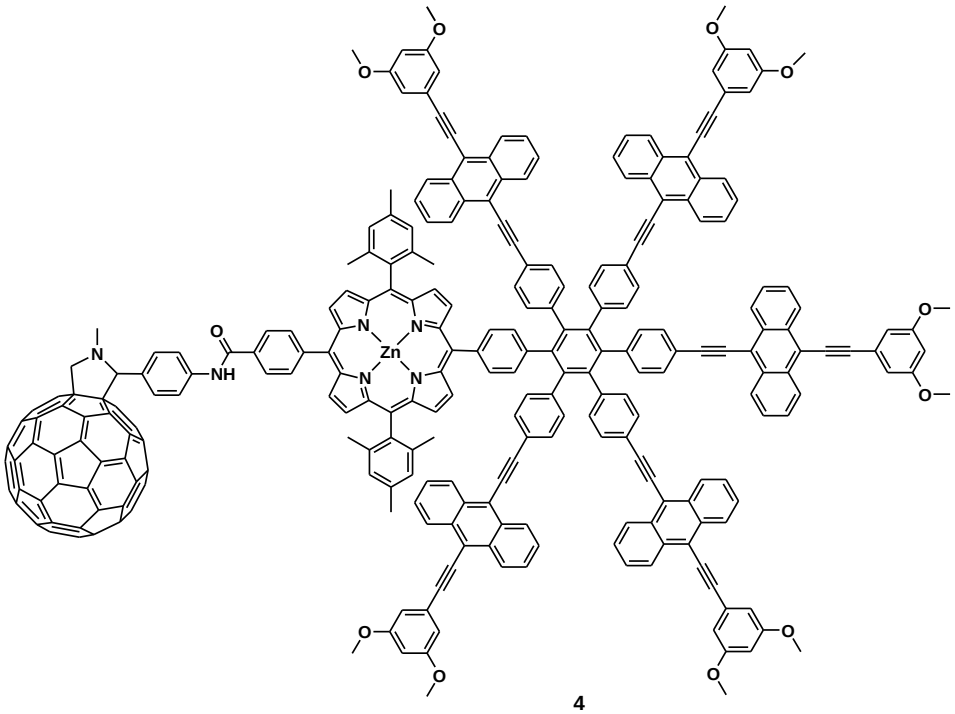

Figure 4. A wheel-shaped hexaphenylbenzene core based artificial photosynthetic antenna-reaction center complex **4**.

Apart from the porphyrin-fullerene dyad this heptad also features five bis(phenylethynyl)anthracene (BPEA) antenna moieties organized on the central hexaphenylbenzene skeleton. The BPEA antenna chromophores afford spectral coverage in the 430-475 nm region of the solar spectrum where chlorophylls and porphyrins do not absorb strongly. Time resolved spectroscopic studies of the complex in 2-methyltetrahydrofuran revealed that complex molecules successfully integrate singlet-singlet energy transfer and photoinduced electron transfer. Energy transfer from the five antennas to porphyrin occurs rapidly on the picoseconds time scale with a quantum yield of 1.0. The excited singlet state of

the porphyrin donates an electron to covalently attached fullerene by photoinduced electron transfer to yield a $P^{\bullet+}$-$C_{60}^{\bullet-}$ charge separated state, which has a lifetime of 15 nanoseconds. The quantum yield of charge separation based on light absorbed by the antenna chromophores is 80% for the free base molecule and 96% for the zinc analogue.

Photoprotection in Photosynthesis

Solar energy harvesting by plants, algae, and certain bacteria provides the usable energy and building materials necessary to support the life on earth. Photosynthesis acts as a sink for carbon dioxide and keeps the global warming in check by controlling the greenhouse gases in the atmosphere. Photosynthetic apparatus and mechanism are very complex in nature. They have been developed by nature over billions of years for optimum performance and safeguard of the machinery. The photosynthesis nano-factories are housed in cells within a complex matrix of proteins and other cofactors.

Light Harvesting Pigments

The most important components of the photosynthetic machinery are light harvesting complexes (LHC) and reaction center (RC). Light harvesting materials such as chlorophylls, carotenoids, and other auxiliary pigments are located within the protein matrix.[47, 48] Light harvesting pigments are non-covalently assembled in the proteins forming pigment-protein complexes. There are arrays of chlorophyll and carotenoid pigments around the reaction center. Light harvesting complexes absorb the sunlight and transfer the energy to the reaction centers where

photoinduced electron transfer events take place to generate long-lived charge-separated states.[49] Purple bacteria have less complex photosynthetic systems than that of the green plants. There are two types of light harvesting complexes in purple bacteria (*Rhodopseudomonas acidophila*), light harvesting complex 1 (LH1) and light harvesting complex 2 (LH2).[50, 51] LH1 is the main complex which is located close to the reaction center. LH2 complex is located at the periphery and is called auxiliary antenna. The structure of LH2 has been determined by X-ray diffraction method.[52] It consists of bacteriochlorophyll, carotenoid, and a circular aggregate of α and β polypeptides. Photosynthetic system in plants consists of two systems, photosystem I (PSI) and photosystem II (PSII). PSII contains the major light harvesting complex (LHCII). The structure of LHCII in green peas has been determined by X-ray crystallography (Figure 5).[53, 54]

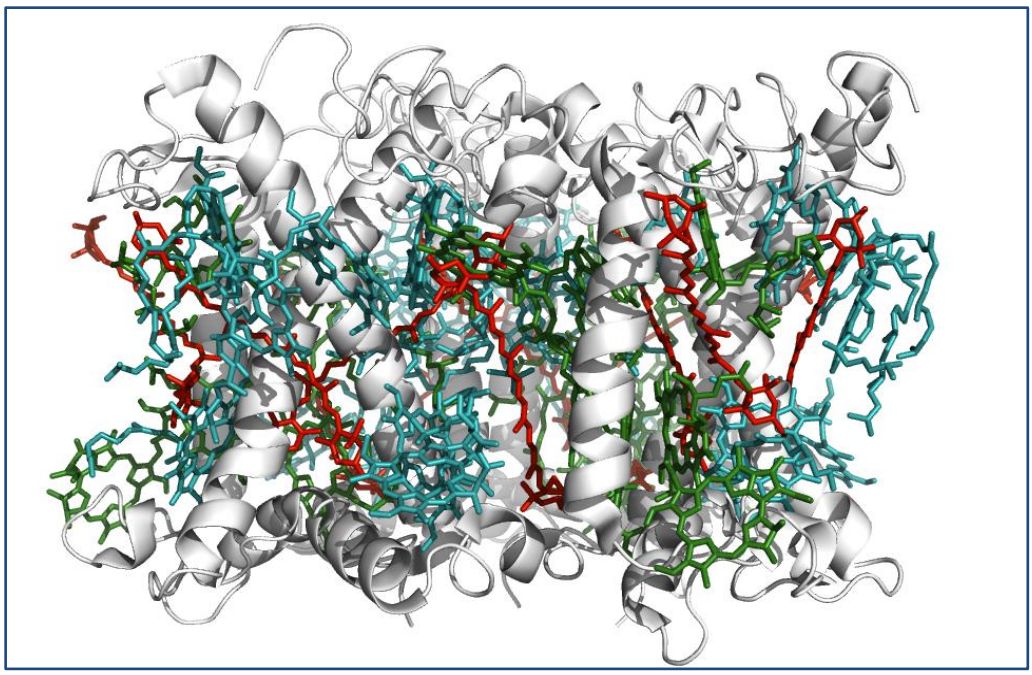

Figure 5: The structure of LHCII trimer: side view from the stromal side. Chl *a* is shown in blue, Chl *b* in green, carotenoids in red, and protein in light grey color.[53, 54]

The structure revealed that it contains chlolorophyll *a*, chlolorophyll *b*, and carotenoids along with proteins. The carotenoids and the proteins in LHCII hold the complex together for stability, and optimum absorption and transfer of energy.

Carotenoids as Light Harvesters and Photoprotectors

The arrays of chlorophylls and carotenoids are the most important and abundant light harvesting pigments found in natural photosynthetic systems. Carotenoids absorb in the blue-green region of the solar spectrum where chlorophylls have low absorption capacity. Carotenoids then transfer the energy

to adjacent chlorophylls thereby acting as efficient antennas.[55] Carotenoids also function as essential components for structural stability of light harvesting proteins.[56] The proteins complexes may disintegrate in the absence of carotenoids. The carotenoids also help the light harvesting complexes achieve proper topological orientation for efficient light harvesting and photoprotection. Carotenoids prevent oxidative photodamage of photosystems by dissipating excess energy as heat.

In low light ambient conditions, plants maximize their light absorption and photosynthesis process. When the absorption of light exceeds the capacity of light energy utilization, the photosynthetic apparatus and organisms become susceptible to photodamage. When photoinduced charge separation outpaces the process by which the redox potential is used in the later steps of dark reactions, high energy, harmful byproducts such as chlorophyll triplet states ($^3Chl^*$) and oxygen singlet states ($^1O_2{}^*$) are formed.[57, 58] These highly reactive species, if not consumed rapidly, react with cell tissue and other vital components such as PSII D1 reaction center protein, lipid bilayer, and pigments, causing photodamage.[59, 60] Photodamage results in decreased photosynthetic efficiency, and injury to the organisms. In extreme oxidative conditions, irreversible photodamage can even cause the death of the organisms.

In natural photosynthetic reaction center, photoinduced electron transfer generates chlorophyll radical cation and a reduced quinone. In normal photosynthetic process, the reduced quinone is replaced with a new quinone before a new photoinduced electron transfer occurs. If the photoinduced electron

transfer events outpace the quinone replacements, an electron combines with chlorophyll radical cation generating $^{3}Chl^{*}$, which generates $^{1}O_{2}^{*}$ from ground state oxygen, which can cause photodamage by attacking the organism tissues.[61] Plants and organisms have developed various mechanisms to outmaneuver the photodamage processes. Photosynthetic organisms employ carotenoid polyenes as photoprotective agents. Carotenoid polyenes found in natural photosynthetic systems have low lying triplet excited states, which absorb the energy of these excited state species converting the excess energy to heat, and thereby providing photoprotection to the organisms.

These photoprotective mechanisms of carotenoid polyenes have been explored in artificial reaction centers.[62-67] A representative example of this type of photoprotective mechanism is described by time-resolved fluorescence studies of a porphyrin-carotene (P-C) dyad **5** which features a carotenoid polyene covalently linked to a porphyrin chromophore (Figure 6).[64]

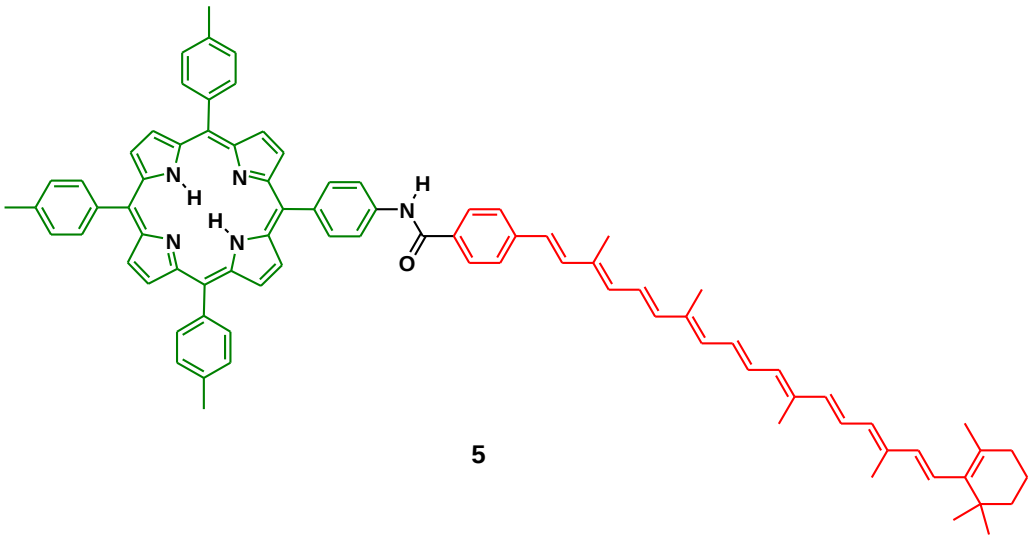

5

Figure 6. A covalently linked porphyrin-carotene (P-C) dyad **5** which demonstrates the photoprotection from singlet oxygen photodamage *via* rapid quenching of the porphyrin triplet states by the carotenoid by triplet-triplet energy transfer.[64]

When a deoxygenated solution of **5** in toluene is excited with a 590 nm laser pulse, porphyrin excited singlet state (^{1}P-C) is generated. The ^{1}P-C decays with a time constant of 5.2 ns, and one of the decay pathways generates the porphyrin triplet state (^{3}P-C). The ^{3}P-C state decays to its ground state with a time constant of 5.7 μs. The ^{3}P-C state can generate singlet oxygen by interacting with ground state oxygen. Transient absorption studies of **5** with a 650 nm laser pulse revealed that ^{3}P-C is converted to P-^{3}C with a triplet-triplet energy transfer with a time constant of less than 10 ns. The rate of triplet energy transfer is possibly greater than that of decay of porphyrin singlet state. Thus the dyad cannot generate singlet oxygen because ^{3}P-C is quenched much faster than the diffusional

quenching by molecular oxygen in oxygenic environment. Therefore, the dyad successfully mimics the role of carotenoid polyenes in photosynthetic photoprotection in green plants and algae.

NPQ in Cyanobacteria

To avoid photodamage and increase photosynthesis efficiency, organisms employ various photoprotective mechanisms to dissipate the excess energy as heat. One of the photoprotective mechanisms is called NPQ in which carotenoid polyenes absorb the energy of exited states of $^{3}Chl^{*}$ and $^{1}O_{2}^{*}$ and dissipate it as heat. In cyanobacteria, excitation energy for water oxidation is absorbed by phycobilisome antennas which contain orange carotenoid protein (OCP).[68, 69] Thermally stable form of the OCP absorbs blue-green light and does not quench the excited singlet states of chlorophylls. However, light absorption by the carotenoids of these proteins leads to structural changes, producing a less stable form of OCP. This form absorbs the red light, and quenches the chlorophyll excited singlet states, preventing the chlorophylls from transferring the energy to reaction centers. This form can thermally revert to the stable blue-green light absorbing form. The ratio of these two forms of OCP depends on the intensity of the light and the temperature. Therefore, at intense light levels, photosynthesis is down regulated by cyanobacteria by NPQ by invoking structural changes in OCP. A self-regulating artificial photosynthetic reaction center pentad **6** has been reported which mimics the role of this process (Figure 7).[70]

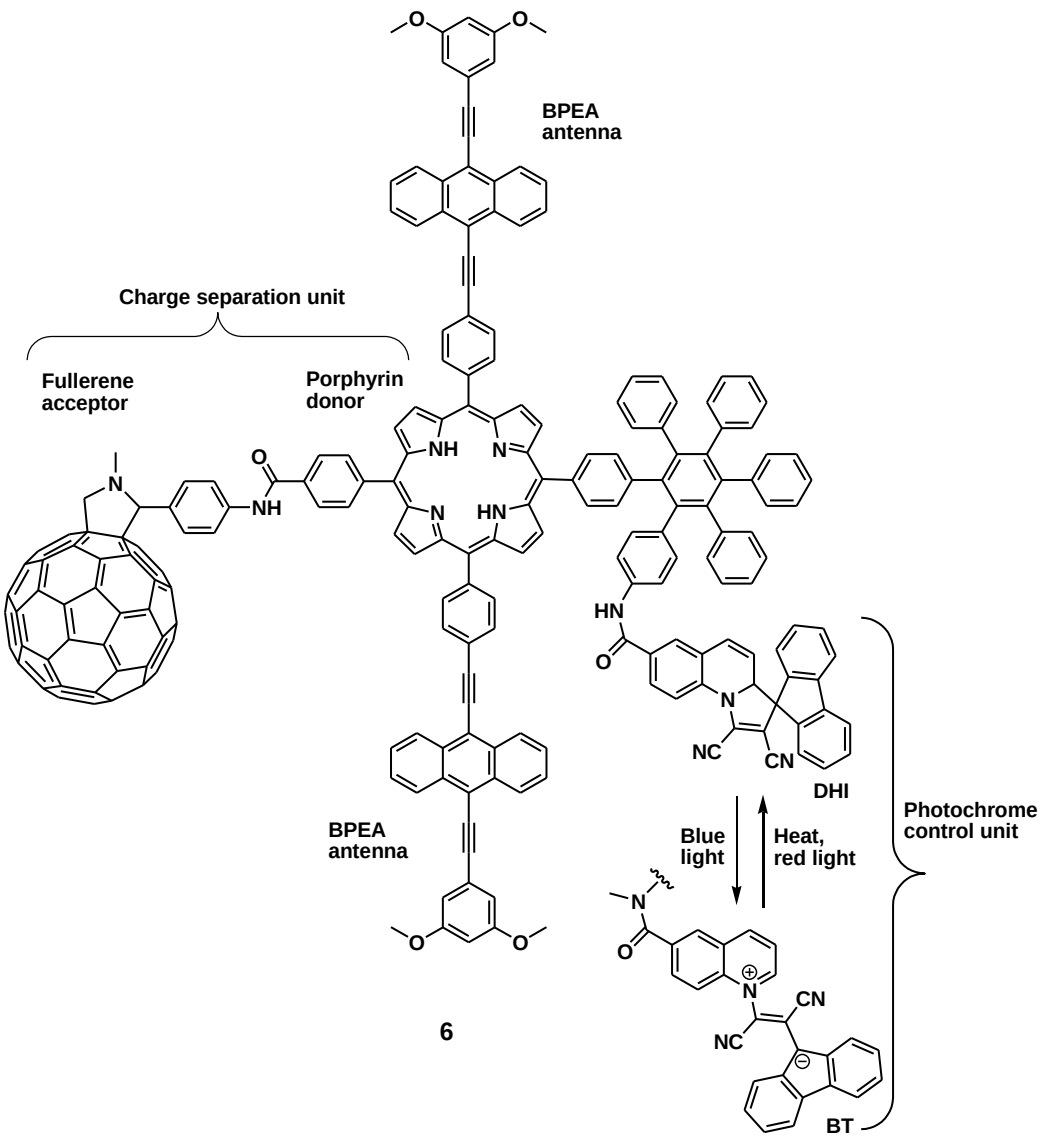

Figure 7. A self-regulating molecular model artificial photosynthetic reaction center pentad **6**. It features two BPEA antennas, a photochromic control unit, and a charge separation unit organized on a hexaphenylbenzene framework. It functionally mimics the role of OCP in NPQ in cyanobacteria.

Pentad **6** features two bis(phenylethynyl)anthracene (BPEA) antenna moieties, a free-base porphyrin (P), a quinoline-derived dihydroindolizine photochrome (DHI) organized on the central hexaphenylbenzene skeleton, and a fullerene electron acceptor (C_{60}) covalently linked to the porphyrin electron donor. The closed, spirocyclic form of DHI is thermodynamically more stable isomer than the open, betaine isomer (BT). DHI has no effect on the photochemistry of the rest of the pentad. BT is generated by photoisomerization initiated by the UV and blue light, and it can rapidly quench the excited states of the porphyrin and BPEA antennas by singlet-singlet energy transfer. When a solution of **6** in 2-methyltetrahydrofuran is irradiated with low intensity light, the BPEA antennas absorb in the 430-475 nm region and efficiently transfer excitation energy to the porphyrin (($\Phi = 1.0$, $\tau = 4.0$ ps) to generate the porphyrin first excited singlet state (^1P), which decays by photoinduced electron transfer to fullerene ($\Phi = 1.0$, $\tau = 2.4$ ns) to generate charge-separated state ($P^{\bullet+}$-$C_{60}^{\bullet-}$). Therefore, when the control unit is in its spirocyclic form, the pentad behaves like a normal photosynthetic reaction center. As the light intensity is increased, the fraction of BT form increases. BT quenches the first excited singlet state of the porphyrin to 33 ps, and the quantum yield of the $P^{\bullet+}$-$C_{60}^{\bullet-}$ state is also reduced to 1%. In the same experiment when the light intensity is decreased, DHI form start to increase, and at the initial level of light, the quantum yield returns to its initial value. Therefore, pentad **6** acts as a self-regulating molecular model nonlinear transducer that functionally mimics the role of the OCP in cyanobacteria.

NPQ in Green Plants and Algae

A different type of NPQ operates in green plants. In natural photosynthesis the process of photoinduced electron transfer produces and releases protons into the thylakoid lumen. This increase in proton concentration leads to a pH and charge gradient across the photosynthetic membrane. In the course of photosynthesis the sunlight energy stored as chemical potential and the pH gradient are continuously consumed by the subsequent dark reactions. When the production of protons outpaces the utilization of pH gradient in subsequent reactions, the lumen pH drops, which signals that the input of energy is more than what the reaction center can utilize. If the charge-separated states are not rapidly utilized in subsequent steps, harmful, high energy reactive intermediate byproducts are generated. Light absorption generates singlet excited state of chlorophyll ($^1Chl^*$) which deactivates by several pathways, and in the event of excess excitation, NPQ is triggered (Figure 8).[49]

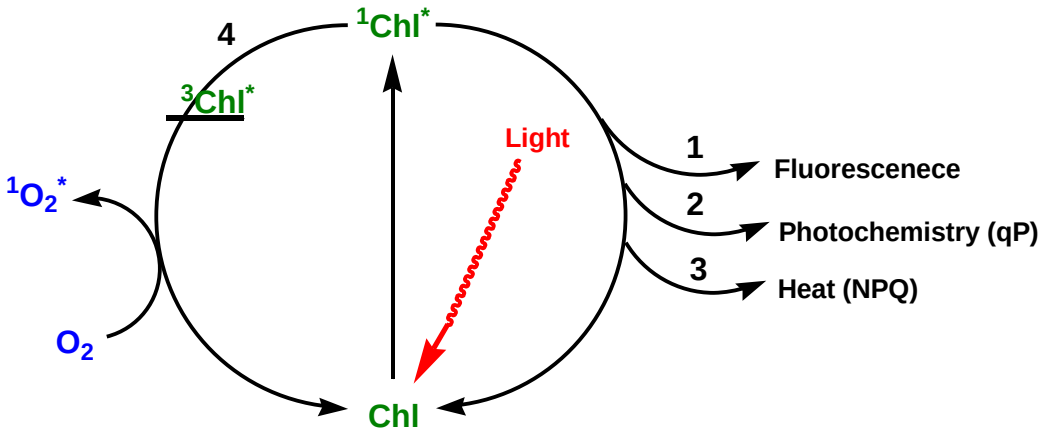

Figure 8. NPQ: green plants' response to excess light energy.[49]

$^1Chl^*$ can come to ground state by normal fluorescence **(1)**, it can initiate photochemistry which is usually associated with photosynthesis **(2)**, it can be deactivated by NPQ **(3)**, or it can relax to $^3Chl^*$ **(4).** The excitation energy from surplus photon absorptions can relax to generate $^3Chl^*$ which reacts with ground state oxygen to generate $^1O_2{}^*$ that causes photodamge to the organisms.[71] Pathway **(3)** which involves NPQ is induced in response to excess excitation of Chl.

Photodamge causes decrease in organisms' photosynthetic efficiency and the ability of carbon fixation. Photodamage is prevented by quenching of $^3Chl^*$ by neighboring carotenoids which have low lying triplet states which do not generate $^1O_2{}^*$. The overall fluorescence quantum yield of Chl is decreased by two processes, photochemical quenching (qP), which is associated with photochemical charge separation in reaction center of PSII, and non-photochemical quenching (NPQ), which is not directly related to charge separation. NPQ can be subdivided into three components, feedback de-excitation quenching (qE), photoinhibition

(qI), and state transitions (qT). Each of these three processes has characteristic induction and relaxation kinetics.[72] The major component of NPQ is the qE. In green plants and algae, qE can quench up to 80% of the ^{1}Chl*.[73-75] Although qE is directly correlated with photosynthetic photoprotection, it is only the manifestation of the excess energy dissipation as heat by green plants and algae.[76, 77] The kinetic observable that characterizes qE is the decrease in the fluorescence lifetime of ^{1}Chl* from about 2.0 ns to about 0.3 ns in the condition when the reaction center is completely closed and the primary electron acceptor, Q_A, is fully reduced.[78] qE is regulated by the pH gradient across the thylakoid membrane, which makes the quenching rapidly reversible.[49,79] As a response to excess light energy, low pH triggers the NPQ to dissipate the excess energy as heat before it reaches to the reaction center. The mechanism of NPQ is not fully understood, but it has been established that a protein, PsbS, which is a member of LHC superfamily, plays a major role in qE. A completely PsbS deficient PSII exhibited normal photochemistry but a pH-dependent quenching was absent, which established that PsbS is necessary for qE.[80, 81] PsbS is a protein subunit of PSII with a molecular mass of 22 kDa.[80-83] In the event of excess sunlight, low pH in thylakoid lumen leads to protonation of carboxylates of two glutamate residues in PsbS protein, and zeaxanthin (Zea) synthesis from violaxanthin (Vio) is induced. Binding of Zea to the protonated from of PsbS produces a PsbS qE state which rapidly quenches the ^{1}Chl* state (Figure 9).

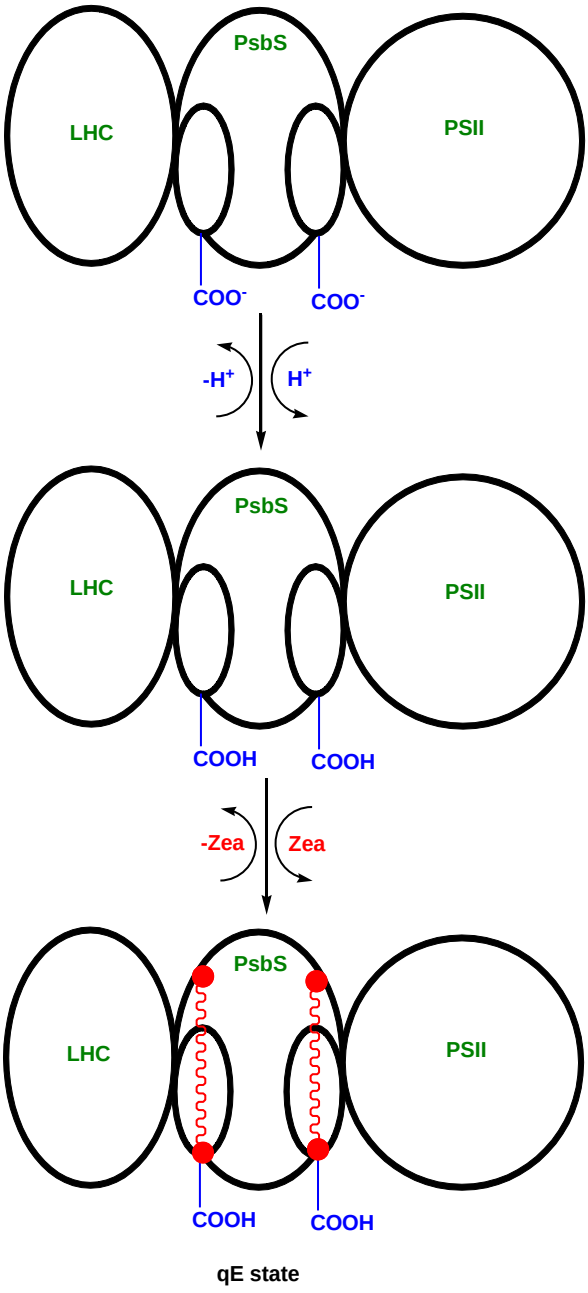

Figure 9. A model for qE in PSII of green plants. In excess sunlight, a low pH in thylakoid lumen leads to protonation of carboxylates of two glutamate residues in PsbS, and Zea synthesis from Vio is induced. Binding of Zea to PsbS results in the qE state in which de-excitation of $^{1}Chl^{*}$ occurs.[57]

NPQ may be triggered by a many factors but the major triggers are considered to be the change in pH of thylakoid membrane, and the activity of xanthophyll cycle. However, it is not clear if the NPQ components are due to the conformational changes in the pigment-protein complexes or due to the location of carotenoids in antenna systems. The conversion of violaxanthin to zeaxanthin via antheraxanthin is known as the xanthophyll cycle (Figure 10).[84]

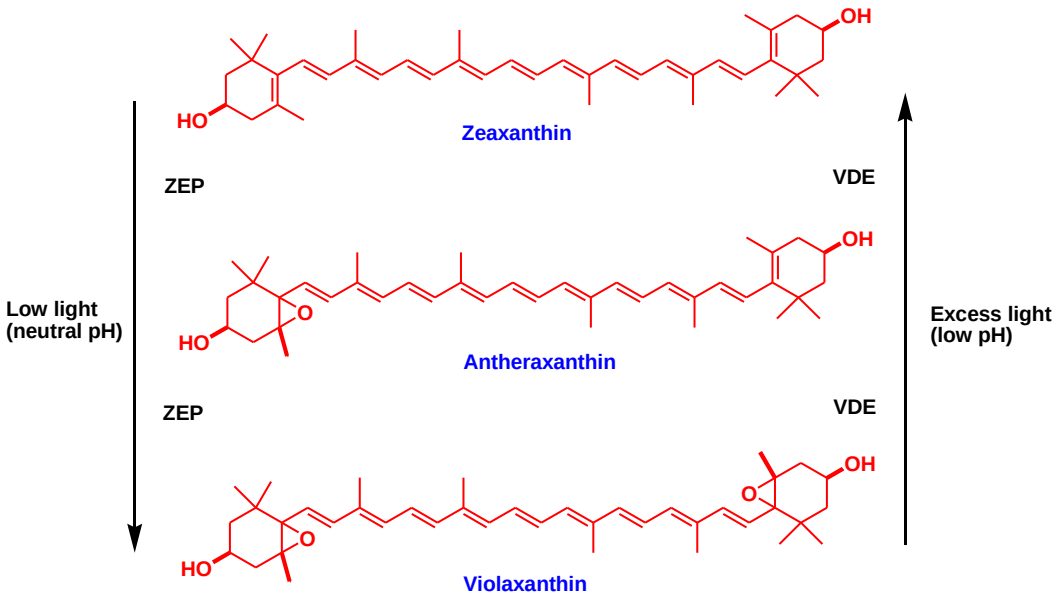

Figure 10. The xanthophyll cycle in photosynthesis.

In xanthophyll cycle in plants, de-epoxidation reaction is carried out by violaxanthin deepoxidase enzyme (VDE) with the help of ascorbic acid to reduce the epoxide ring. The epoxidation reaction is catalyzed by zeaxanthin epoxidase (ZEP). The activity of ZEP is optimum at pH 8; therefore, it is believed to be located on the stromal side of the thylakoid membrane. It is widely accepted that NPQ linearly correlates with the pH, and concentrations of antheraxanthin and zeaxanthin inside the lumen. Violaxanthin and antheraxanthin are not good

acceptors of energy. However, zeaxanthin strongly absorbs the energy thereby quenching the excited states of chlorophylls. The carotenoid polyenes quench chlorophyll excited states by energy and/or by electron transfer.[51, 57, 58, 69, 85-87] Recently, the formation of short-lived exciton states, in some natural and artificial antenna systems, is proposed to be playing a role in the mechanism of NPQ.[67, 88] Recently, A model dyad was synthesized which features a zinc porphyrin and a pH-sensitive dye organized on a hexaphenylbenzene core, which successfully exhibits the pH-dependent quenching in an artificial system (Figure 11).[3]

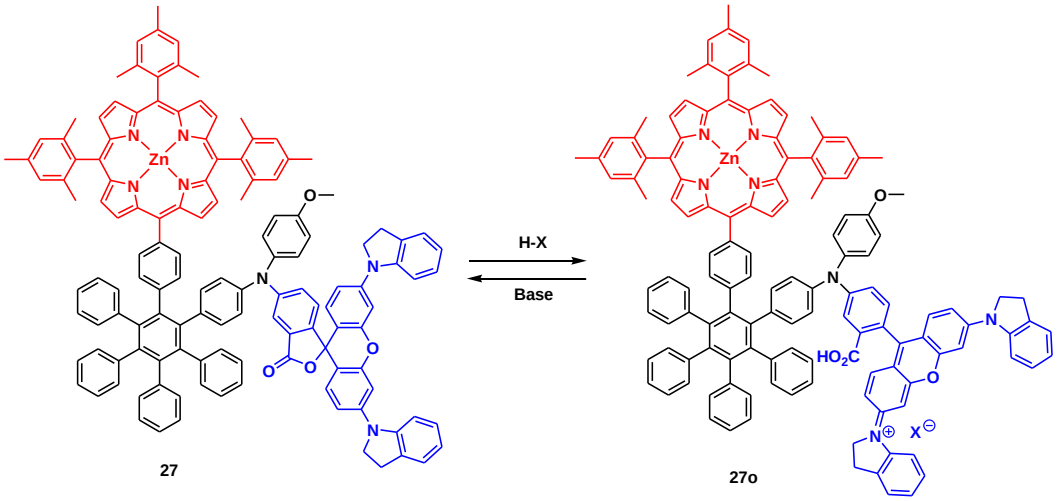

Figure 11. Structures of zinc porphyrin-dye model dyads when dye is in closed form **27**, and open form **27o**. Photoexcitation of a neutral solution of dyad **27** displays the normal photophysical decay behavior of the zinc porphyrin chromophore, however, in acidic medium, the pH-sensitive dye opens to generate **(27o)** and quenches the excited singlet states of the porphyrin to 23 ps.

The antennas play a major role in NPQ by altering their structures from nonabsorbent to strong quencher. Hexad **34** was synthesized (see synthesis) and studied to mimic the function of antennas in NPQ, and get insight into the mechanism of NPQ (Figure 12).[3] The molecular hexad features five zinc porphyrin antennas, and a pH-sensitive dye moiety organized on a hexaphenylbenzene framework. In a neutral solution, the dye stays in its closed spirocyclic, colorless form, and does not absorb light. When the pH of the solution is lowered by adding an acid, the dye converts to its open, colored form which strongly absorbs in the emission region of zinc porphyrins, hence making the quenching of the porphyrin excited states by the dye thermodynamically possible.

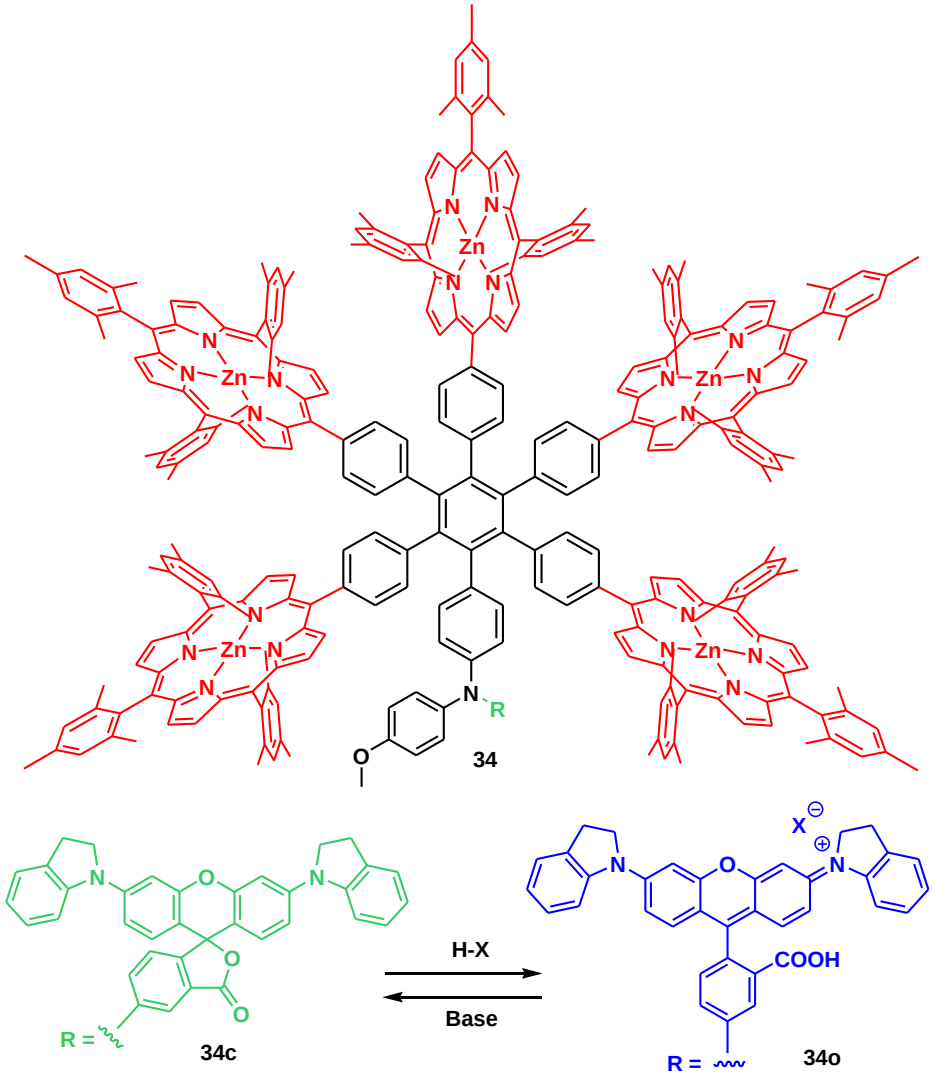

Figure 12. An acid-regulated artificial photosynthetic antenna model hexad **34**. Photoexcitation of a neutral solution of hexad **(34c)** displays the normal photophysical decay behavior of the five zinc porphyrin antennas, however, when an acid H-X is added, the dye opens **(34o)** and quenches the excited singlet states of all five porphyrins to <40 ps, and functionally mimics the role of antenna in NPQ in green plants.

Photoexcitation of a neutral solution of **34** generates the first exited singlet states of the porphyrins, and the porphyrins rapidly exchange excitation energy and decay by normal photophysical processes (τ = 2.1 ns). The closed form of the dye does not have any effect on the porphyrin antenna system. In this case the lifetimes of zinc porphyrin excited states are long enough for photoinduced electron transfer or other photochemistry. However, when acid is added to the same solution, the dye converts to its open form, which rapidly quenches the porphyrin excited states of all five porphyrins, converting the excitation energy to heat. In this case the porphyrins are rendered kinetically incompetent to perform any useful photochemistry. In the same experiment, when a base is added to the acidic solution of the hexad, the dye closes and the dyad reverts to its original 34c form and regains the normal photophysical processes observed at the beginning of the experiment. Therefore the antenna acts as a pH-dependent reversible switch. Therefore, the molecular hexad mimics the role of antennas in green plants NPQ.

Chapter 2

DESIGN OF MOLECULAR MODELS FOR PHOTOSYNTHETIC PHOTOPROTECTION

Goals of the Project

Most of the sunlight powering photosynthesis is absorbed by antenna arrays which transfer as well as regulate the excitation energy reaching the reaction centers. Under normal light conditions the photosynthesis operates at its maximum performance, but at higher light levels the excitation energy received by reaction centers is more than what can be utilized in later steps of photosynthesis. This excess excitation energy produces highly reactive redox species which can harm the photosynthetic apparatus. Nature has developed various mechanisms to dissipate this excess energy and repair the injured photosynthetic components. One of the mechanisms utilized by photosynthetic apparatus to dissipate the excess energy is known as non-photochemical quenching (NPQ). Although the complete mechanism of NPQ is still elusive, it is believed to be started by a signal by a drop in the pH of thylakoid lumen. Low pH in the lumen triggers complex biological processes which alter the structures of nonabsorbent carotenoid polyenes making them strongly absorbent in the emission regions of the antennas thereby dissipating excess excitation energy as heat.

In this research, self-regulating molecular model systems were designed and synthesized which upon acidification of the medium initiate quenching of a bio-inspired light-harvesting antenna mimicking NPQ. In addition to functionally

mimicking a photosynthetic photoprotection process, this research provides an excellent example of adaptive phenomena that can emerge when simple systems are combined. This kind of self-regulating molecular behavior will be needed in not only protecting the artificial photosynthetic components of solar energy conversion devices but also in realizing the modern nanotechnology. The initial goal was to prepare a model system containing one porphyrin chromophore coupled to a pH-sensitive dye molecule. As discussed in the introduction, porphyrins and metalloporphyrins are good mimics of chlorophyll chromophores found in natural photosynthesis.

Hexaphenylbenzene as a Structural Framework

For effective and efficient transfer of energy, the coupling between the porphyrin chromophores and the pH-sensitive dye should be suitable. The chromophores and the dye need to be at optimum distance and spatial orientation. A suitable structural framework is vital, even when this framework does not affect the photophysics or thermodynamics of individual chromophores. Hexaphenylbenzene has been proven to be a very good structural framework due to its special properties which include:

i. The hexaphenylbenzene core can be readily synthesized with various substitution patterns.
ii. The core has additional phenyl rings for attachment of additional chromophores which provides efficient synthetic routes for large array systems.

iii. Hexaphenylbenzene framework is relatively rigid with a high rotational barrier of the peripheral aryl rings about their axes to the central benzene. This to an extent controls the interchromophoric distances and spatial orientation for efficient energy transfer. The structural rigidity of the hexaphenylbenzene framework is also helpful in correlation of energy transfer and electron transfer theories.

iv. In hexaphenylbenzene core the peripheral benzene rings are almost orthogonal to the central benzene ring which promotes the Förster singlet-singlet energy transfer over electron transfer which requires interchromophoric orbital overlap.

v. Many artificial photosynthetic antenna reaction centers based on hexaphenylbenzene structural framework have been synthesized and studied which provide the basic understanding of this type of systems for further research.

A relatively easy synthesis of hexaphenylbenzene core provides a large variety of structural motifs with minimum steps of isomer separations. A general scheme of preparation of hexaphenylbenzene core is illustrated in Figure 13.

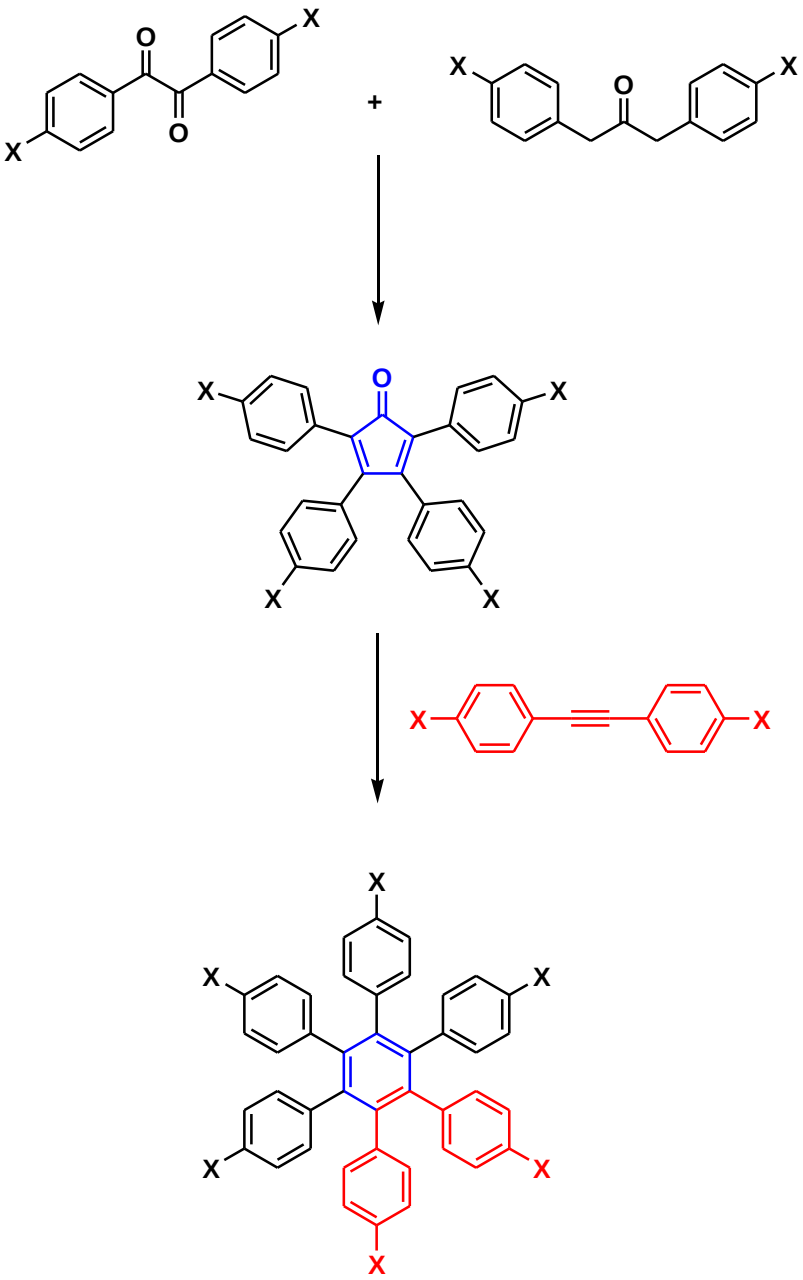

Figure 13. Synthetic scheme of hexaphenylbenzene core based derivatives where X is an atom or a group which can be same or different depending on the synthesis requirement.

pH-Sensitive Dyes

Most pH-sensitive indicator dyes are colorless at low pH and become colored at high pH, but the reverse is needed for this work. The desired properties of the dye are very difficult to achieve. The pH-sensitive dye has the following requirements:

i. The dye should be sufficiently polar in nature to function in polar as well as aqueous environments.

ii. The dye should stay in closed, colorless form at neutral and higher pH.

iii. The dye should open and convert into a colored form by protonation at lower pH.

iv. The dye should open with a suitable pKa value that allows protonation without affecting the porphyrin or metalloporphyrin.

v. The dye should not absorb in its closed form, and should not interfere with the photophysics of the porphyrin chromophore.

vi. The dye should strongly absorb in its acid-stable, open form.

vii. The absorption of open form of the dye should overlap porphyrin emission, thus making energy transfer from the porphyrin to the dye thermodynamically possible.

viii. The dye should be coupled to the porphyrin in a geometry suitable for Förster singlet-singlet energy transfer quenching of the porphyrin by the low-pH form of the dye.

ix. The dye should not fluoresce, if it does fluoresce, its emission should not overlap with the absorption of the porphyrin chromophore, thus preventing the reverse excitation.

Model of a Porphyrin-Dye Dyad

In dichloromethane, free-base porphyrins absorb at about 520 nm, and emit at about 650-700 nm. In similar conditions, zinc porphyrins absorb at about 560 nm, and emit at about 600-650 nm. Therefore, the dye should absorb in 600-650 nm region for coupling with a zinc porphyrin chromophore. A model porphyrin-dye dyad arranged on a hexaphenylbenzene core is illustrated in Figure 14.

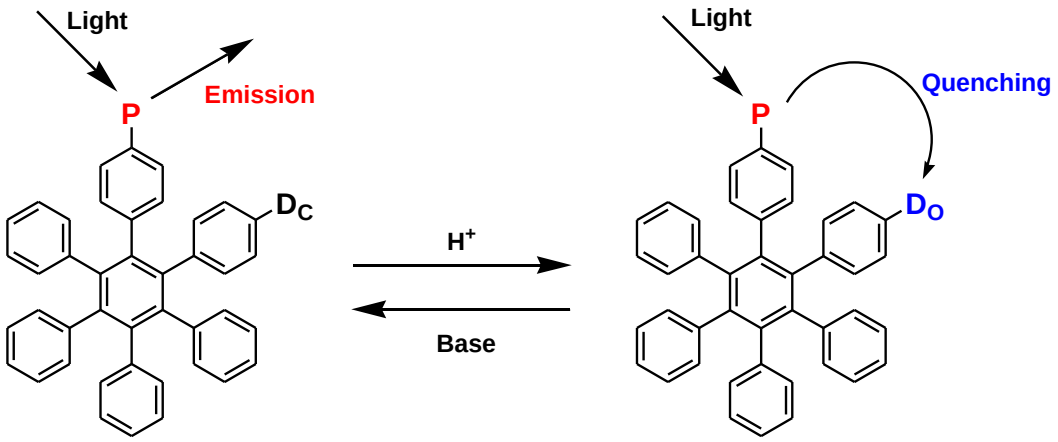

Figure 14. Structures of a model porphyrin-dye dyad in basic and acidic solutions. In basic solution, the dye stays in a nonabsorbent, closed form (D_C) and does not quench porphyrin emission, while in acidic condition; the dye is converted into an open, absorbent form (D_O) which quenches the porphyrin emission.

In the dyad the porphyrin and the dye molecules are covalently attached on para positions of two ortho rings of hexaphenylbenzene. In the proposed dyad, in neutral solution, the dye stays in its closed form (D_C) and does not absorb light, in acidic condition, the dye is converted to its open form (D_O) which absorbs light. When a neutral solution of the dyad is irradiated with light, first excited singlet state of the porphyrin is generated, which comes to ground state by emission of energy by normal photophysical processes. When acid is added to the solution and the solution is irradiated with light, the porphyrin excited state is quenched by energy transfer to the open form of the dye. Addition of a base neutralizes the solution and closes the dye moiety. The closed form of the dye does not quench porphyrin emission, and the porphyrin emission increases to its initial value observed at the beginning of the same experiment.

Tin Porphyrin-CVL Dye Dyad

On the basis of the above principles, a tin porphyrin-dye dyad **7** was synthesized and studied (Yuichi Terazono, unpublished results). The dyad features a tin porphyrin, and a crystal violet lactone (CVL) type dye (Figure 15).

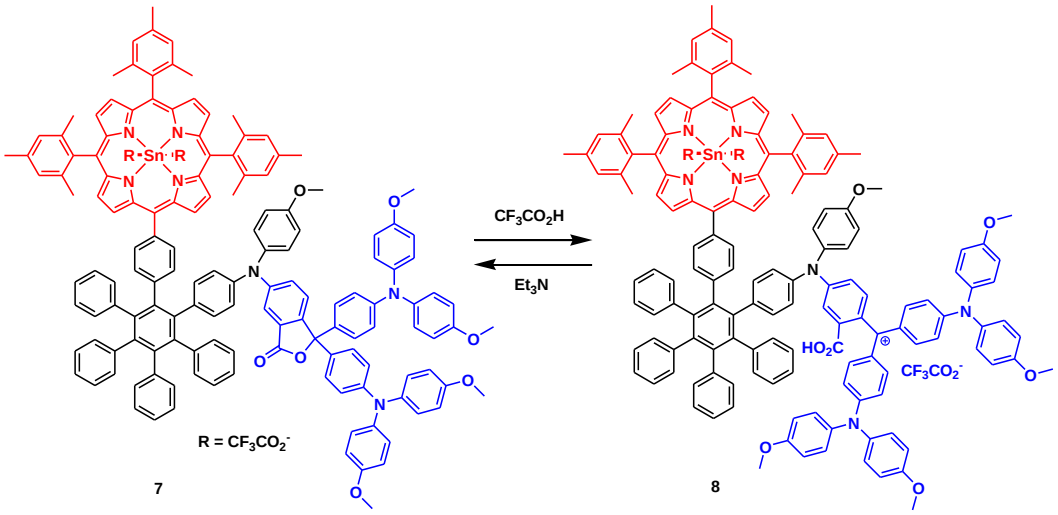

Figure 15. Structures of a tin porphyrin- CVL dye dyad in basic solution **7** and acidic solution **8**. In neutral solution, the dye stays in a nonabsorbent, closed form, and does not affect photophysics of the dyad, while in acidic condition; the dye is converted into an open, absorbent form which quenches the porphyrin emission. Addition of a base such as triethylamine closes the dye and converts the dyad into its neutral closed form.

Absorption and emission behavior of the dyad in its closed and open form are illustrated in Figure 16.

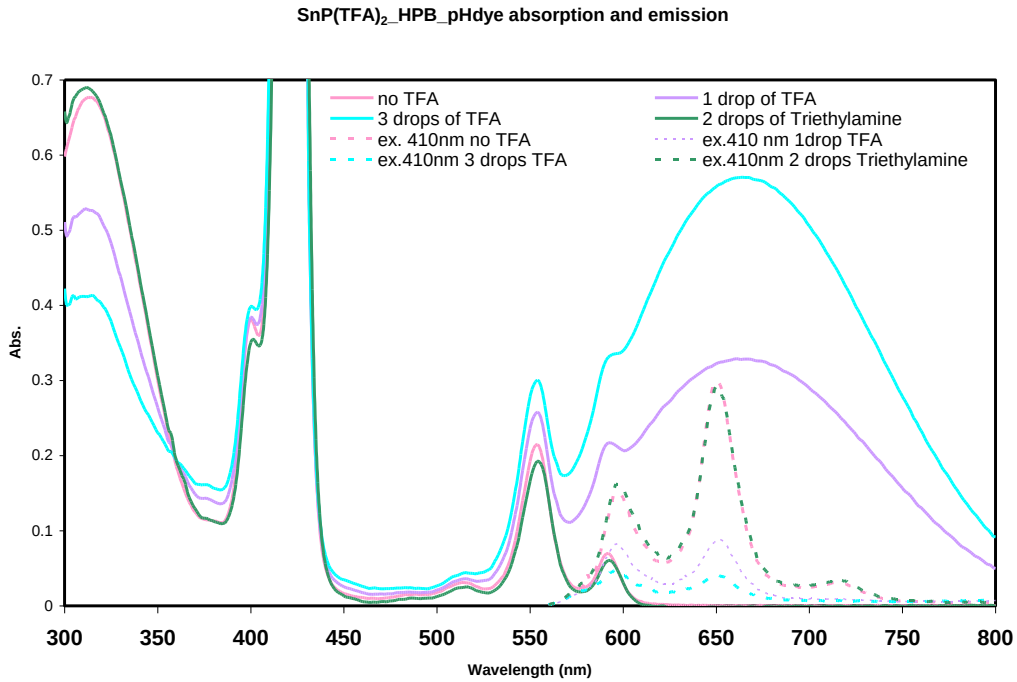

Figure 16. Absorption and emission spectra of a model tin porphyrin-CVL dye dyad organized on hexaphenylbenzene [SnP(TFA)$_2$_HPB_pHdye] in closed and open forms. A neutral solution of the dyad in dichloromethane exhibits normal absorption and emission of the porphyrin as seen in similar tin porphyrins. Addition of trifluoroacetic acid (TFA) opens the dye and quenches the porphyrin emission. Addition of a base triethylamine closes the dye, and the porphyrin emission increases to its initial value of the same experiment.

The closed form of the dye has no effect on the photophysics of the dyad, in neutral solution the tin porphyrin exhibits usual photophysics observed in similar tin porphyrins. When a drop of TFA is added to the dyad solution, the dye opens and its absorption band increases, at three drops of TFA, the dye absorption almost reaches the maximum. Open form of the dyad formed due to addition of

TFA quenches the porphyrin emission, and porphyrin emission band significantly decreases due to quenching by the open dye. Addition of two drops of triethylamine closes the dye and the porphyrin emission increases to its initial value of the experiment. Thus the dyad successfully demonstrates the basic premise of the project. However, there are some inherent problems associated with this dyad:

i. The CVL dye in **7** does not switch cleanly between colored and colorless forms in the presence of protic or other polar solvents.

ii. The CVL dye in **7** requires relatively acidic conditions to fully convert to the colored form. This low pH requirement limits the metals used in porphyrin, because many metals such as zinc and magnesium in porphyrins are acid labile.

iii. For the ease of synthesis and thermodynamic reasons the use of a zinc porphyrin is desired in the dyad, as well as in a model triad where the competition between the energy transfer and electron transfer will be studied.

Xanthene-based Dyes

Due to these limitations new dyes were sought and researched that would be protonated at higher pH, and allow the use of zinc rather than tin porphyrin. Xanthene-based dyes seemed to be promising candidates (Figure 17).

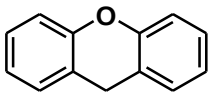

Xanthene

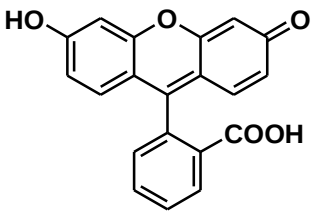

Fluorescein

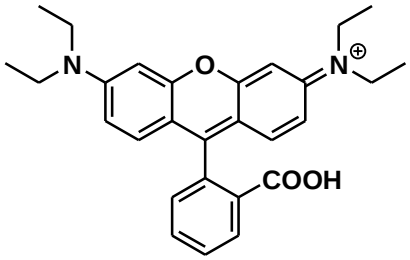

Rhodamine B

Figure 17. Xanthene-based dyes: Fluorescein and Rhodamine B. In dichloromethane, the absorption maxima of Fluorescein and Rhodamine B in their acid-stable forms are found at 494 nm and 542 nm, respectively.

Xanthene-based dyes are quite polar in nature, and they can stay in neutral (closed, colorless), and acid-stable (open, colored) forms. Fluorescein and Rhodamine B are well-known dyes of this class that function well in aqueous environments. However, in dichloromethane, their absorption maxima in their acid-stable forms are found at 494 nm and 542 nm, respectively. These wavelengths are too short to provide substantial overlap with porphyrin emission spectra, and thus these dyes would not quench a porphyrin first excited singlet state by singlet energy transfer. Therefore, other rhodamine-based dyes were synthesized (Figure 18) and their absorptions were determined in dichloromethane and ethanol.

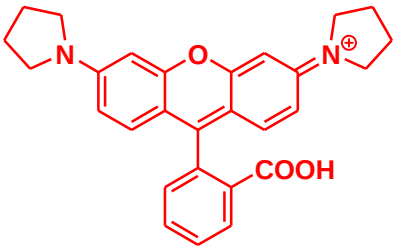

10

3',6'-Pyrrolidinorhodamine (red)

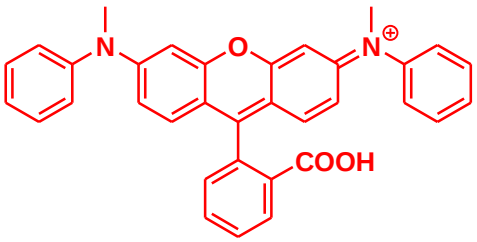

12

3',6'-N-Methylanilinorhodamine (red)

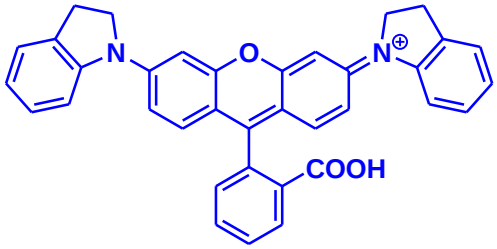

14

3',6'-Indolinorhodamine (blue)

Figure 18. Structures of rhodamine-based dyes: 3',6'-pyrrolidinorhodamine **10**, 3',6'-N-methylanilinorhodamine **12**, and 3',6'-indolinorhodamine **14**. In dichloromethane, the absorption maxima of these dyes in their acid-stable forms are found at 550 nm, 552 nm, and 640 nm, respectively.

Initial attempts to design a suitable dye turned out to be fruitless. In dichloromethane, the absorption maxima of acid-stable forms of 3',6'-pyrrolidinorhodamine and 3',6'-N-methylanilinorhodamine were observed at 550 nm and 552 nm, respectively. These wavelengths are too short for significant overlap with a zinc porphyrin emission spectrum. The lower wavelengths resulted due to limited delocalization of the positive charge. Therefore, another dye molecule exhibiting a greater degree of delocalization of positive charge was

envisioned. In the light of these dyes and their wavelengths, a new pH-indicator dye 3',6'-indolinorhodamine **14** was designed and synthesized which features a greater degree of delocalization of the positive charge in the acid-stable form, and thus absorbs at longer wavelengths. In dichloromethane, this dye has an absorption maximum at 640 nm, which is ideal for accepting energy from zinc porphyrin chromophores. This dye also functions in alcohols and other protic or polar solvents. It can be protonated using only acetic acid, instead of the much stronger trifluoroacetic acid. Thus, a dye of this general class seems to be ideal for our proposed experiments. Model dye **14** lacks functionality for attachment of other chromophores. Therefore, model dyes **18** and **19** (Figure 19) were synthesized (synthetic details in Chapter 3).

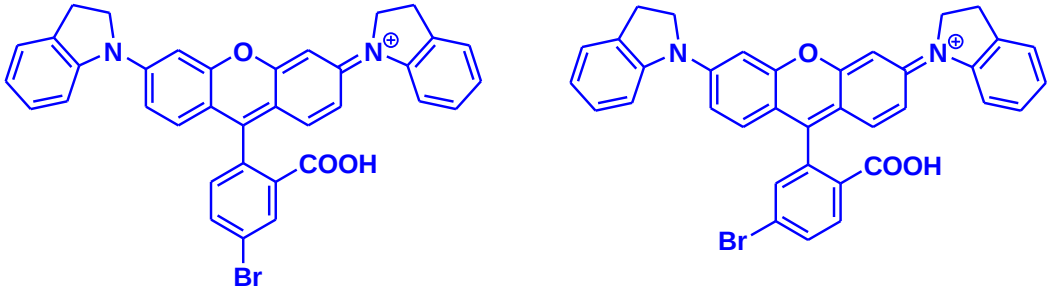

18

3',6'-Indolino-5-bromorhodamine

19

3',6'-Indolino-6-bromorhodamine

Figure 19. Structures of functionalized rhodamine-based dyes: 3',6'-indolino-5-bromorhodamine **18** and 3',6'-indolino-6-bromorhodamine **19**.

Zinc Porphyrin-Rhodamine Dye Dyads and Hexad

Based on the model dyes **18** and **19**, two model porphyrin-dye dyads **27** and **28** were synthesized (Figure 20).

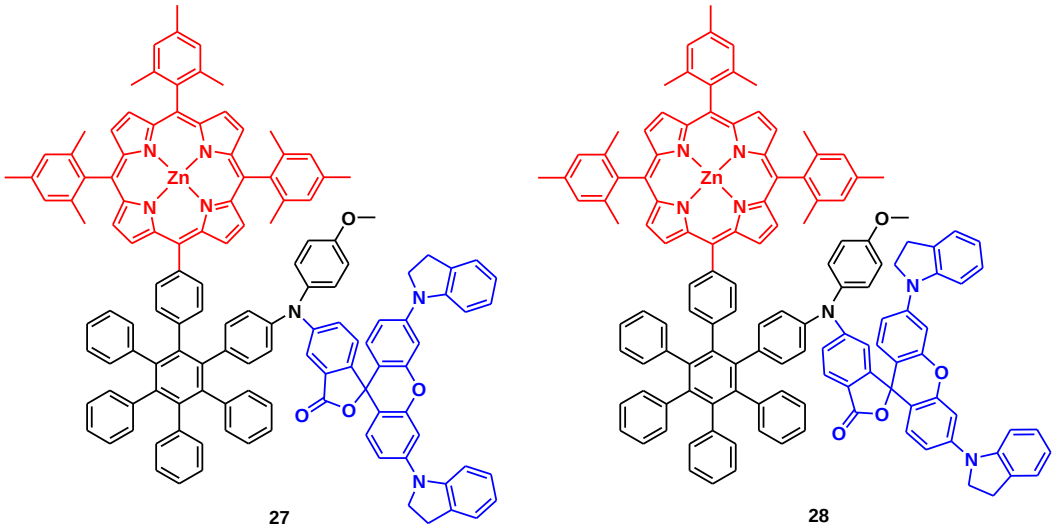

Figure 20. Structures of the porphyrin-dye dyads: para-dyad **27** and meta-dyad **28,** where the indolinorhodamine dyes are in their closed forms.

In order to mimic the function of the antenna in photosynthetic photoprotection, a model hexad **34** was synthesized, which features an indolinorhodamine dye and five zinc porphyrins organized on a hexaphenylbenzene framework (Figure 21). The hexad demonstrates rapid interchromophoric singlet energy transfer, and pH guided quenching of the zinc porphyrin chromophores.

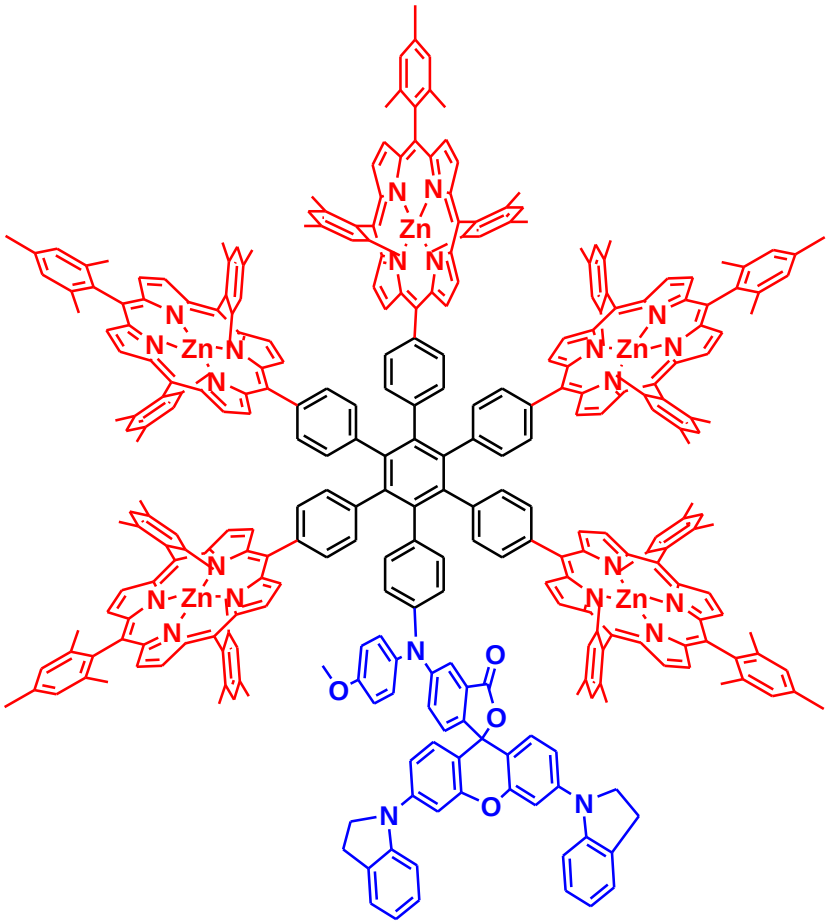

34

Figure 21. Structure of the hexad **34** where the indolinorhodamine dye is shown in its closed form.

Chapter 3

SYNTHESIS OF THE COMPOUNDS

Synthesis of Model Dyes

Steady state absorption and emission spectra of the tin porphyrin-CVL dye dyad revealed that the CVL based dyes had some inherent limitations and would not be suitable for this research. Therefore, new dyes were sought. Xanthenes-based dyes seemed to be promising due to their desirable properties. Several xanthene-based rhodamine-type dyes were synthesized according to a procedure employed by Woodroofe *et al.*[89] Absorption spectra of the dyes were recorded. A rhodamine-based model dye 3',6'-pyrrolidinorhodamine was synthesized and its absorption spectrum was obtained in dichloromethane (Scheme 1). 3-Bromophenol was stirred with phthalic anhydride in methanesulfonic acid solvent at 140 ^{0}C for 16 h to obtain an intermediate compound 3',6'-dibromofluoran **9** (49% yield). 3',6'-Dibromofluoran was stirred with pyrrolidine in presence of anhydrous zinc chloride catalyst at 170 ^{0}C for 4 h, acidic workup of reaction mixture with dilute hydrochloric acid afforded 3',6'-pyrrolidinorhodamine **10** (95% yield) in its acid-stable form. Treatment of acidic solution of **10** afforded 3',6'-pyrrolidinofluoran **11**, which is a neutral form of **10**. A solution of compound **10** in dichloromethane is red in color.

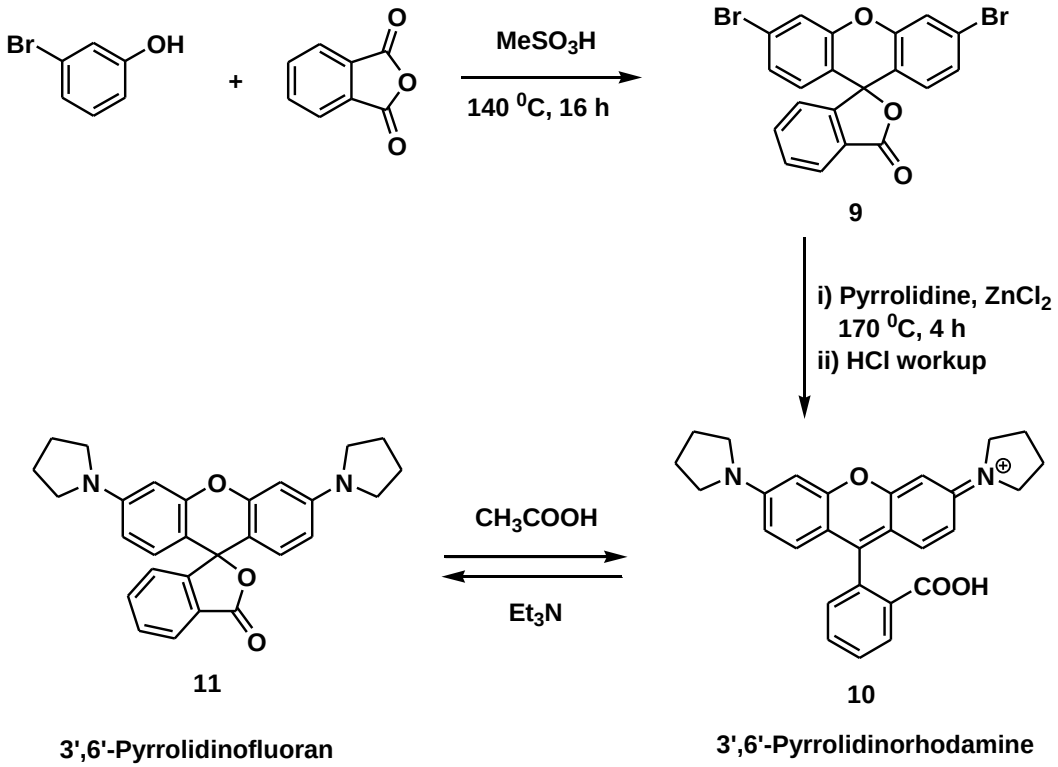

Scheme 1. Synthesis of a rhodamine-based dye 3',6'-pyrrolidinorhodamine **10**.

In dichloromethane, compound **10** has an absorption maximum at 550 nm, which is too short for a significant overlap with a zinc porphyrin emission spectrum. Therefore, 3',6'-N-methylanilinorhodamine **12** was synthesized using similar methods and reaction conditions (Scheme 2). Compound **12** was expected to have a greater delocalization of positive charge of its acid-stable form and therefore absorb at longer wavelengths. The precursor compound **9** was reacted with N-methylaniline under similar reaction conditions that of compound **10** to obtain compound **12** (90% yield). A solution of compound **10** in dichloromethane is red in color.

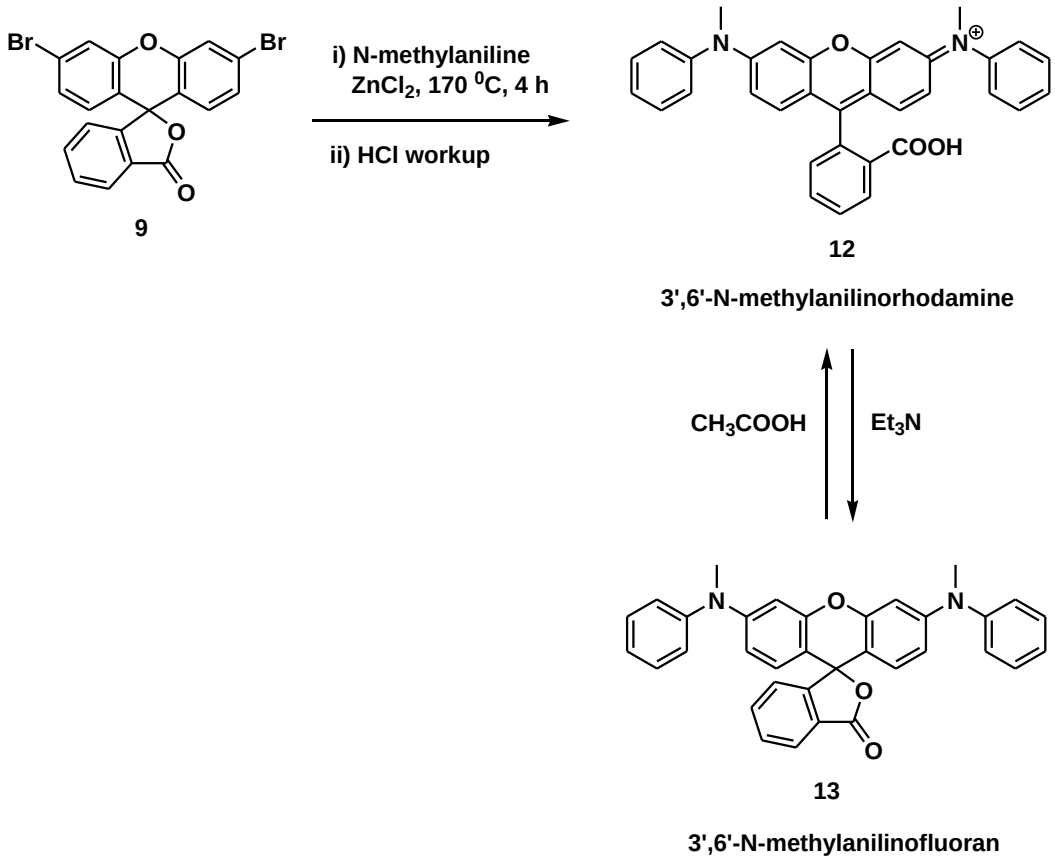

Scheme 2. Synthesis of a rhodamine-based dye 3',6'-N-methylanilinorhodamine **12**.

A treatment of acid solution of **12** with a base such as triethylamine gives the closed form of **12**, 3',6'-N-methylanilinofluoran **13**. An absorption spectrum of **12** in dichloromethane exhibited absorption maximum at 552 nm, which is still too short for desired wavelength. Perhaps a relatively free rotation of the phenyl ring attached to amine nitrogen prevents the greater degree of delocalization of the positive charge generated in the acid-stable form of the dye **12**. Therefore, another rhodamine-based dye 3',6'-indolinorhodamine **14** was designed and synthesized which would feature greater degree of delocalization of positive

charge due to restricted motion of benzene ring in respect to the nitrogen atom. Compound **14** was synthesized using halide coupling of **9** with indoline (Scheme 3).

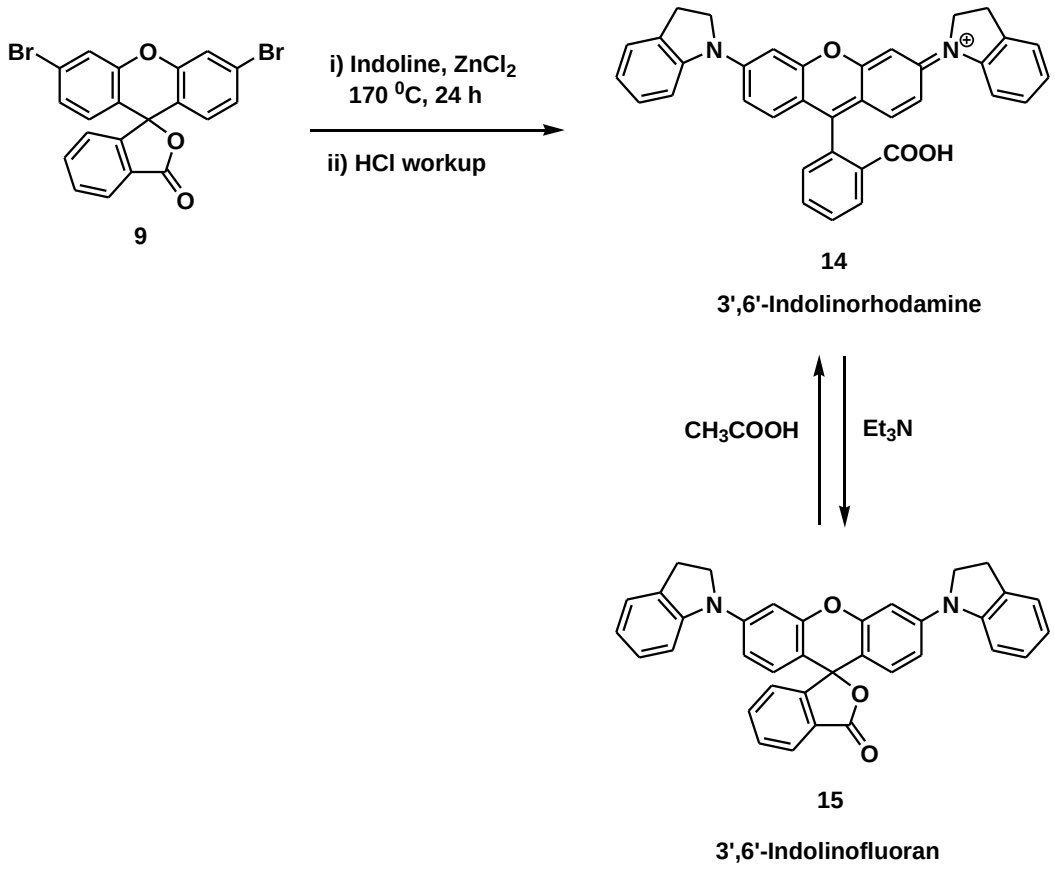

9

14

3',6'-Indolinorhodamine

15

3',6'-Indolinofluoran

Scheme 3. Synthesis of a rhodamine-based dye 3',6'-indolinorhodamine **13**.

Acidic workup of the reaction mixture afforded **14** (90% yield). Compound **14** is dark blue in color. Addition of triethylamine to the solution of **14** gives compound **15** which is the closed, colorless form of **14**. Absorption maximum of a solution of **14** in dichloromethane is found at 640 nm, which is ideal for the absorption of a zinc porphyrin emission.

Synthesis of Functionalized Dyes

Model dye compound **14** lacks functionality for attachment of porphyrin chromophores. Therefore, functionalized indolinorhodamine-based dyes 3',6'-indolino-5-bromorhodamine **18** and 3',6'-indolino-6-bromorhodamine **19** were synthesized (Scheme 4). Condensation of 3-iodophenol and 4-bromophthalic anhydride gave two isomers of substituted fluoran **16** (21% yield) and **17** (23% yield). Alkylation of **16** and **17** with indoline, and subsequent acidic workup gave model dyes **18** (92% yield) and **19** (92% yield). Addition of a base such as triethylamine to the solutions of **18** and **19** gives their closed, colorless forms **20** and **21** (Scheme 5).

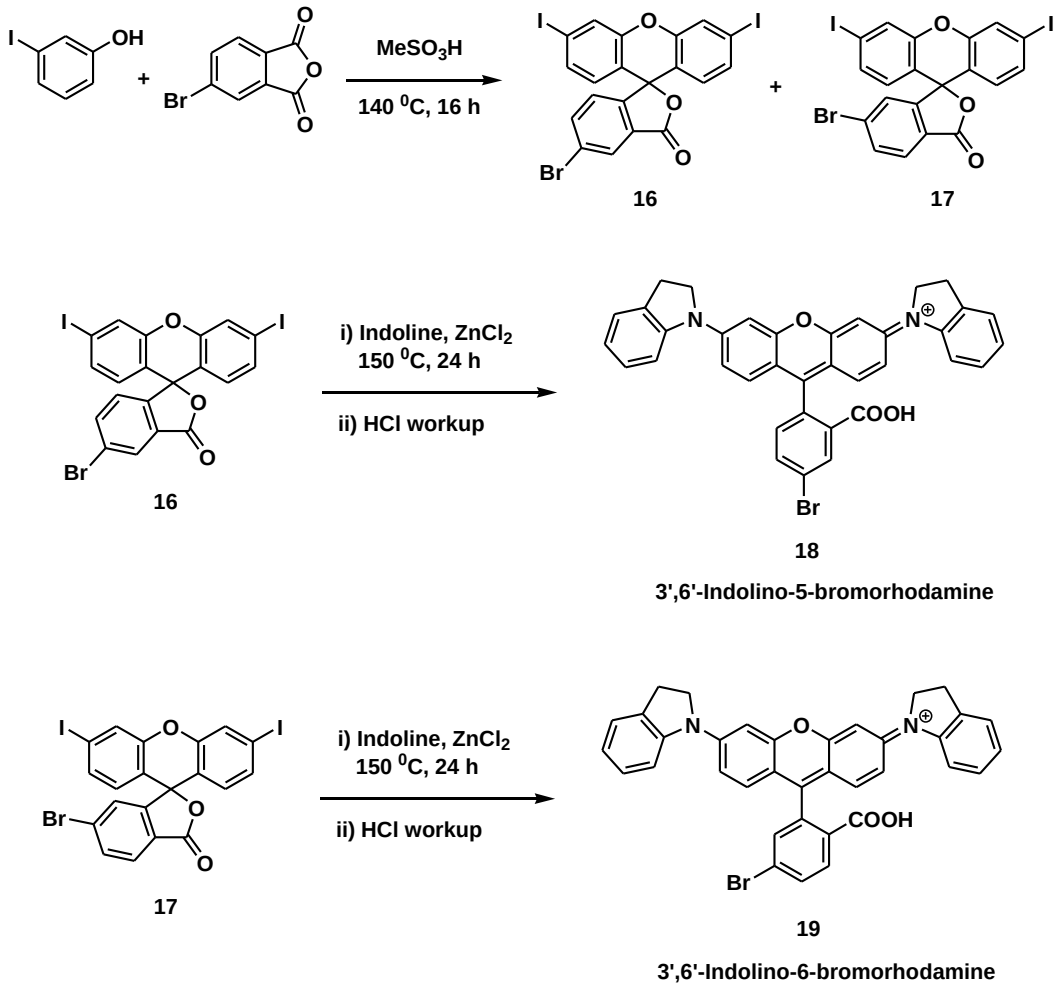

Scheme 4. Synthesis of functionalized dyes 3’,6’-indolino-5-bromorhodamine **18** and 3’,6’-indolino-6-bromorhodamine **19**.

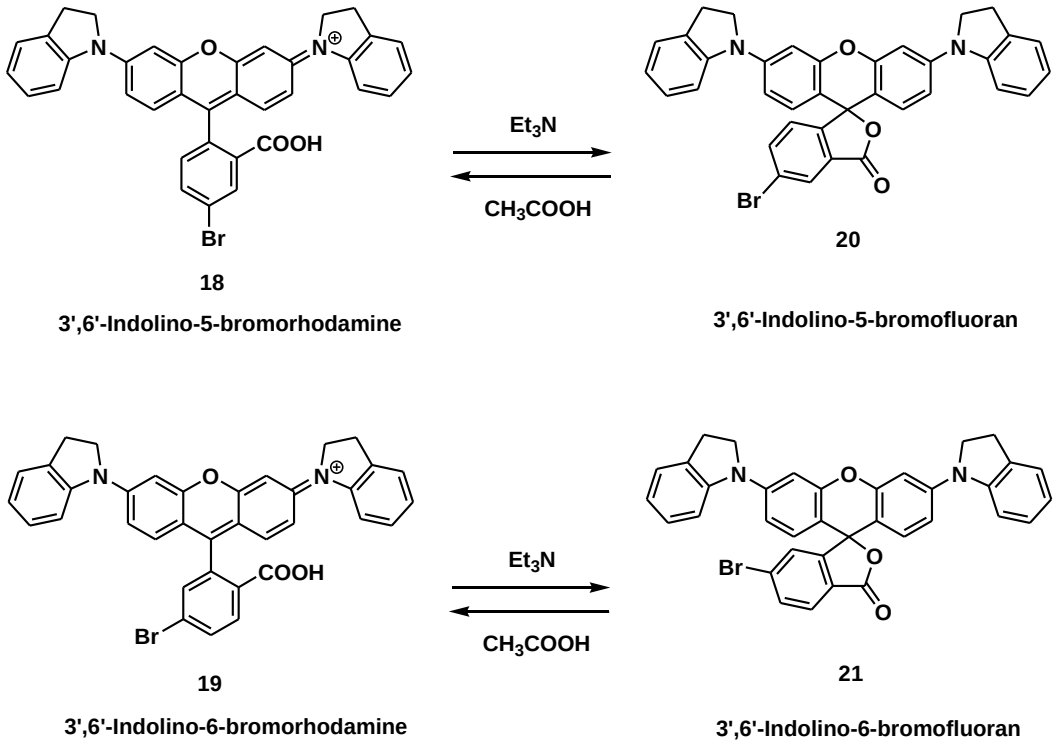

Scheme 5. Conversion of functionalized dyes 3',6'-indolino-5-bromorhodamine **18** and 3',6'-indolino-6-bromorhodamine **19** into their closed forms 3',6'-indolino-5-bromofluoran **20** and 3',6'-indolino-6-bromofluoran **21**.

Synthesis of a Porphyrin Chromophore

Compound **22**, 4-(4-bromophenylethynyl)benzaldehyde, a precursor to a free-base porphyrin **24** was synthesized by Sonogashira coupling of 4-bromo-1-ethynylbenzene with 4-iodobenzaldehyde (Scheme 6). The reaction mixture was chromatographed on silica gel (flash column, DCM/hexanes 3/2 to 2/1) to get 66% yield of the desired product. Porphyrin **24** was synthesized by acid catalyzed condensation of **22**, mesityldipyrromethane **23** and mesitaldehyde. After purification 18% yield of **24** was obtained.

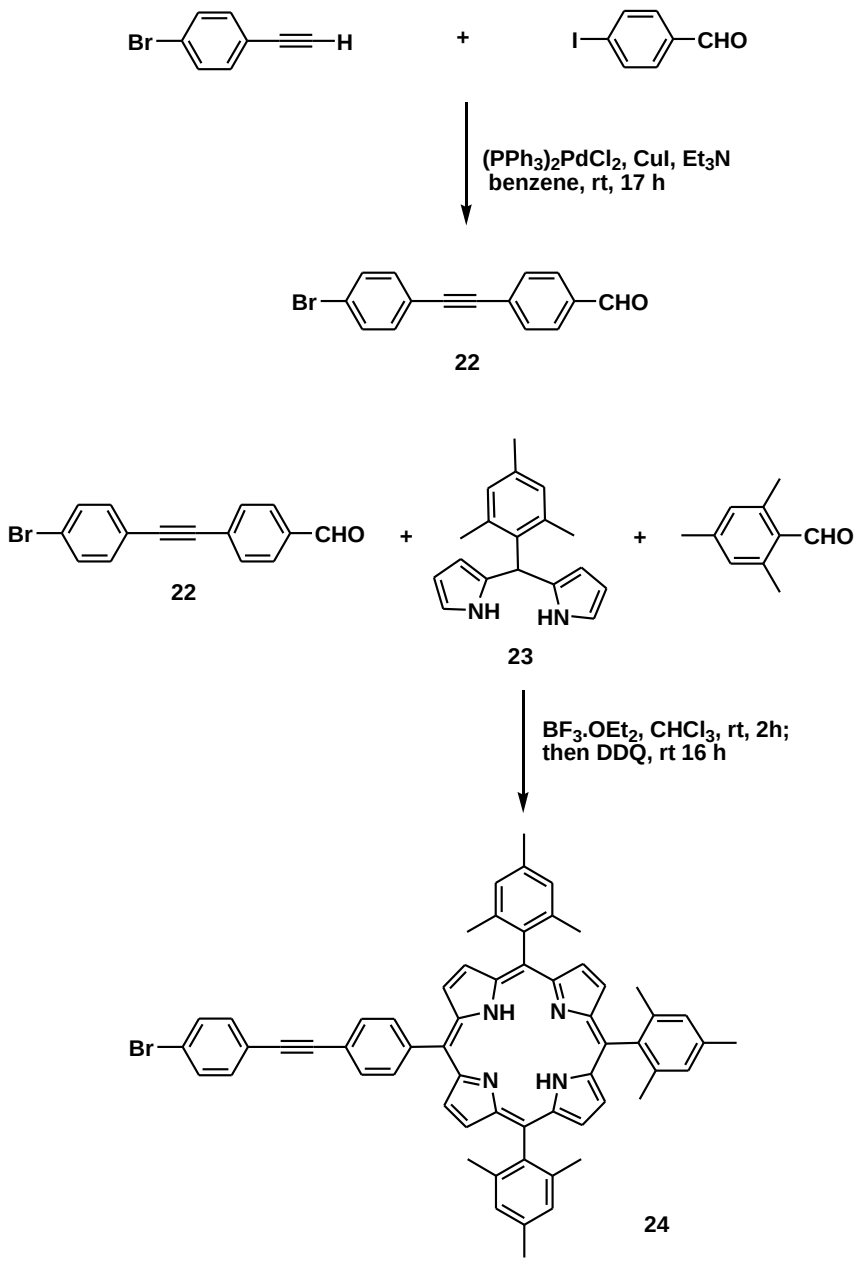

Scheme 6. Synthesis of a porphyrin precursor **22** and a free-base porphyrin **24**.

Synthesis of Hexaphenylbenzene Core

Compound **24** and cyclopentadienone were refluxed in presence of diphenyl ether for 4 h (Scheme 7). Purification of the reaction mixture with flash column chromatography afforded the hexaphenylbenzene core bearing a free-base porphyrin. Regular metallation of free-base porphyrin with zinc acetate gave the hexaphenylbenzene core bearing a zinc porphyrin **25**.

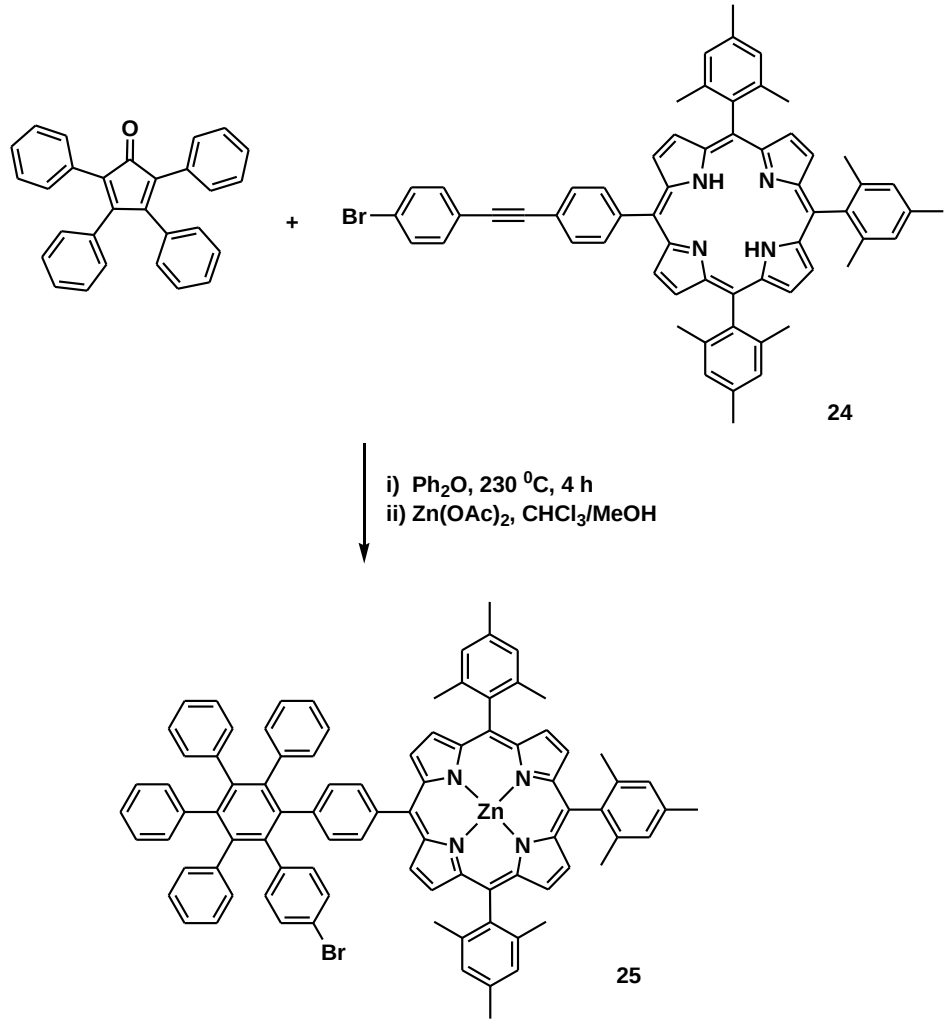

Scheme 7. Synthesis of hexaphenylbenzene core bearing a zinc porphyrin **25**.

Amination of Hexaphenylbenzene Core

Compound **25** was prepared by a palladium catalyzed coupling of **25** with p-anisidine (Scheme 8). Purification of the reaction mixture with flash column chromatography afforded the aminated hexaphenylbenzene core **26 (**47% yield).

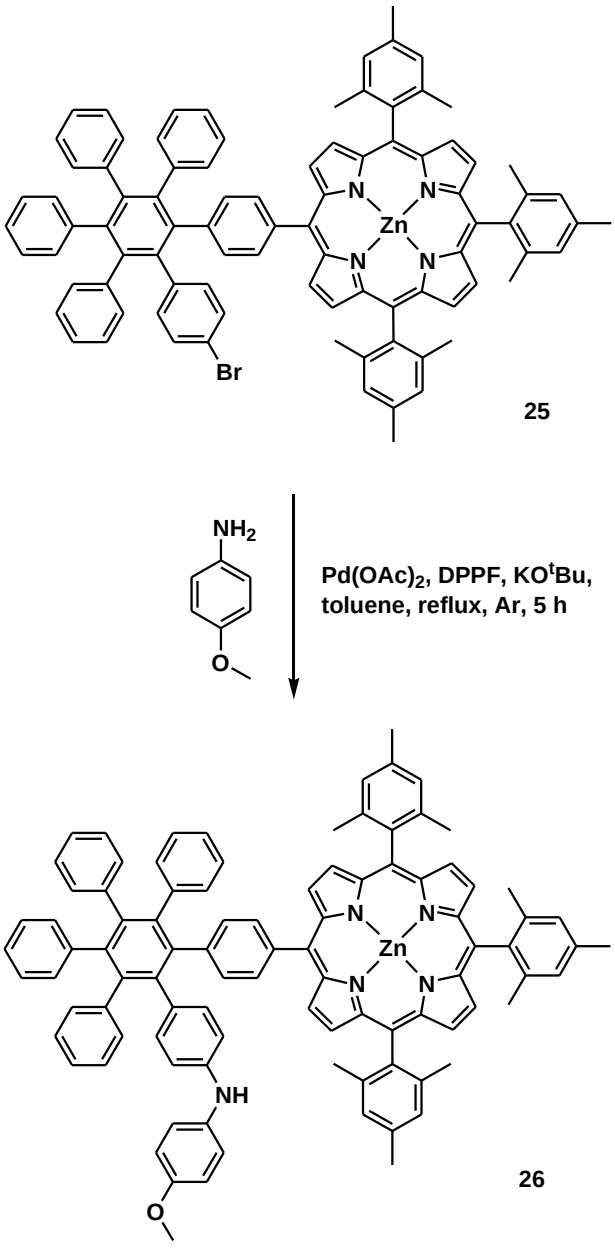

Scheme 8. Synthesis of aminated hexaphenylbenzene core **26**.

Synthesis of p-Dyad

Dyad **27** was synthesized by a palladium catalyzed coupling of **26** with the dye compound **20** (Scheme 9). Purification of the reaction mixture with flash column chromatography afforded the pure p-dyad **(**57% yield).

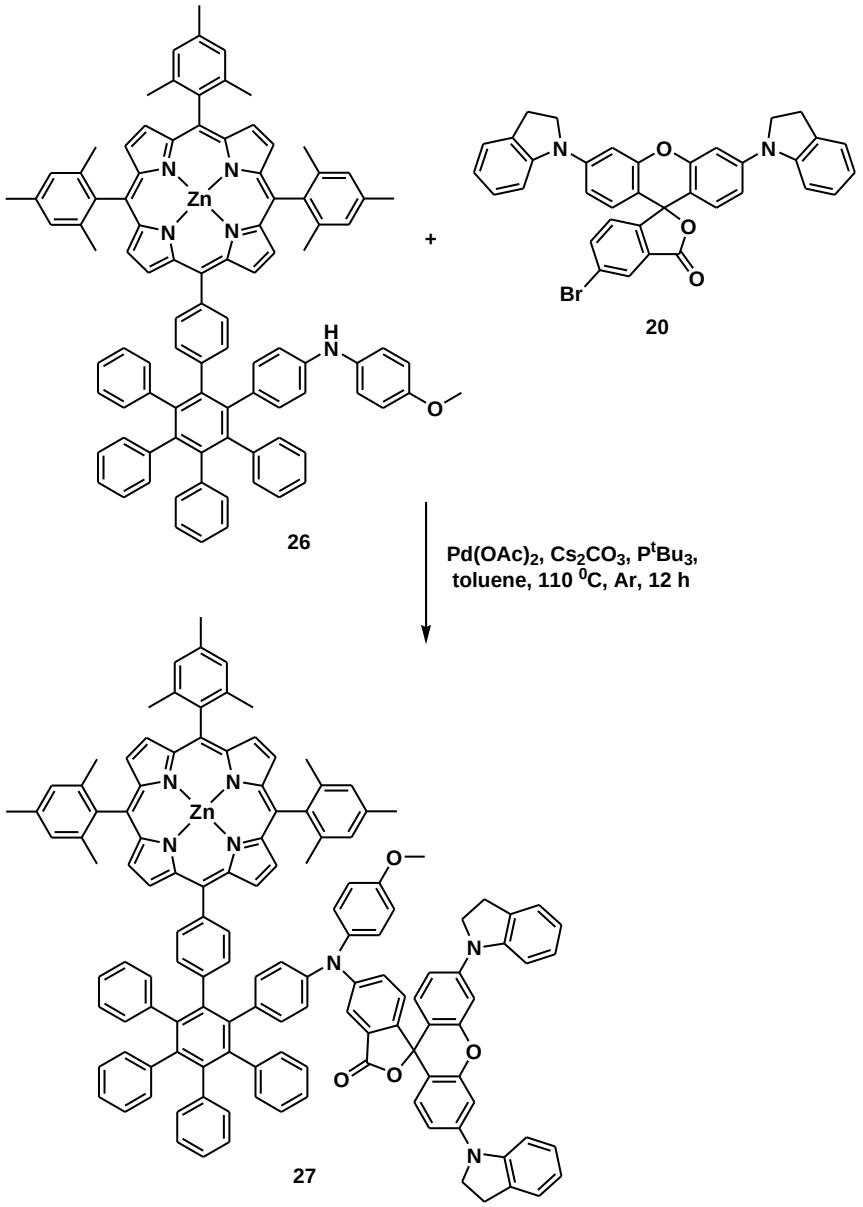

Scheme 9. Synthesis of zinc porphyrin-dye Dyad **27**.

Synthesis of m-Dyad

Dyad **28** was synthesized by a palladium catalyzed coupling of **26** with the dye compound **21** (Scheme 10). Purification of the reaction mixture with flash column chromatography afforded the pure m-dyad **28**.

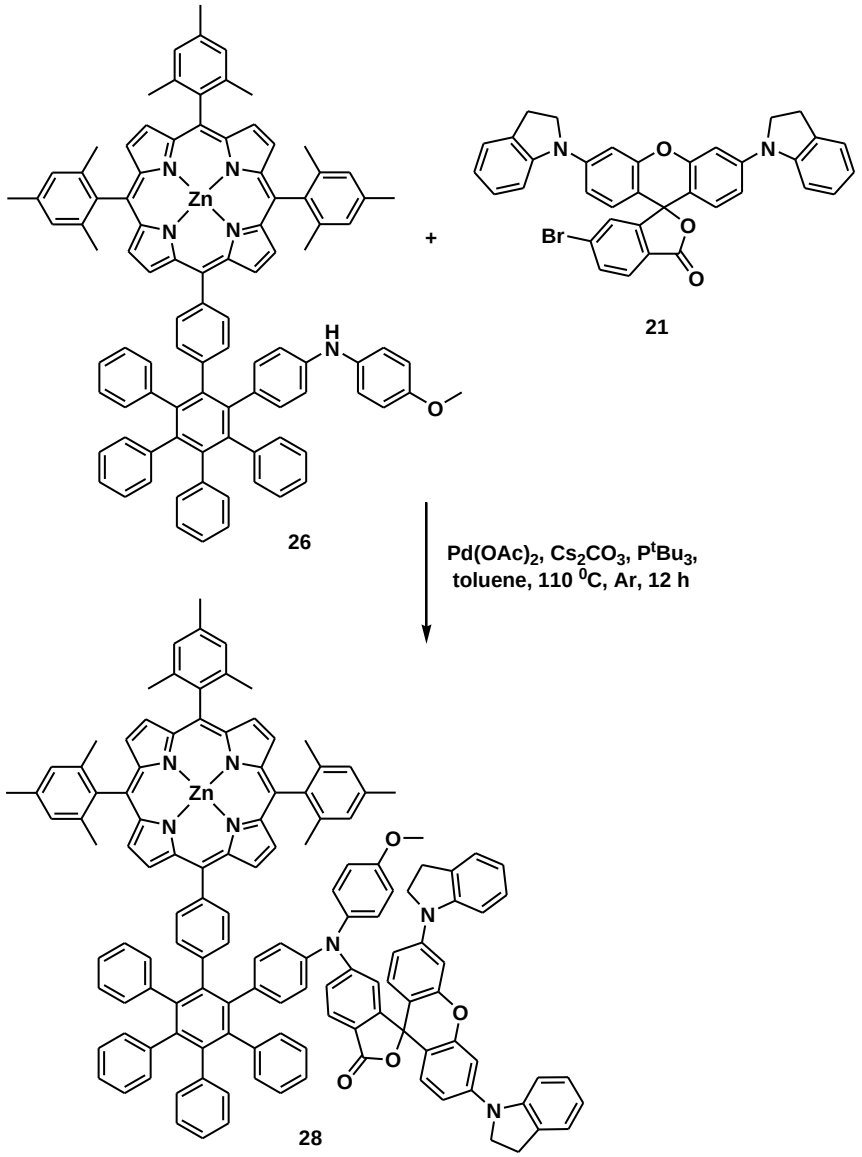

Scheme 10. Synthesis of zinc porphyrin-dye m-Dyad **28**.

Synthesis of a Hexaphenylbenzene-Dye Model Compound

A hexaphenylbenzene-based dye model compound **30** was synthesized by a palladium catalyzed coupling of aminated hexaphenylbenzene **29** with the dye compound **20** (Scheme 11). Purification of the reaction mixture with flash column chromatography afforded the pure dye compound **30** with 82 % yield (synthesis: Yuichi Terazono).

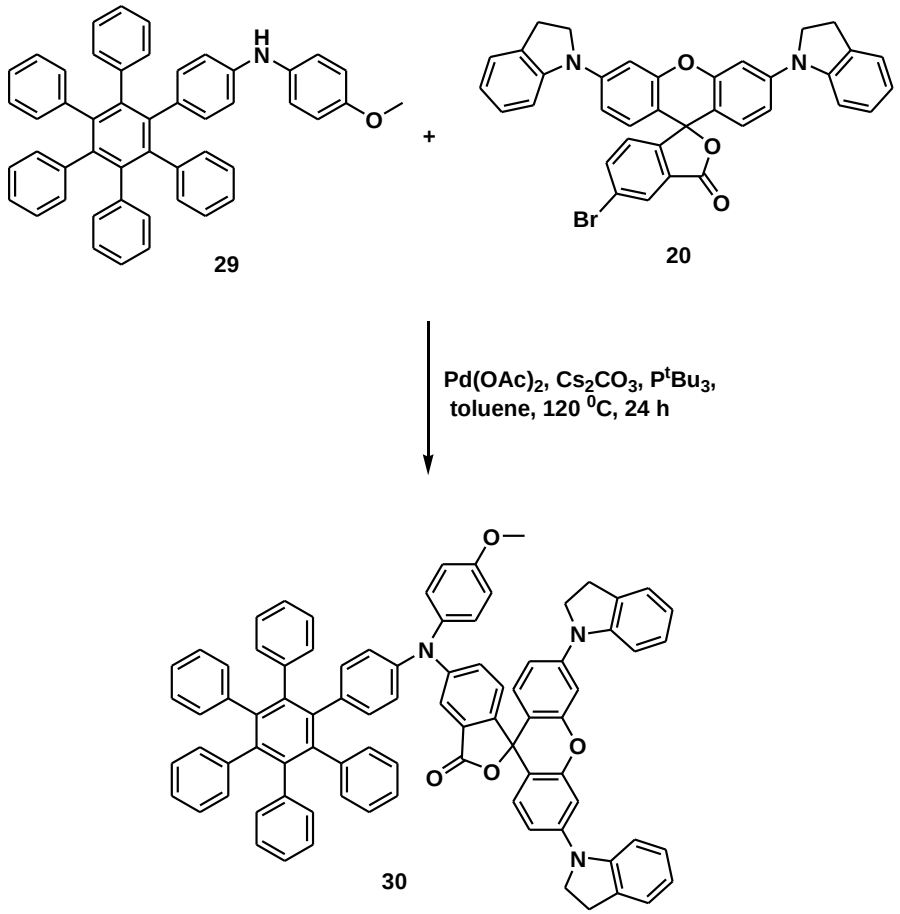

Scheme 11. Synthesis of a model dye compound **30**.

Synthesis of Hexad 34

The general outline of synthesis of **34** is as follows. The hexaphenylbenzene skeleton was synthesized by a variation of the cyclotrimerization method reported by Takase *et al.*[90] Two acetylene moieties, each bearing two nickel porphyrins, and a third acetylene bearing a nickel porphyrin and a substituted aniline were cyclized using a dicobalt octacarbonyl catalyst. After removal of the nickel with sulfuric acid and insertion of zinc into the porphyrins, the resulting hexaphenylbenzene precursor bearing five zinc porphyrins was coupled to the dye precursor via a palladium-catalyzed amination (Scheme 12). Purification of the reaction mixture with flash column chromatography afforded the pure hexad **34** with 47 % yield (synthesis: Yuichi Terazono).

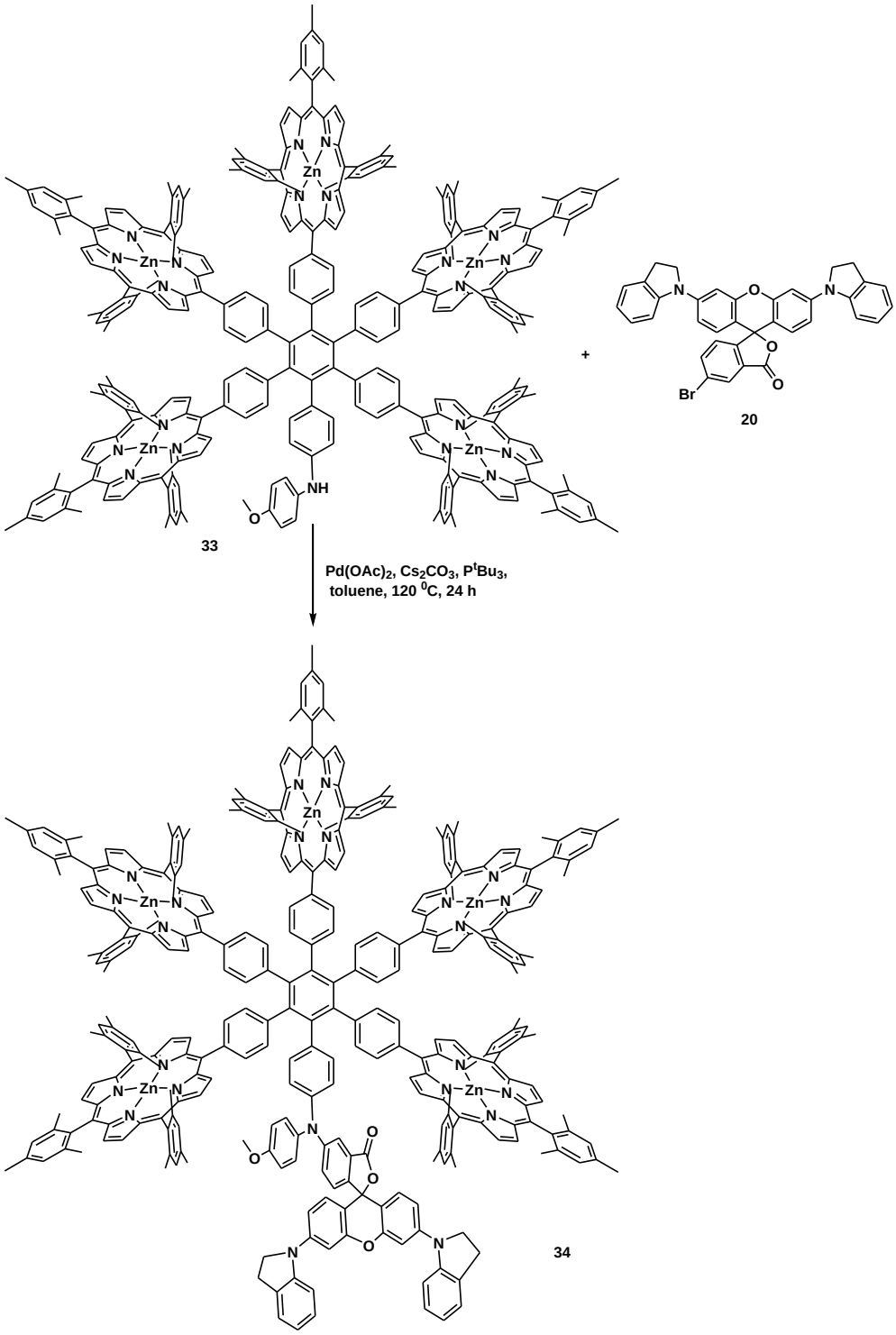

Scheme 13. Synthesis of hexad **34**.

Chapter 4

RESULTS AND DISCUSSION

pH-Sensitive Dyes

Steady state absorption and emission spectra of the tin porphyrin-CVL dye dyad did not exhibit desired properties, and it had some inherent limitations. Therefore, time-resolved studies were not conducted on this dyad and alternative dyes were researched. Xanthenes-based dyes seemed to be promising candidates due to their desirable properties. To overcome the limitations, a rhodamine-based model dye 3',6'-pyrrolidinorhodamine **10** was synthesized. Closed form of this dye 3',6'-pyrrolidinofluoran **11** is colorless, and it does not absorb light significantly. However, when acetic acid is added to 11, it opens and converts to its colored form. This open red colored form strongly absorbs light. In dichloromethane, compound **10** has an absorption maximum of 550 nm. Although this model dye cleanly opens and closes in acidic and basic medium respectively but its absorption wavelengths are too short for effective overlap with the emission of a zinc porphyrin, which is about 600-650 nm. Therefore, alternative rhodamine-based dyes were sought which would have a greater degree of delocalization of positive charge in their acid-stable forms. Therefore, another model dye 3',6'-N-methylanilinorhodamine **12** was synthesized. An absorption spectrum of **12** was taken in dichloromethane (Figure 22).

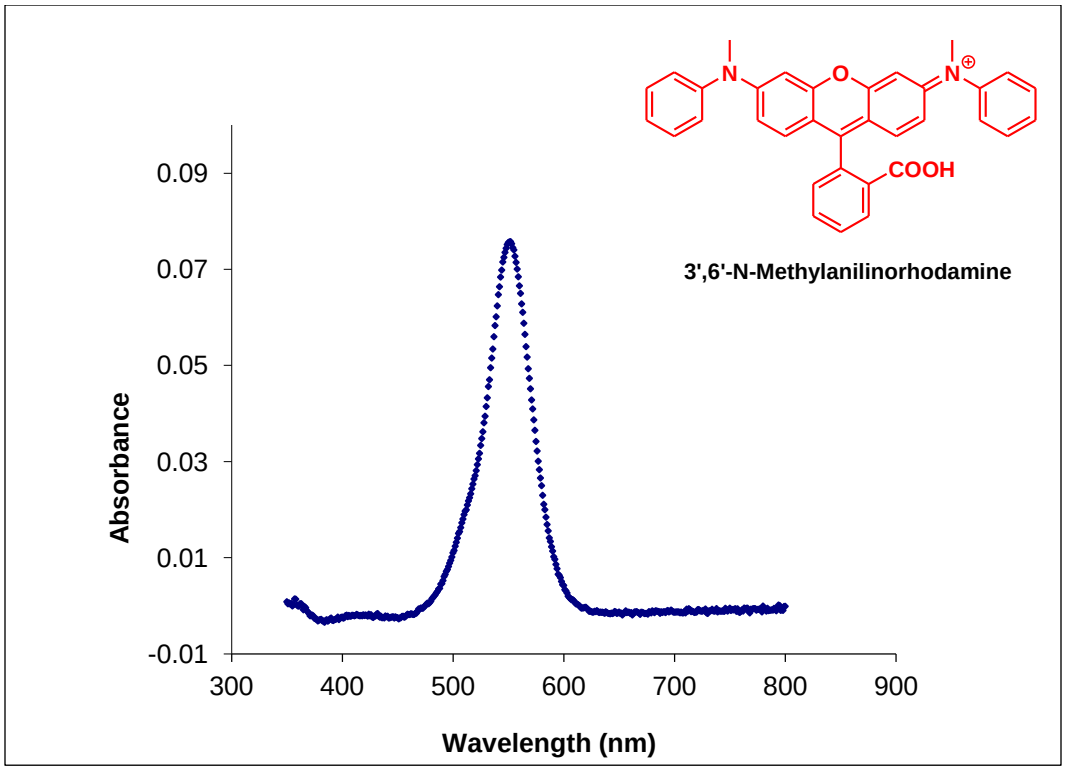

Figure 22. Absorption spectrum of 3',6'-N-methylanilinorhodamine **12** in dichloromethane. Absorption maximum: 552 nm.

The absorption spectrum of **12** revealed its absorption maximum at 552 nm, which is again too short for the purpose of this research. Perhaps the positive charge in its acid-stable form is not very delocalized due to relatively unrestricted rotation of the phenyl ring attached to the nitrogen atom. Therefore, it was envisioned that introducing a greater degree of delocalization of the positive charge can be achieved by restricting the motion of the benzene ring adjacent to nitrogen atom. Based on these hypotheses, 3',6'-indolinorhodamine **14** was synthesized. Compound 14 features a greater degree of delocalization of positive charge. In dichloromethane, compound **14** has an absorption maximum of 640 nm (Figure 23), which is excellent for the purpose of this project as this dye is

suitable for the absorption of zinc porphyrin emission. Compound **14** is blue in color, and it can be converted into its closed, colorless, nonabsorbent form **15** by addition of a base such as triethylamine.

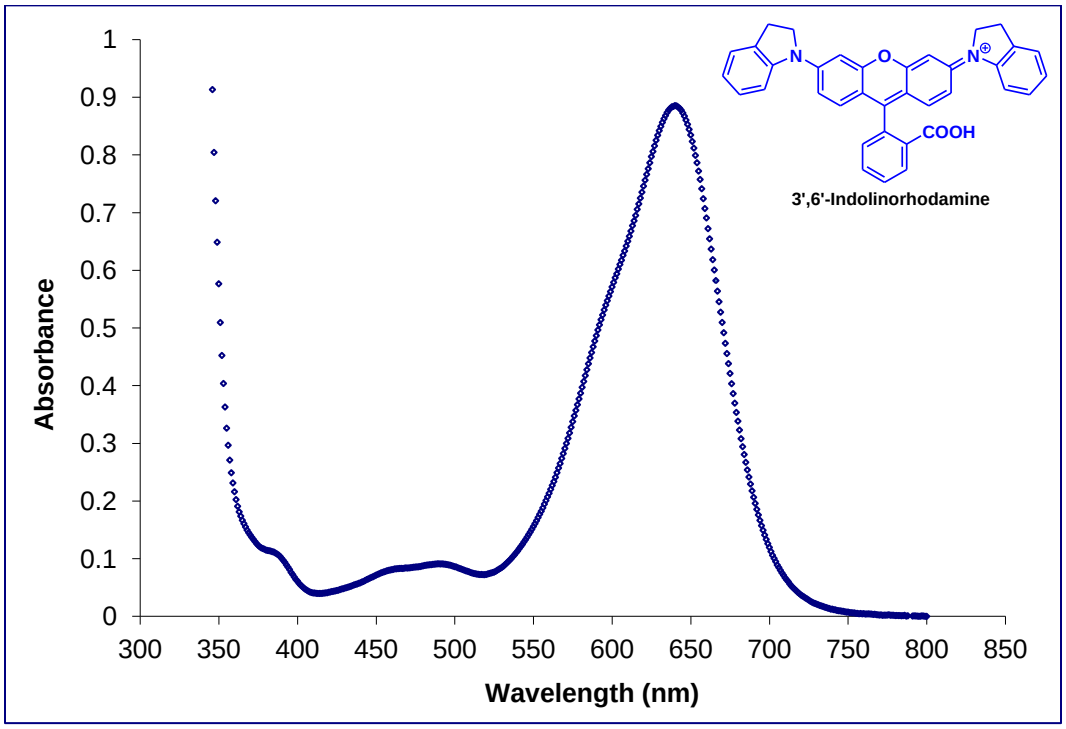

Figure 23. Absorption spectrum of 3',6'-indolinorhodamine **14** in dichloromethane. Absorption maximum: 640 nm.

To demonstrate the opening and closing of the dye, a solution of the dye in dichloromethane was titrated with acetic acid and triethylamine respectively. Absorption spectra were taken with a neutral solution of 3',6'-indolinofluoran **15** and upon gradual addition of acetic acid (Figure 23). The dye opens upon the addition of acetic acid, the absorption band grows in and at the addition of 1.0 mL of acetic acid most of the dye molecules are converted into their open form. To

this solution of open dye, triethylamine was gradually added and absorption spectra were taken (Figure 25). Addition of triethylamine closes the dye and the absorption band decreases as more amine is added. Addition of 1.2 mL of triethylamine closes most of the dye molecules and the absorption band reaches its approximate original value at the beginning of the titration.

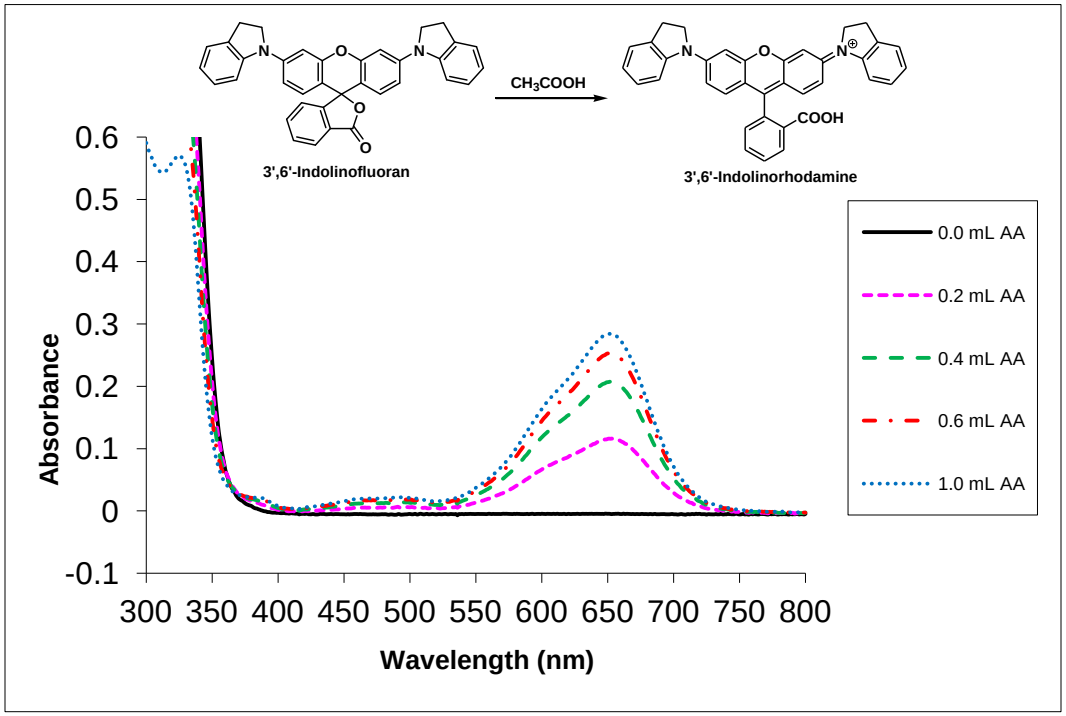

Figure 24. Absorption spectra of 3',6'-indolinofluoran **15** in dichloromethane and upon addition of acetic acid (AA).

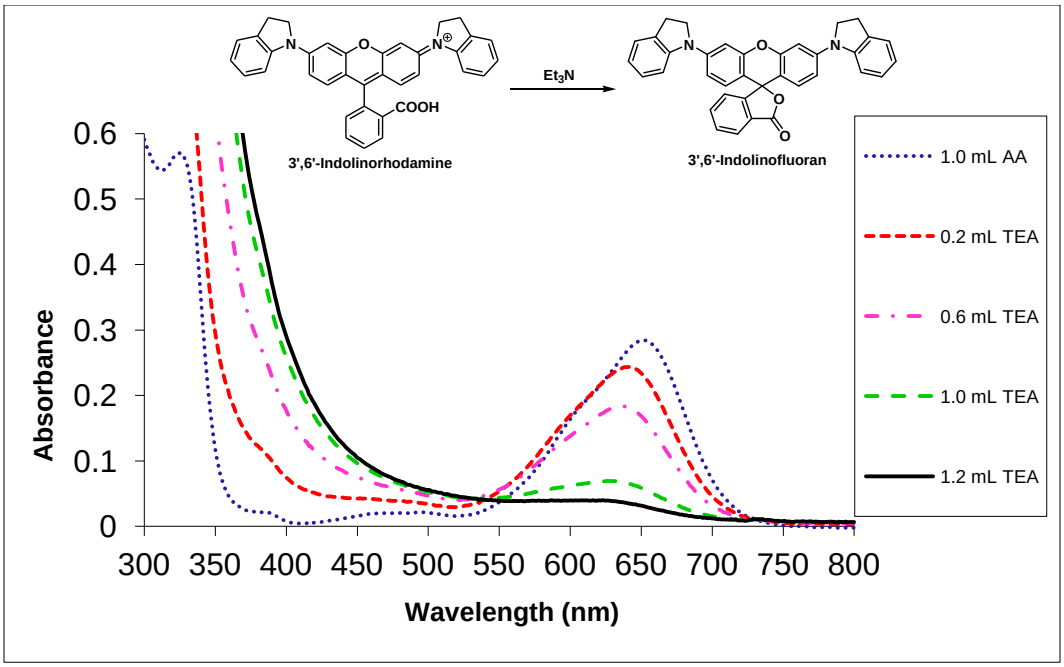

Figure 25. Absorption spectra of 3',6'-indolinorhodamine **14** in dichloromethane and upon addition of triethylamine (TEA).

Next step of the project was to synthesize this class of dyes bearing a suitable functional group so that they could be attached with porphyrin chromophores. Therefore, two functionalized indolinorhodamine-based dyes 3',6'-indolino-5-bromorhodamine **18** and 3',6'-indolino-6-bromorhodamine **19** were synthesized. Two zinc porphyrin-dye dyads **27** and **28** were synthesized.

Solvent-Acid Systems for Photophysical Studies

To study the photophysical properties of the dyads, the dyads **27** and **28** were dissolved in dichloromethane and their steady-state absorption and emission spectra were taken in their neutral, closed form and after portion-wise addition of acetic acid. Addition of acid protonates the dye in the dyad and an open form of the dyad is obtained. The open, protonated form of the dye quenches the

porphyrin emission. Steady-state absorption and emission spectra of **27** are illustrated in Figure 30. Steady-state absorption and emission spectra of dyad **28** showed identical spectral feature those of **27**. Therefore, time-resolved photophysical studies were only carried out on **27**. Although addition of acetic acid to a solution of the dyad in dichloromethane effectively opens the dye moiety, quite a large amount of acid is needed to open most of the dye. Therefore, alternative solvent-acid systems, with a stronger acid, were investigated. Formic acid was explored as it is a stronger acid than acetic acid. Although the dyad is soluble in 2-methyltetrahydrofuran solvent but the dye does not open cleanly by addition of acetic acid or even a much stronger formic acid. Small amount of demetallation of the zinc porphyrin occurs when formic acid is added to a solution of the dyad in dichloromethane. Demetalllation was also observed when monochloroacetic acid was used instead of acetic acid in a solution of the dyad in dichloromethane. Formic acid works well in ethanol solvent and demetallation does not occur, but ethanol being much more polar than dichloromethane has the potential to promote electron transfer rather than energy transfer as the electron transfer is a function of solvent polarity, which affects reorganization energies as well as driving force. Therefore, dichloromethane-acetic acid solvent-acid system was selected for time-resolved studies of **27** and the hexad **34**.

Photophysical Studies of the Hexad

In order to study the photophysical properties of artificial photosynthetic antenna hexad **34**, a model dye **30**, and a model zinc porphyrin **32** were synthesized **(**Figure 26). Photophysical studies were conducted by Gerdenis Kodis.

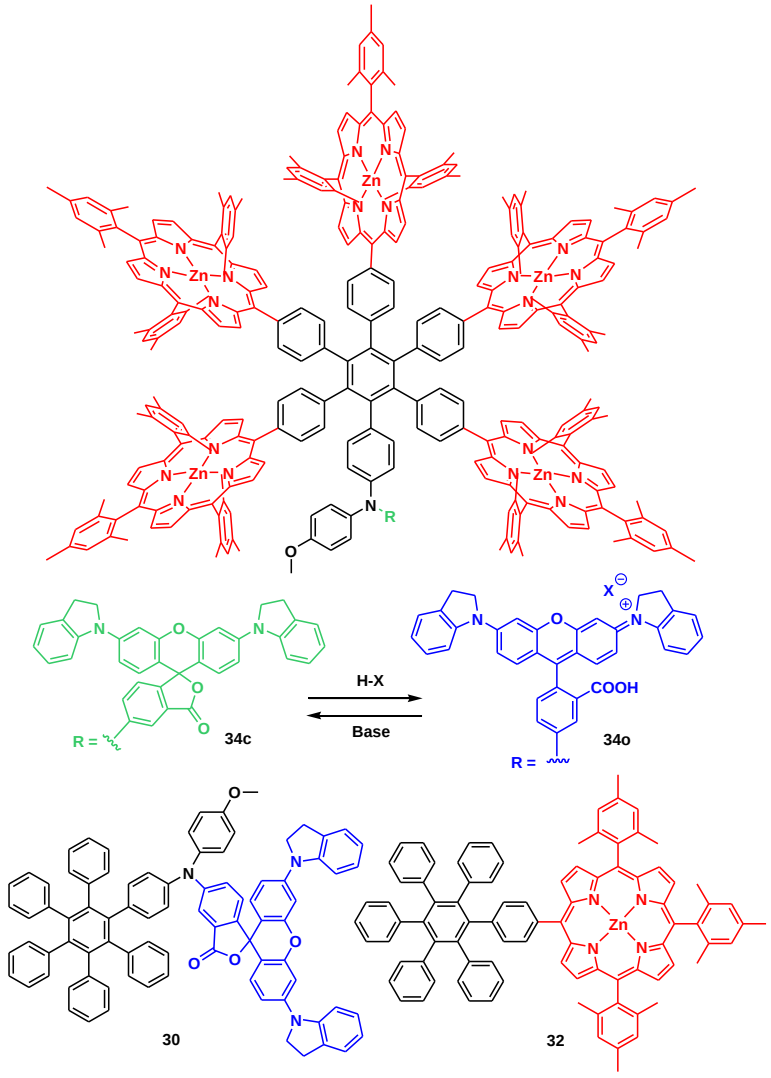

Figure 26. Structures of the hexad when the dye is in closed, spirocyclic form **34c** and when the dye is in open form **34o**, a model dye **30**, where the dye is shown in only closed form, and a model zinc porphyrin **32**.

The hexad features five zinc porphyrin chromophores organized on a hexaphenylbenzene framework. The zinc porphyrins are covalently linked to hexaphenylbenzene core at meso positions. The hexaphenylbenzene core also bears a pH-sensitive rhodamine-based dye moiety. The hexaphenylbenzene core provides structural rigidity for controlling electronic interactions between chromophores, and predicting the rate constants. Under neutral conditions, in dichloromethane, the dye remains in closed, spirocyclic form and the hexad exists in closed form **34c**. When an acid is added to the hexad solution, the dye is protonated. Protonated form of the dye takes the open, positively charged form, and the hexad converts to its open form **34o**, where X^- represents the counterion around the positive charge of the open form of the dye. The closed dye does not absorb in the visible spectral region but has bands at 309 and 336 nm. The closed form of the dye does not affect the photophysical properties of the hexad, only open form of the dye absorbs the porphyrin emissions. In hexad when the dye is in closed form, the porphyrins rapidly exchange energy and come to ground state. The absorption of the porphyrin chromophores in the hexad is similar to that of the model compound **32** comprising a single porphyrin and the porphyrin in dyad **27**. However, there are exitonic interactions between the porphyrins of the hexad, which result in the broadening of the shoulder and slight red shift of the Soret band (Figure 27).

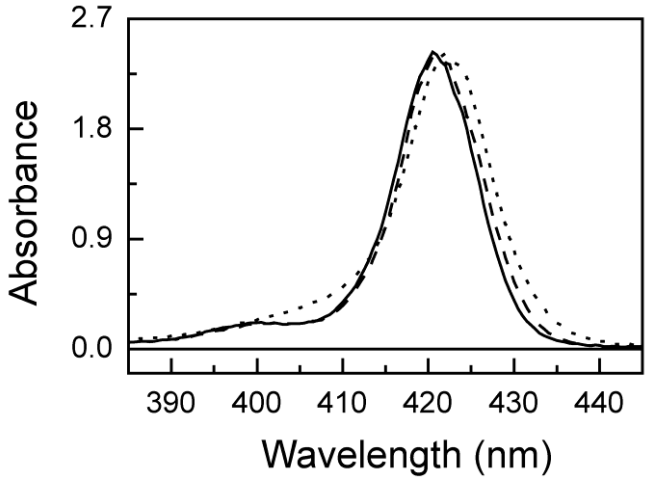

Figure 27. Absorption spectra in the Soret region of dichloromethane solutions of model porphyrin **32** (solid), porphyrin-dye dyad **27** with the dye in the closed, form (dash), and hexad **34c** with the dye in the closed form (dot). The slight broadening and shift of the hexad Soret band indicates excitonic interactions among the porphyrin chromophores.

The broadening of Soret band of **34c** and slight shift to longer wavelengths, relative to model compound indicated weak excitonic splitting (~10 nm) among adjacent porphyrin chromophores. These types of excitonic interactions have been observed in similar compounds,[41, 42, 91] and explained in some details in a closely related compound containing a porphyrin array.[92]

Steady-state Absorption and Emission Spectra of the Hexad

The hexad solution was prepared in dichloromethane. The absorption and emission spectra of the hexad in its neutral form and after addition of acetic acid, and reversion of **34o** to **34c** are shown in Figure 28.

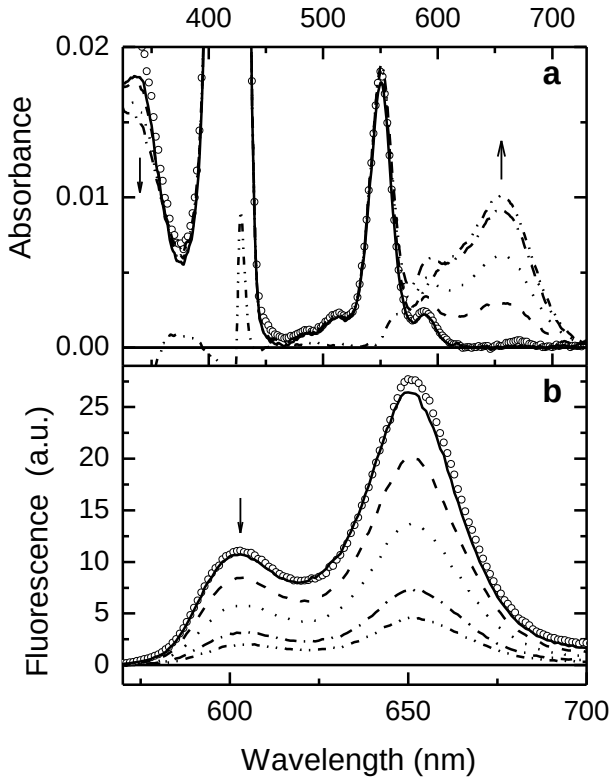

Figure 28. Absorption and emission spectra of the hexads. (a) Absorption spectra of **34c** in dichloromethane (solid) and after addition of acetic acid, which converts some of the **34c** to **34o**: acetic acid at 123 mM (dash), 244 mM (dot), 482 mM (dash dot) and 826 mM (dash dot dot). (b) Fluorescence emission spectra (λ_{ex} = 396 nm) of the solutions described in (a). The absorption and emission spectra of the resulting solution after base treatment (reversion of **34o** to **34c**) are shown (circles).

The amplitudes of the spectra were corrected for dilution factor. The absorption spectrum of **34c** is shown in Figure 28a. It features the porphyrin Soret band shoulder at ~410 nm (seen clearly in Figure 27) and 423 nm, and Q-bands at 514, 551 and 590 nm. The Q-band shapes and wavelengths of hexad are essentially

identical to those in **32**. As acetic acid is added, portion-wise, to the solution of hexad**,** a new absorbance with a maximum at 656 nm grows in (Figure 28a). The new band is characteristic of the open form of the dye, signalling conversion of **34c** to **34o** by protonation of the dye. The zinc porphyrin spectral features remain same after the addition of acetic acid, indicating that zinc is not removed from the porphyrins by the acid.

The hexad **34c** exhibits typical zinc porphyrin fluorescence emission with bands at 602 and 650 nm (Figure 28b). The hexad **34o** formed due to the addition of acetic acid displays significant changes in the emission spectrum. The shape of the emission is unchanged after the addition of acid but the amplitude of emission decreases profoundly which demonstrates the quenching of the porphyrin emission by the open form of the dye generated upon the addition of the acid. Infect the emission of all five porphyrins chromophores was strongly quenched by the open form of the dye. After completion of the measurements, the acidic solution was neutralized by treating with excess granular sodium carbonate and filtering. This treatment led to the reversion of **34o** to **34c** and the original absorption and emission values were recovered (Figure 28). It also caused the appearance of a very small absorption at 670 nm, and a small emission band (not shown) at ~720 nm. These features are ascribed to a small amount of impurity or decomposition due to the neutralization process. Thus the amount of **34c** and **34o** in the solution is a function of the amount of acid added.

The recovery of the absorbance and emission spectra demonstrates the reversibility of the protonation and the quenching processes. This experiment demonstrates the function of the antenna and quencher in pH-controlled reversible quenching of excess energy in NPQ in plants.

Transient Spectroscopy and Quenching Process in Hexad

Information about the quenching process was obtained from transient spectroscopy. Fluorescence emission data were obtained from two different spectrometers: a streak camera setup and a conventional single-photon-timing apparatus. In each case, the decays were analyzed by least-squares fitting as a sum of exponentials, with reconvolution to remove effects from the instrument response as described in the experimental section in chapter 5. Both apparatus produced reliable time constants down to ca. 5 ps, with the goodness-of-fit (χ^2) values reported below. When a dichloromethane solution of **34c** was excited at 550 nm, where the light is absorbed by the porphyrin Q-bands, the decay of the fluorescence emission (monitored at 650 nm) measured with the streak camera showed (Figure 29) that the emission could be fitted with a single exponential with a time constant of 2.14 ns (Figure 29, $\chi^2 = 1.16$). This lifetime is typical of a zinc porphyrin of this class (*vide infra*).

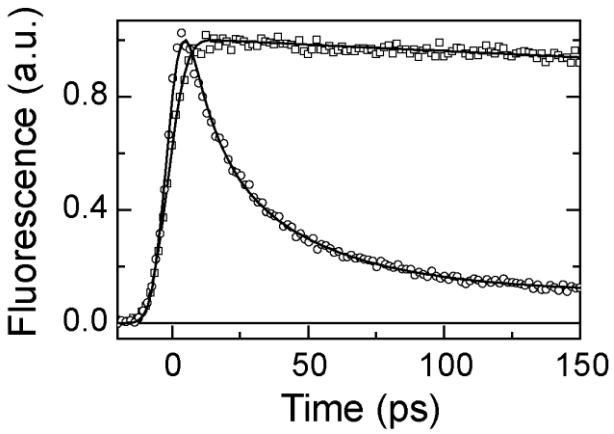

Figure 29. Emission decays for **34** measured at 650 nm following excitation at 550 nm with a 130 fs laser pulse. Decays were obtained from **34c** in dichloromethane (squares) and from an acidified solution highly enriched in **34o** (circles). The solid lines are best fits to exponential functions with time constants.

The fluorescence decay of the solution of **34** was measured again (Figure 29) after addition of acetic acid, which converted most of the sample to **34o**. The decay was fitted (χ^2 = 1.21) with exponential components having time constants of 10.3 ps (49%), 39.4 ps (31 %), and 2.10 ns (20%). The ps components represent the profound reduction of the lifetimes of porphyrin first excited singlet states, and the 2.1 ns component is due to the residual **34c**. For **34o**, the rate constants of the quenching processes are 9.7×10^{10} s^{-1} and 2.5×10^{10} s^{-1}. The quantum yield of fluorescence quenching is essentially unity, as calculated based on either of the two ps time constants and the lifetime of **34c**.

Photophysical Studies of the Dyad 27

In order to understand better the quenching process in **34o**, model dyad **27** (Figure 11) was studied. Dyad **27** features a single zinc porphyrin and a pH-sensitive dye, identical to that in **34**, organized on a hexaphenylbenzene framework. Steady-state absorbance and emission spectra of a neutral solution of **27** in dichloromethane and after addition of acetic acid are shown in figure 30.

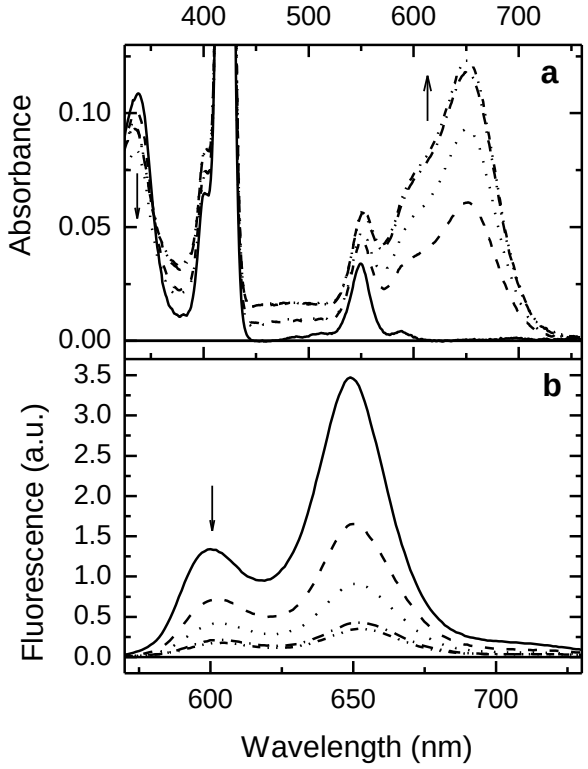

Figure 30. Dyad absorption (a) and fluorescence (b) with the addition of acetic acid, 0 (solid), 100 (dash), 200 (dot), 400 (dash dot), 500 μL (dash dot dot). Fluorescence quenching is 90% at 500 μL.

The zinc porphyrin at a position *ortho* to the dye is covalently linked at meso position to the hexaphenylbenzene core. A solution of **27** in dichloromethane, when the dye is in closed form, showed Soret and Q-band absorption maxima and fluorescence maxima at wavelengths similar to those observed for **34c**, although no excitonic splitting or significant band broadening were observed. In absorption spectra, the absorption maxima were found at 336 (closed dye), 402 (sh), 422 (Soret), 550, 589, 651 (open dye) nm. The fluorescence maxima were at 600 and 650 nm with excitation at 399 nm.

Time resolved fluorescence experiments of **27** using the single-photon-timing method with excitation at 425 nm and emission at 600 nm yielded a lifetime for the porphyrin first excited singlet state of 2.09 ns (Figure 31).

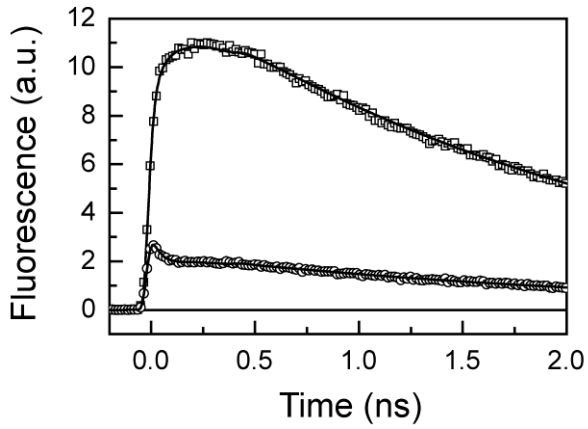

Figure 31. Fluorescence emission decays at 600 nm following excitation at 425 nm of a solution of dyad **27** in 2.5 mL of dichloromethane. The squares indicate the data for the dyad in the closed form, and the circles indicate data for the solution after addition of 250 μL of acetic acid (**27o**). The accompanying solid line is a best exponential fit to the data.

The fluorescence of model porphyrin **32**, measured using the same apparatus, decayed as a single exponential with a lifetime of 2.13 ns (χ^2 = 1.02).

The best exponential fit to the data of **27** gives lifetimes of 2.09 ns (99.3%) and 8.2 ns (0.7%), with χ^2 = 1.16. The small component of 8.2 ns decay is ascribed to the presence of free-base porphyrin. Addition of 250 μL acetic acid converts most of 27 to open, protonated form **27o**. Exponential fitting of the data for **27o** gives time constants of 23 ps (70%) and 2.12 ns (30%), with χ^2 = 1.13. The longer time constant is associated with **27** and the shorter time constant is associated with **27o**, which represents the quenching of the first excited singlet state of the porphyrin by open form of the dye. The apparent rise at early times is due to the convolution of the decay kinetics with the instrument response function.

Turning again to the results of hexad, the 10 ps decay observed for **34o** is associated mainly with quenching of the two porphyrins *ortho* to the dye by the dye moiety. Given the fact that the two molecules are not identical, this time constant is comparable to that measured for the similar process in **27o** (23 ps). In the hexad, the porphyrins next to the dye moiety experience strong steric interactions with it and the adjacent porphyrins, which result in conformational changes that affect the rates of energy transfer. These type of steric interactions are absent in the dyad **27**. The 39 ps decay must result from some combination of direct quenching of the porphyrins *meta* and *para* to the dye by the dye moiety and singlet energy transfer among the porphyrins. In a detailed study of a porphyrin array with very similar, but not identical, porphyrin structures, a time

constant for exchange of energy between adjacent porphyrins of ~180 ps was estimated from fluorescence anisotropy results.[92] If it is assumed that a similar time constant is appropriate for **34**, then it is clear that the rapid (ca. 39 ps) transfer of excitation to the open dye from the porphyrin moieties *meta* and *para* to it must involve energy transfer directly from these porphyrins to the dye moiety. The time constants for energy transfer involving the porphyrins in the *meta* and *para* locations are definitely different from one another, but drawing out of additional time constants was not justified by data analysis. Although excitation hopping is possible between porphyrins but it has a negligible effect on the porphyrin first excited singlet state decay profile. The studies clearly demonstrate that the open, protonated form of the dye rapidly quenches the excited singlet states of all five porphyrin chromophores.

When studied by single-photon-timing methods, model dye **30** (Figure 26) in its open, protonated form did not show measurable fluorescence. Therefore the singlet excited state lifetime of the dye was measured in ethanol by using femtosecond transient absorption spectroscopy with excitation at 640 nm (Figure 32) The data shows excited state relaxation to the ground state (decay of ground state bleaching at 640 nm) and an exponential least-squares fit with a time constant of 5.0 ps.

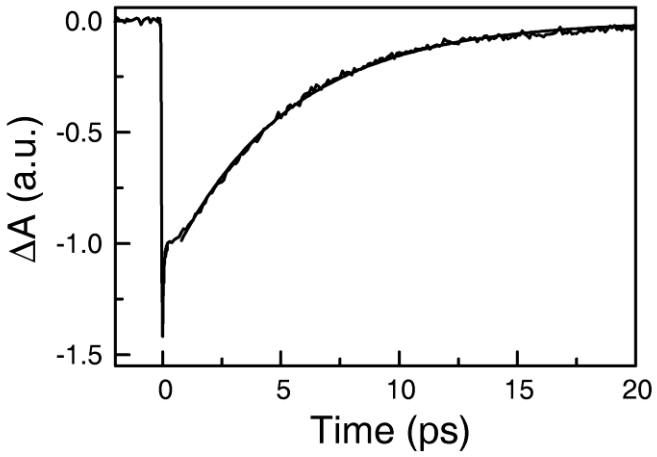

Figure 32. Transient absorption at 640 nm (arbitrary units) of an ethanol solution of model dye **30** excited with a 54-fs laser pulse at 640 nm. The solution contained sufficient formic acid to convert the molecule to its open, protonated form. The data show the decay of the dye ground-state bleach as the first excited singlet state returns to the ground state. The smooth curve is an exponential fit to the decay with a time constant of 5.0 ps. The χ^2 value (unreduced) is 0.16.

Quenching Mechanism

There are two possible mechanisms for quenching of the porphyrin excited states by the open, protonated form of the dye. First is singlet-singlet energy transfer from the porphyrin to the dye resulting in the excited state of the dye which comes to the ground state, and second is photoinduced electron transfer from the porphyrin to the dye resulting in a charge-separated state. In order to investigate the thermodynamic feasibility for quenching by photoinduced electron transfer, the electrochemical properties of model dye **30** were measured (Figure 33).

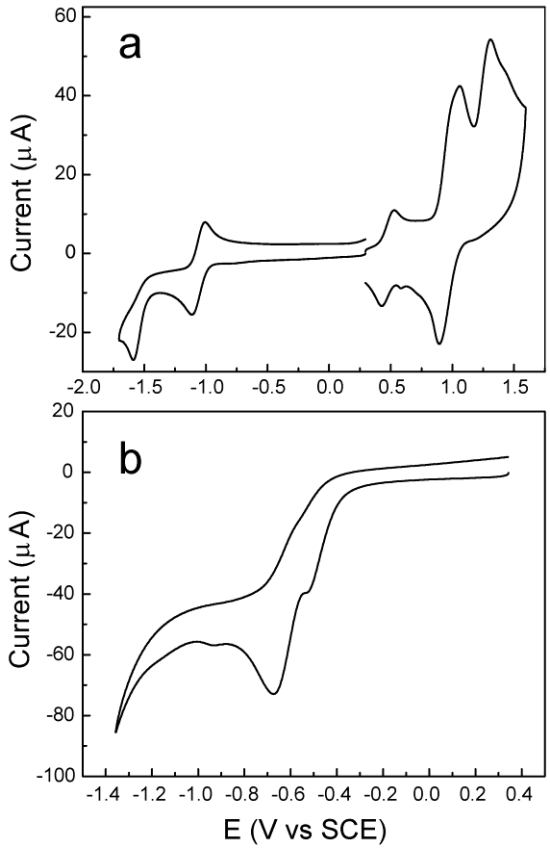

Figure 33. Cyclic voltammograms of model dye **30** dissolved in dichloromethane containing 0.1 M tetra-*n*-butylammonium hexafluorophosphate (a) and the same solution after addition of sufficient acetic acid to convert most of the dye to the open form (b). The potentials were measured with ferrocene as an internal reference and are reported relative to SCE. The waves around 0.5 V are due to ferrocene.

The results of cyclic voltammetric experiments in dichloromethane containing 0.1 M tetra-*n*-butylammonium hexafluorophosphate are shown in Figure 33. The working electrode was glassy carbon, the counter electrode was platinum foil, and the reference electrode was a silver wire in 10 mM silver nitrate in acetonitrile

containing the same electrolyte. The potentials were converted to the SCE scale using ferrocene as an internal reference compound. Representative results for **30** in the closed, spirocyclic form are shown in Figure 33a. The first oxidation was observed at 0.94 V vs SCE, and the first reduction at -1.11 V vs SCE. Both waves were essentially reversible. The waves around 0.5 V are due to ferrocene. A representative voltammogram after converting most of the dye to open, protonated form by addition of 80 μL of acetic acid is shown in Figure 33b. The voltammogram is not reversible but it is evident that reductive processes occur in the -0.5 to -0.6 V region.

Based on the reduction behavior of the dye **30** and the oxidation potential of zinc tetramesitylporphyrin (0.68 V vs SCE[93]), quenching via photoinduced electron transfer from the excited porphyrin to the protonated dye is thermodynamically possible. However, electron transfer requires overlap of donor and acceptor molecular orbitals, which is expected to be rather weak in **34o**, given the large number of bonds between the porphyrins and dye moiety *ortho*, *meta,* and *para* to them. Also, the steric hindrance at the center of the hexaphenylbenzene core leads to near-orthogonality of the central and peripheral benzene rings,[94-96] which would hinder the electron transfer.

On the other hand, singlet-singlet energy transfer usually occurs by the Förster mechanism,[97] which does not require orbital overlap and depends in part on interchromophore separation and orientation. In **34o**, the energy overlap of the porphyrin emission and dye absorption, and spatial proximity of the zinc porphyrins and the dye are favorable for singlet-singlet energy transfer. The rate

constants for singlet-singlet energy transfer from porphyrin moieties of **34o** to the dye moiety in the open form, calculated using the Förster theory, also suggested the singlet-singlet energy transfer. In these calculations, the transition dipole moment for the protonated dye molecule was assumed to lie in the same position as it does in the related rhodamine 6G.[98] The fluorescence quantum yield for the zinc porphyrins in the absence of energy transfer was taken as 0.04.[99] The extinction coefficient for the open form of the model dye **30** at 656 nm was measured to be 5.7×10^4 M^{-1} cm^{-1}. Molecular modeling using molecular mechanics (MM2) showed that several conformations for the dye relative to the porphyrins were likely. For the porphyrin *para* to the dye, distances between the transition dipoles ranged from 20.9 Å to 21.5 Å. Assuming an orientation factor κ^2 equal to 2/3 (random orientation), these distances gave energy transfer rate constants of 40.6 ps and 48.1 ps, respectively. Energetically reasonable conformations for the molecule featured distances between the dipoles of the dye and a porphyrin *ortho* to it ranging between 12.5 Å and 15.3 Å. A κ^2 of 2/3 yielded rate constants of 1.9 ps and 6.25 ps for these separations. Transfer rates between the open dye and a porphyrin *meta* to it were not calculated, but are expected to exist between those for the *ortho* and *para* porphyrins. The calculated rate constants for energy transfer from a porphyrin to a dye moiety *ortho* and *para* to it are relatively close to the measured lifetimes of 10 and 39 ps. Thus, it is most likely that the quenching in **34o** is due to energy transfer from porphyrins to the open, protonated dye.

Quenching mechanism by energy transfer was also strongly supported by the fact that the time constants for decay of the zinc porphyrin excited states of **34o** measured in ethanol (9 ps and 39 ps) were almost identical to those in dichloromethane. Energy transfer is generally not a strong function of solvent polarity. The dielectric constant of ethanol (24) is significantly larger than that of dichloromethane (9), and electron transfer rates are strongly dependent on solvent polarity, which affects both driving force and reorganization energies. The lifetime of the first excited singlet state of model dye **30** in its open form, measured by transient absorption spectroscopy, is only 5 ps (Figure 32), which is shorter than the time constants of the processes that populate it, which would make it difficult to directly measure the energy transfer in **34o** by transient spectroscopy.

Conclusions

A rhodamine-based pH-sensitive dye was designed and synthesized, which in its neutral form does not absorb in the visible region. However, an open, protonated form of the dye strongly absorbs in the emission spectral region of a zinc porphyrin, making the energy transfer from porphyrin to the dye thermodynamically possible. The model dyad **27**, which bears a single porphyrin and this dye moiety, clearly exhibits the profound quenching of the zinc porphyrin by open, protonated form of the dye, which reduces the lifetime of first excited singlet state of a typical zinc porphyrin from 2.0 ns to 23 ps.

The results of photophysical studies of hexad clearly demonstrate that excitation of a neutral solution of **34c** by visible light displays normal photophysical behaviour of the zinc porphyrin chromophore, and rapid exchange of excitation among the porphyrins is observed. The lifetimes (2.1 ns) of the porphyrins in **34c** are long enough to initiate useful photochemistry such as photoinduced electron transfer. The dye, when in closed, spirocyclic form, has no effect on the decay behaviour of the hexad, however when the solution becomes sufficiently acidic by addition of acetic acid, the protonated form of the dye quenches all porphyrin excited singlet states to less than 40 ps, rendering the porphyrins incompetent to do a useful photochemistry, and dissipating the energy as heat. The quenching is ascribed to singlet-singlet energy transfer from excited state porphyrins to the open form of the dye moiety. The quenching is a function of the acidity and open form of the dye. Therefore, the antenna system in hexad down-regulates the energy as the acidity of the system is increased. Thus the hexad functionally mimics the role of antenna in NPQ in green plants, where quenching of antenna chlorophyll excited state is triggered by decreasing pH in the thylakoid lumen. Therefore, in addition to providing a functional mimic exhibiting the phenomenon of natural NPQ, the hexad shows the self-regulation of function in response to external stimuli, and could be useful in photoprotection of solar energy conversion devices.

Chapter 5

EXPERIMENTAL PROCEDURES

This chapter describes the methods and instrumentation used, and synthesis and characterization details of the compounds related to this research.

General Methods

The ^{1}H NMR spectra were recorded on Varian spectrometers at 300, 400 or 500 MHz. Samples for NMR were dissolved in deuteriochloroform ($CDCI_3$) with tetramethysilane (TMS) as an internal reference unless otherwise specified. $CDCl_3$ for NMR was stored over K_2CO_3. Chemical shifts are reported in ppm, and are referenced either to TMS (0.00 ppm) or the residual proton peak from CDCI3 (7.24 ppm). Mass spectra were obtained with matrix-assisted laser desorption/ionization time-of-flight spectrometer (MALDI-TOF) unless otherwise noted. Spectroscopic studies were carried out on dilute (ca. 10^{-5} M) solutions in dichloromethane and acetic acid was added to convert the dye to the protonated form, unless otherwise specified. Random errors associated with the reported lifetimes were typically $\leq 5\%$.

Solvents and Reagents

Reagents used in the research were purchased from common chemical suppliers (Sigma-Aldrich, Alfa Aesar, Acros, EM Science etc.), and used without prior purification unless otherwise noted. Solvents were generally used without purification, except some cases to run a reaction or column. Tetrahyrdofuran (THF) was distilled from sodium metal and benzophenone in nitrogen or an argon

atmosphere immediately prior to use. Dichloromethane was distilled from potassium carbonate, and toluene was distilled from CaH_2.Thin layer chromatography (TLC) and Preparative TLC were done using silica coated glass plates from Analtech. Column chromatography was carried out using silica gel or alumina as stationary phase. Palladium catalyzed reactions were carried out under argon atmosphere.

Steady-state Spectroscopy

Absorption spectra were measured on a Shimadzu UV2100U UV-vis and/or UV-3101PC UV-vis-NIR spectrometer. Steady-state fluorescence spectra were measured using a Photon Technology International MP-1 spectrometer and corrected for detection system response. Excitation was provided by a 75 W xenon-arc lamp and single grating monochromator. Fluorescence was detected 90^o to the excitation beam via a single grating monochromator and an R928 photomultiplier tube having S-20 spectral response and operating in the single photon counting mode.

Time-resolved Fluorescence

Fluorescence decay measurements were performed employing two different systems: a conventional single-photon-timing apparatus and a streak camera setup. The excitation source for the single-photon-timing system was a mode-locked Ti:Sapphire laser (Spectra Physics, Millennia-pumped Tsunami) with a 130 fs pulse duration operating at 80 MHz. The laser output was sent through a frequency doubler and pulse selector (Spectra Physics Model 3980) to

obtain 370-450 nm pulses at 4 MHz. Fluorescence emission was detected at the magic angle using a double grating monochromator (Jobin Yvon Gemini-180) and a microchannel plate photomultiplier tube (Hamamatsu R3809U-50). The instrument response function was 35-55 ps. The spectrometer was controlled by software based on the LabView programming language and data acquisition was done using a single photon counting card (Becker-Hickl, SPC-830).

Time vs. wavelength fluorescence intensity surfaces were recorded on the streak camera system, with excitation provided by an ultrafast laser. Laser pulses of ~130 fs at 800 nm were generated from an amplified, mode-locked Titanium Sapphire 250 kilohertz laser system (Verdi/Mira/RegA, Coherent). The excitation light wavelength was adjusted using an optical parametric amplifier (Coherent). Fluorescence with polarization set to the magic angle was collected 90^{o} to the excitation beam and focused on the entrance slit of a Chromex 250IS spectrograph, which was coupled to a Hamamatsu C5680 streak camera with a M5675 synchroscan sweep unit. The streak images were recorded on a Hamamatsu C4742 CCD camera and curvature corrected (corrections for shading and system detection sensitivity at different wavelengths were not performed). The instrument response function was ca. 5 - 20 ps.

Data analysis of results from both systems was carried out using locally written software (ASUFIT) developed in a MATLAB environment (Mathworks Inc.). Data were fitted as a sum of exponential decays, which were reconvoluted with the appropriate instrument response function. Goodness of fit was established by examination of residuals and the reduced χ^2 value.

Transient Absorption Spectroscopy

Transient absorption spectroscopy was carried out by the pump-probe technique. The femtosecond light source was an optical parametric amplifier (Coherent OPA) pumped by a 250 kHz Ti:Sapphire regenerative amplifier (Coherent RegA 9050) that was seeded by a Ti:Sapphire oscillator (Coherent Mira Seed). The output of the OPA was tuned to 640 nm and compressed with prisms to 54 fs. These pulses were divided by a beam splitter and the probe beam was attenuated with a neutral density filter to 20 microwatts. The pump beam was sent through an optical delay line and the beams were crossed at the sample position. The power of the pump at the sample was 1 mW. The probe beam intensity was measured with a photodiode (Thorlabs DET 210) connected to a lock-in amplifier (Stanford Research Systems SR830) that was synchronized with a mechanical chopper modulating the pump path at 499 Hz. The observed kinetics were independent of both pump and probe intensity. The measured transient absorption signal was fit with a single exponential decay using least squares analysis, and goodness of fit was established from residuals. The fitting was restricted to the part of the curve where the effects of the excitation pulse and coherence artifacts were negligible.

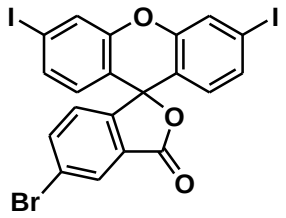

16

3', 6'-Diiodo-5-bromofluoran (16). Portions of 3-iodophenol (2.20 g, 10 mmol) and 4-bromophthalic anhydride (1.135 g, 5 mmol) were combined in 5 mL of methanesulfonic acid and heated at 140ºC for 16 h. The reaction mixture was poured in 200 mL of ice water, stirred for 30 min, and then filtered. The resulting damp gray solid was dissolved in dichloromethane and filtered through a short plug of silica gel. The product isomers 3', 6'-diiodo-5-bromofluoran (**16**) and 3', 6'-diiodo-6-bromofluoran (**17**) were separated by silica gel column chromatography with toluene/dichloromethane (4/1) to yield 0.663 g (21 %) of **16** and 0.758 g (24 %) of **17**.

16: ^{1}H NMR (400 MHz, $CDCl_3$): δ, ppm 6.542 (2H, d, *J* = 8 Hz, Ar-*H*), 7.003 (1H, d, *J* = 8.4 Hz, Ar-*H*), 7.397 (2H, dd, *J* = 8.4 Hz, *J* = 1.2 Hz, Ar-*H*), 7.691 (2H, d, *J* = 1.6 Hz, Ar-*H*), 7.781 (1H, dd, *J* = 8 Hz, *J* = 1.6 Hz, Ar-*H*), 8.158 (1H, d, *J* = 1.6 Hz, Ar-*H*). MALDI-TOF-MS *m/z*: calcd for $C_{20}H_9BrI_2O_3$ + H 630.790, obsd 630.835 (98 % intensity) 632.833 (100 % intensity).

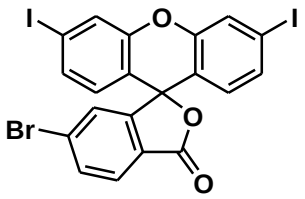

17

3', 6'-diiodo-6-bromofluoran (17). ^{1}H NMR (400 MHz, $CDCl_3$): δ, ppm 6.562 (2H, d, *J* = 8.4 Hz, Ar-*H*), 7.176 (1H, d, *J* = 7.6 Hz, Ar-*H*), 7.418 (2H, dt, *J* = 8.4 Hz, *J* = 0.8 Hz, Ar-*H*), 7.698 (2H, d, *J* = 1.6 Hz, Ar-*H*), 7.762 (1H, dd, *J* = 8.4 Hz, *J* = 1 Hz, Ar-*H*), 7.885 (1H, d, *J* = 8.4 Hz, Ar-*H*). MALDI-TOF-MS *m/z*: calcd for $C_{20}H_9BrI_2O_3$ + H 630.790, obsd 630.784 (77 % intensity) 506.886 (100 % intensity).

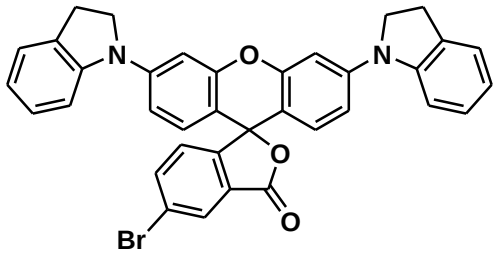

20

3', 6'-Diindolino-5-bromofluoran (20).

Method A. 3', 6'-Diiodo-5-bromofluoran (126 mg, 0.2 mmol) and anhydrous zinc chloride (136 mg, 1 mmol) were mixed in a 10 mL round bottom flask. Indoline (225 μL, 2 mmol) was added to above mixture and the reaction mixture was stirred at 150 ºC under argon for 24 h.

The reaction mixture was dissolved in dichloromethane and filtered through a short plug of silica gel (1 to 2% methanol in dichloromethane). The desired product (31 mg, 25 % yield) was purified by a silica gel preparative thin layer chromatography plate (1 to 2% methanol in dichloromethane).

Method B. A mixture of compound **16** (400 mg, 0.634 mmol), indoline (282 μL, 2.53 mmol), (±)2,2'-bis(diphenylphosphino)-1,1'-binaphthyl (17 mg, 0.027 mmol), palladium(II) acetate (5.6 mg, 0.025 mmol), and cesium carbonate (2.1 g, 6.44 mmol) in toluene (15 mL) was refluxed for 24 h. The solvent was removed and the residue was chromatographed on a silica gel column (1 to 3 % MeOH in dichloromethane) to yield 350 mg (0.57 mmol) of compound **20** (90 % yield). ^{1}H NMR (400 MHz, $CDCl_3$): δ, ppm 3.161 (4H, t, *J* = 8.4 Hz, -C*H*$_2$-), 3.992 (4H, m, -C*H*$_2$-), 6.734 (2H, d, *J* = 8.4 Hz, Ar-*H*), 6.822 (2H, t, *J* = 7.4 Hz, Ar-*H*), 6.941 (2H, dd, *J* = 8.8 Hz, *J* = 2.4 Hz, Ar-*H*), 7.06 (2H, d, *J* = 2.4 Hz, Ar-*H*), 7.097-7.145 (3H, m, Ar-*H*), 7.201 (2H, d, *J* = 7.2 Hz, Ar-*H*), 7.252 (2H, d, *J* = 6.4 Hz, Ar-*H*), 7.799 (1H, dd, *J* = 8.4 Hz, *J* = 1.8 Hz, Ar-*H*), 8.166 (1H, d, *J* = 1.6 Hz, Ar-*H*). MALDI-TOF-MS *m/z*: calcd for $C_{36}H_{25}BrN_2O_3$ + H 615.11, obsd 614.96.

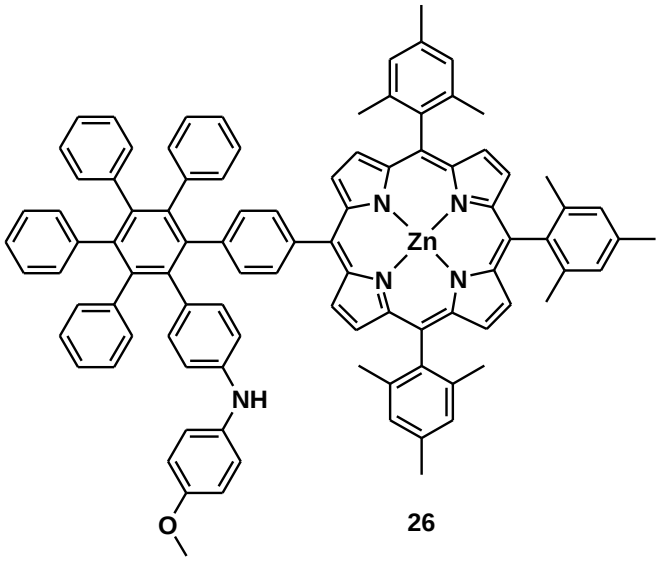

26

Porphyrin 26. Porphyrin **25**[45] (116 mg, 0.0867 mmol), palladium(II) acetate (1.2 mg, 0.0053 mmol), 1,1'-bis(diphenylphosphino)ferrocene (11.8 mg, 0.0213 mmol), *p*-anisidine (14 mg, 0.11 mmol), and potassium *t*-butoxide (14 mg, 0.12 mmol) were placed in a 25mL pear-shaped flask under argon. Deoxygenated toluene (1 mL) was added to the flask. The mixture was refluxed under argon for 5 h. After cooling to room temperature, the mixture was chromatographed on silica gel columns (column 1: dichloromethane/hexanes, 5/5; column 2: toluene) to yield 56 mg (47 %) of compound **26**. ^{1}H NMR (400 MHz, $CDCl_3$): δ, ppm 1.804 (6H, s, -C*H*$_3$), 1.817 (6H, s, -C*H*$_3$), 1.829 (6H, s, -C*H*$_3$), 2.614 (3H, s, -C*H*$_3$), 2.625 (3H, s, -C*H*$_3$), 2.639 (3H, s, -C*H*$_3$), 3.759 (3H, s, -OC*H*$_3$), 5.448 (1H, s, -N*H*), 6.722 (2H, d, *J* = 8.8 Hz, Ar-*H*), 6.764 (2H, d, *J* = 8.8 Hz, Ar-*H*), 6.86-7.01 (18H, m, Ar-*H*), 7.036 (2H, d, *J* = 9.2 Hz, Ar-*H*), 7.12-7.16 (6H, m, Ar-*H*), 7.190 (2H, d, *J* = 8.0 Hz), 7.26-7.28 (6H, m, Ar-*H*), 7.731 (2H, d, *J* = 8.0 Hz,

Ar-*H*), 8.480 (1H, d, *J* = 4.4 Hz, β-*H*), 8.554 (1H, d, *J* = 4.4 Hz, β-*H*), 8.652 (1H, d, *J* = 4.8 Hz, β-*H*), 8.67-8.69 (5H, m, β-*H*). MALDI-TOF-MS *m/z*: calcd for $C_{96}H_{77}N_5OZn$ 1379.542, obsd 1379.525. UV-vis (CH_2Cl_2): λ_{max}, nm 421, 550, 586.

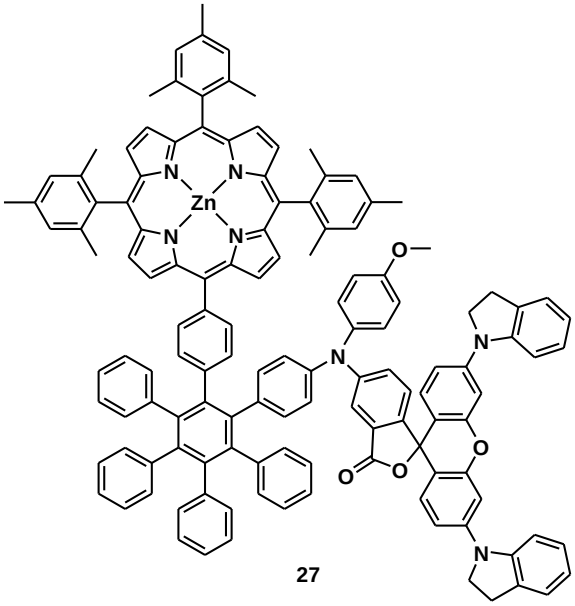

27

Dyad 27. Porphyrin compound **26** (15 mg, 0.011 mmol), dye compound **20** (13 mg, 0.021 mmol), palladium acetate (2.0 mg, 0.0089 mmol), cesium carbonate (55 mg, 0.17 mmol), and 1 M tri-*t*-butylphosphine in toluene (15 μL, 0.015 mmol) were mixed in deoxygenated toluene (1 mL) under argon. The mixture was stirred at 110 ºC under argon overnight. After cooling to room temperature, insoluble salts were filtered off and the filter cake was washed with dichloromethane. Solvents were distilled from the filtrates under reduced pressure. The residue was chromatographed on a silica gel column (dichloromethane/methanol, 98/2) to yield 12 mg (57 %) of **27**.

^{1}H NMR (400 MHz, $CDCl_3$): δ, ppm 1.699 (6H, s, -C*H*$_3$), 1.805 (6H, s, -C*H*$_3$), 1.816 (6H, s, -C*H*$_3$), 2.462 (3H, s, -C*H*$_3$), 2.610 (3H, s, -C*H*$_3$), 2.638 (3H, s, -C*H*$_3$), 3.102 (4H, t, *J* = 8.4 Hz, -C*H*$_2$-), 3.492 (3H, s, -OC*H*$_3$), 3.930 (4H, m, -C*H*$_2$-), 6.442 (2H, d, *J* = 8.8 Hz, Ar-*H*), 6.74-6.81 (5H, m, Ar-*H*), 6.87-7.28 (45H, m, Ar-*H*), 7.512 (1H, m, Ar-*H*), 7.744 (2H, d, *J* = 7.6 Hz, Ar-*H*), 8.498 (1H, d, *J* = 4.4 Hz, β-*H*), 8.59-8.70 (7H, m, β-*H*). MALDI-TOF-MS *m/z*: calcd for $C_{132}H_{101}N_7O_4Zn$ 1911.721, obsd 1911.783 (100 % intensity) 1866.783 (45 % intensity). UV-vis (CH_2Cl_2): λ_{max}, nm 421, 551, 588.

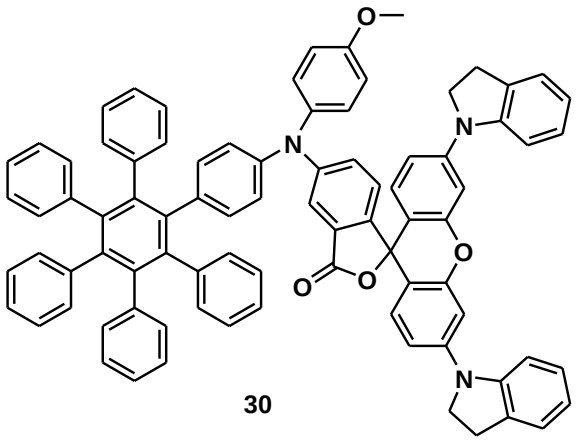

30

Model Dye 30. A hexaphenylbenzene precursor compound[3,100] (25 mg, 0.038 mmol), dye compound **20** (24 mg, 0.039 mmol), palladium(II) acetate (2.3 mg, 0.010 mmol), cesium carbonate (50 mg, 0.15 mmol), and 10 % tri-*t*-butylphosphine (52 μL) were mixed in deoxygenated toluene (1 mL). The mixture was refluxed under argon for 18 h. After cooling to room temperature, the mixture was chromatographed on a silica gel column (dichloromethane/methanol, 99.5/0.5) to yield 37 mg (82 %) of compound **30**. ^{1}H NMR (400 MHz, $CDCl_3$): δ, ppm 3.155 (4H, t, *J* = 8.4 Hz, -C*H*$_2$-), 3.808 (3H, s, -OC*H*$_3$), 3.988 (4H, t, *J* = 8.4 Hz, -C*H*$_2$-), 6.670 (2H, d, *J* = 8.4 Hz, Ar-*H*), 6.746 (2H, d, *J* = 8.4 Hz, Ar-*H*), 6.79-6.97 (36H, m, Ar-*H*), 7.00-7.04 (3H, m, Ar-*H*), 7.111 (2H, t, *J* = 7.6 Hz, Ar-*H*), 7.194 (2H, d, *J* = 7.6 Hz, Ar-*H*), 7.24-7.28 (3H, m, Ar-*H*). MALDI-TOF-MS *m/z*: calcd for $C_{85}H_{61}N_3O_4$ + H 1188.47, obsd 1188.30 (97 % intensity) 1143.31 (100 % intensity).

References

1. Gupta, C. L. *Renewable and Sustainable Energy Reviews* **2003**, 7, 155-174.

2. Ciamician, G. *Science* **1912**, 36, 385-394.

3. Terazono, Y.; Kodis, G.; Bhushan, K.; Zaks, J.; Madden, C.; Moore, A. L.; Moore, T. A.; Fleming, G. R.; Gust, D. *J. Am. Chem. Soc.* **2011**, 133, 2916-2922.

4. http://photoscience.la.asu.edu/photosyn/education/photointro.html

5. Gust, D.; Moore, T. A.; Moore, A. L. *Acc. Chem. Res.* **2001**, *34*, 40.

6. Gust, D.; Moore, T. A.; Moore, A. L. Mimicking Bacterial Photosynthesis. In *Artificial Photosynthesis.* Collings, A. F.; Critchley, C. Eds. Wiley-VCH: Weinheim, **2005**, pp 187-210.

7. Wasielewski, M. R. *Chem. Rev.* **1992**, *92*, 435.

8. Bard, A. J.; Fox, M. A. *Acc. Chem. Res.* **1995**, 28, (3), 141-145.

9. Steinberg-Yfrach, G.; Liddell, P. A.; Hung, S. C.; Moore, A. L.; Gust, D.; Moore, T. A. *Nature* **1997**, 385, 239-241.

10. Gust, D.; Moore, T. A. *The Porphyrin Handbook.* Kadish, K.; Smith, K. M.; Guilard, R. Eds. Academic Press: New York, **1999**, pp 153-190.

11. Imahori, H.; Sakata, Y. *Eur. J. Org. chem.* **1999**, 2445-2457.

12. Kuciauskas, D.; Liddell, P. A.; Lin, S.; Johnson, T. E.; Weghorn, S. J.; Lindsey, J. S.; Moore, A. L.; Moore, T. A.; Gust, D. *J. Am. Chem. Soc.* **1999**, 121, 8604-8614.

13. Burrell, A. K.; Officer, D. L.; Plieger, P. G.; Reid, D. C. W. *Chem. Rev.* **2001**, 101, (9), 2751-2796.

14. Imahori, H.; Tamaki, K.; Guldi, D. M.; Luo, C. P.; Fujitsuka, M.; Ito, O.; Sakata, Y.; Fukuzumi, S. *J. Am. Chem. Soc.* **2001**, 123, 2607-2617.

15. Guldi, D. M. *Chem. Soc. Rev.* **2002**, 31, 22-36.

16. Wasielewski, M. R. *J. Org. Chem.* **2006**, 71, (14), 5051-5066.

17. Herrero, C; Lassalle-Kaiser, B.; Leibl, W.; Rutherford, A. W.; Aukauloo, A. *Coord. Chem. Rev.* **2008**, 252, (3+4), 456-468.

18. Tamiaki, H.; Miyatake, T.; Tanikaga, R.; Holzwarth, A. R.; Schaffher, K. *Angew. Chem. Int. Ed. Engl.* **1996,** 35, (7), 772-774.

19. Ahrens, M. J.; Sinks, L. E.; Rybtchinski, B.; Liu, W.; Jones, B. A.; Giaimo, J. M.; Gusev, A. V.; Goshe, A. J.; Tiede, D. M.; Wasielewski, M. R. *J. Am. Chem. Soc.* **2004**, 126, (26), 8284-8294.

20. Balaban, T. S. *Acc. Chem. Res.* **2005**, 38, (8), 612-623.

21. Roger, C; Miloslavina, Y.; Brunner, D.; Holzwarth, A. R.; Wurthner, F. *J. Am. Chem. Soc.* **2008**, 130, (18), 5929-5939.

22. Förster, T. *Ann. Phys.* **1948**, 2, 55-75.

23. Förster, T. *Naturforsch.* **1949**, 4, 321.

24. Dexter, D. L. *J. Chem. Phys.* **1953**, 21, 836.

25. Marcus, R. A. *J. Chem. Phys.* **1956**, 24, 966-978.

26. Hush, N. S. *J. Chem. Phys.* **1958**, 28, 962-972.

27. Levich, V. G.; Dogonadze, R. R. *Collect. Czech. Chem. Commun.* **1961**, 26, 193-214.

28. Jortner, J. *J. Chem. Phys.* **1976**, 64, (12), 4860-4867.

29. Closs, G. L.; Miller, J. R. *Science* **1988**, 240, (4851), 440-447.

30. Moore, T. A.; Gust, D.; Mathis, P.; Mialocq, J. C; Chachaty, C.; Bensasson, R. V.; Land, E. J.; Doizi, D.; Liddell, P. A.; et al. *Nature* **1984**, 307, (5952), 630-632.

31. Connolly, J. S.; Bolton, J. R. *Photoinduced Electron Transfer*. Fox, M. A.; Chanon, M. Eds. Elsevier: Amsterdam, **1988**, pp 303-393.

32. Maggini, M.; Scorrano, G.; Prato, M. *J. Am. Chem. Soc.* **1993**, *115*, 9798-9799.

33. Liddell, P. A.; Sumida, J. P.; Macpherson, A. N.; Noss, L.; Seely, G. R.; Clark, K. N.; Moore, A. L.; Moore, T. A.; Gust, D. *Photochem. Photobiol.* **1994**, 60, (6), 537-541.

34. DeGraziano, J. M.; Liddell, P. A.; Leggett, L.; Moore, A. L.; Moore, T. A.; Gust, D. *J. Phys. Chem. B.* **1994**, 98, (7), 1758-1761.

35. Kuciauskas, D.; Lin, S.; Seely, G. R.; Moore, A. L.; Moore, T. A; Gust, D.; Drovetskaya, T.; Reed, C. A.; Boyd, P. D. W. *J. Phys. Chem. B* **1996**, 100, (39), 15926-15932.

36. Liddell, P. A.; Kuciauskas, D.; Sumida, J. P.; Nash, B.; Nguyen, D.; Moore, A. L.; Moore, T. A.; Gust, D. *J. Am. Chem. Soc.* **1997**, 119, (6), 1400-1405.

37. Bahr, J. L.; Kuciauskas, D.; Liddell, P. A.; Moore, A. L.; Moore, T. A.; Gust, D. *Photochem. Photobiol.* **2000**, 72, (5), 598-611.

38. Kuciauskas, D.; Liddell, P. A.; Lin, S.; Stone, S. G.; Moore, A. L.; Moore, T. A.; Gust, D. *J. Phys. Chem. B.* **2000**, 104, (18), 4307-4321.

39. Liddell, P. A.; Kodis, G.; de la Garza, L.; Bahr, J. L.; Moore, A. L.; Moore, T. A.; Gust, D. *Helv. Chim. Acta.* **2001**, 84, (9), 2765-2783.

40. Kodis, G.; Liddell, P. A.; Moore, A. L.; Moore, T. A.; Gust, D., *J. Phys. Org. Chem.* **2004**, 17, (9), 724-734.

41. Liddell, P. A.; Kodis, G.; de la Garza, L.; Moore, A. L.; Moore, T. A.; Gust, D. *J. Phys. Chem. B* **2004**, *108*,10256-10265.

42. Terazono, Y.; Kodis, G.; Liddell, P. A.; Garg, V.; Moore, T. A.; Moore, A. L.; Gust, D. *J. Phys. Chem. B.* **2009**,113, (20), 7147-7155.

43. Kodis, G.; Liddell, P. A.; de la Garza, L.; Clausen, P. C; Lindsey, J. S.; Moore, A. L.; Moore, T. A.; Gust, D. *J. Phys. Chem. A.* **2002,** 106, (10), 2036-2048.

44. Moore, A. L.; Moore, T. A.; Gust, D. *Acc. Chem. Res.* **2009**, 42, (12), 1890-1898.

45. Terazono, Y.; Liddell, P. A.; Garg, V.; Kodis, G.; Brune, A.; Hambourger, M.; Moore, A. L.; Moore, T. A.; Gust, D. *J. Porphyrins Phthalocyanins* **2005**, 9, 706-723.

46. Kodis, G.; Terazono, Y.; Liddell, P. A.; Andreasson, J.; Garg, V.; Hambourger, M.; Moore, T. A.; Moore, A. L.; Gust, D. *J. Am. Chem. Soc.* **2006**, *128*,1818-1827.

47. Gust, D.; Moore, T. A. *Science* **1989**, *244*, 35.

48. Gust, D.; Moore, T. A.; Moore, A. L. *Acc. Chem. Res.* **1993**, *26*, 198.

49. Muller, P.; Li, X. P.; Niyogi, K. K. *Plant Physiol.* **2001**, *125*, 1558-1566.

50. Ahn, T. K.; Avenson, T. J.; Ballottari, M.; Cheng, Y. C.; Niyogi, K. K.; Bassi, R.; Fleming, G. R. *Science* **2008**, *320*, 794.

51. Ruban, A. V.; Berera, R.; Ilioaia, C.; van Stokkum, I. H. M.; Kennis, J. T. M.; Pascal, A. A.; van Amerongen, H.; Robert, B.; Horton, P.; van Grondelle, R. *Nature* **2007**, *450*, 575.

52. Vaswani, H. M.; Holt, N. E.; Fleming, G. R. *Pure Appl. Chem.* **2005**, *77*, 925.

53. Standfuss, R.; van Scheltinga, A. C. T.; Lamborghini, M.; Kuhlbrandt, W. *Embo J.* **2005**, *24*, 919.

54. Pillai, S. In *Dissertation*, Arizona State University, Tempe, Arizona, **2011**.

55. Dreuw, A.; Fleming, G. R.; Head-Gordon, M. *Phys. Chem. Chem. Phys.* **2003**, *5*, 3247.

56. Frank, H. A.; Cogdell, R. *J. Photochem. Photobiol.* **1996**, *63*, 257.

57. Holt, N. E.; Fleming, G. R.; Niyogi, K. K. *Biochem*. **2004**, 43, (26), 8281-8280.

58. Külheim, C.; Ågren, J.; Jansson, S. *Science* **2002**, 297, 91-93.

59. Barber, J.; Andersson, B. *Trends Biochem. Sci.* **1992**, 17, 61-66.

60. Niyogi, K. K. *Annu. Rev. Plant Physiol. Plant Mol. Biol.* **1999**, 50, 333-359.

61. Gust, D.; Moore, T. A.; Moore, A. L. *Faraday Discuss.* **2012**, 155, 9-26.

62. Bensasson, R. V.; Land, E. J.; Moore, A. L.; Crouch, R. L.; Dirks, G.; Moore, T. A. Gust, D. *Nature*, **1981**, 290, 329.

63. Moore, A. L.; Joy, A. M.; Tom, R.; Gust, D.; Moore, T. A.; Bensasson, R. V.; Land, E. J. *Science*, **1982**, 216, 982.

64. Gust, D.; Moore, T. A.; Moore, A. L.; Devadoss, C.; Liddell, P. A.; Hermant, R. M.; Nieman, R. A.; Demanche, L. J.; DeGraziano, J. M.; Gouni, I. *J. Am. Chem. Soc.* **1992**, 114, 3590.

65. Gust, D.; Moore, T. A.; Moore, A. L.; Kuciauskas, D.; Liddell, P. A.; Halbert, B. D. *J. Photochem. Photobiol. B* **1998**, 43, 209.

66. Kodis, G.; Herrero, C.; Palacios, R.; Marino-Ochoa, E.; Gould, S. L.; de la Garza, L.; van Grondelle, R.; Gust, D.; Moore, T. A.; Moore, A. L.; Kennis, J. T. M. *J. Phys. Chem. B* **2004**, 108, 414.

67. Kloz, M.; Pillai, S.; Kodis, G.; Gust, D.; Moore, T. A.; Moore, A. L.; van Grondelle, R.; Kennis, J. T. M. *J. Am. Chem. Soc.* **2011**, 133, 7007.

68. Wilson, A.; Ajlani, G.; Verbavatz, J. M.; Vass, I.; Kerfeld, C. A.; Kirilovsky, D. *Plant Cell* **2006**, 18, 992.

69. Wilson, A.; Punginelli, C.; Gall, A.; Bonetti, C.; Alexandre, M.; Routaboul, J. M.; Kerfeld, C. M.; van Grondelle, R.; Robert, B.; Kennis, J. T. M.; Kirilovsky, D. *Proc. Natl. Acad. Sci. U. S. A.* **2008**, 105, 12075.

70. Straight, S. D.; Kodis, G.; Terazono, Y.; Hambourger, M.; Moore, T. A.; Moore, A. L.; Gust, D. *Nat. Nanotechnol.* **2008**, 3, 280.

71. Havaux, M.; Niyogi, K. K. *Proc. Natl. Acad. Sci. U.S.A.* **1999**, 96, 8762-8767.)

72. Horton, P.; Hague, A. *Biochim. Biophys. Acta* **1988**, 932, 107-115.

73. Demmig-Adams, B.; Adams, W. W. III; Barker, D. H.; Logan, B. A.; Bowling, D. R.; Verhoeven, A. S. *Physiol. Plant.* **1996**, 98, 253-264.

74. Bassi, R.; Caffarri, S. *Photosynth. Res.* **2000**, 64, 243-256.

75. Li, X.-P.; Bjorkman, O.; Shih, C.; Grossman, A. R.; Rosenquist, M.; Jansson, S.; Niyogi, K. K. *Nature* **2000**, 403, 391-395.

76. Demmig-Adams, B. *Biochim. Biophys. Acta* **1990**, *1020*, 1-24.

77. Li, X.-P.; Muller-Moule, P.; Gilmore, A. M.; Niyogi, K. K. *Proc. Natl. Acad. Sci. U.S.A. 2002, 99*, 15222-15227.

78. Gilmore, A. M.; Hazlett, T. L.; Govindjee *Proc. Natl. Acad. Sci. U.S.A.* **1995**, 92, 2273-2277.

79. Horton, P.; Ruban, A. V.; Walters, R. G. *Annu. Re*v. *Plant Phys.* **1996**, 47, 655-684.

80. Wedel, N.; Klein, R.; Ljungberg, U.; Andersson, B.; Herrmann, R. G. *FEBS Lett*. **1992**, 314, 61-66.

81. Kim, S.; Sandusky, P.; Bowlby, N. R.; Aebersold, R.; Green, B. R.; Vlahakis, S.; Yocum, C. F.; Pichersky, E. *FEBS Lett.* **1992**, 314, 67-71.

82. Ljungberg, U.; Akerlund, H. E.; Andersson, B. *Eur. J. Biochem.* **1986**, *158*, 477-482.

83. Ghanotakis, D. F.; Waggoner, C. M.; Bowlby, N. R.; Demetrious, D. M.; Babcock, G. T.; Yocum, C. F. *Photosynth. Res.* **1987**, 14, 191-199.

84. Young, A. J.; Phillip, D.; Ruban, A. V.; Horton, P.; Frank, H. A. *Pure Appl. Chem.* **1997**, *69*, 2125.

85. Horton, P.; Ruban, A. V. *J. Exp. Bot.* **2004**, 56, 365.

86. Pascal, A. A.; Liu, Z. F.; Broess, K.; van Oort, B.; van Amerongen, H.; Wang, C.; Horton, P.; Robert, B.; Chang, W. R.; Ruban, A. *Nature,* **2005**, 436, 134.

87. Berera, R.; Herrero, C.; van Stokkum, L. H. M.; Vengris, M.; Kodis, G.; Palacios, R. E.; van Amerongen, H.; van Grondelle, R.; Gust, D.; Moore, T. A.; Moore, A. L.; Kennis, J. T. M. *Proc. Natl. Acad. Sci. U. S. A.* **2006**, 103, 5343.

88. Liao, P. N.; Pillai, S.; Gust, D.; Moore, T. A.; Moore, A. L.; Walla, P. J. *J. Phys. Chem. A* **2011**, 115, 4082.

89. Woodroofe, C. C.; Lim, M. H.; Bu, W. M.; Lippard, S. J. *Tetrahedron* **2005**, 61, 3097-3105.

90. Takase, M.; Ismael, R.; Murakami, R.; Ikeda, M.; Kim, D.; Shinmori, H.; Furuta, H.; Osuka, A. *Tetrahedron Lett.* **2002**, 43, 5157-5159.

91. Terazono, Y.; Kodis, G.; Liddell, P. A.; Garg, V.; Gervaldo, M.; Moore, T. A.; Moore, A. L.; Gust, D. *Photochem. Photobiol.* **2007**, 83, 464-469.

92. Cho, H. S.; Rhee, H.; Song, J. K.; Min, C.-K.; Takase, M.; Aratani, N.; Cho, S.; Osuka, A.; Joo, T.; Kim, D. *J. Am. Chem. Soc.* **2003**, 125, 5849-5860.

93. Barzilay, C. M.; Sibilia, S. A.; Spiro, T. G.; Gross, Z. *Chem. Eur. J.* **1995**, 1, 222-231.

94. Almenningen, A.; Bastiansen, O.; Skancke, P. N. *Acta Chem. Scand.* **1958**, 12, 1215-1220.

95. Bart, J. C. J. *Acta Crystallogr., Sect. B* **1968**, 24, 1277-1287.

96. Larson, E. M.; Von Dreele, R. B.; Hanson, P.; Gust, D. *Acta Cryst.* **1990**, C46, 784-788.

97. Förster, T. *Disc. Faraday Soc.* **1959**, *27*, 7-17.

98. Penzkofer, A.; Wiedmann, J. *Optics Commun.* **1980**, 35, 81-86.

99. Hsiao, J.-S.; Krueger, B. P.; Wagner, R. W.; Johnson, T. E.; Delaney, J. K.; Mauzerall, D. C.; Fleming, G. R.; Lindsey, J. S.; Bocian, D. F.; Donohoe, R. J. *J. Am. Chem. Soc.* **1996**, 118, 11181-11193.

100. Kubel, C.; Chen, S. L.; Mullen, K. *Macromolecules* **1998**, 31, 6014-6021.